To the Graduate Council:

I am submitting herewith a thesis written by George Jacob entitled "Energy Absorption in Polymer Composite Materials for Automotive Crash Worthiness". I have examined the final copy of this thesis for form and content and recommend that it be accepted in partial fulfillment of the major requirements for the degree of Master of Science, with a major in Polymer Engineering.

John F. Fellers

John F. Fellers, Major Professor

We have read this thesis and recommend its acceptance:

Roberto Benson

Accepted for the Council:

Interim Vice Provost

and Dean of the Graduate School

Energy Absorption in Polymer Composite Materials for Automotive Crash Worthiness

A Thesis Presented for the Master of Science Degree

The University of Tennessee, Knoxville

George Jacob

May 2001

To All Those Who Hope

&

Pray For My Well Being

Acknowledgements

I would like to thank my committee, Dr. John F. Fellers, Dr. Joseph E. Spruiell and Dr. Roberto S. Benson, for their interest in my research as well as education. Dr. John F. Fellers who guided me in the capacity of a graduate advisor has always been extremely supportive and encouraging to all my thoughts and actions during my stay in this university. I would also like to thank Dr. J. Michael Starbuck from the Engineering Technology Division, Oak Ridge National Laboratory, for supervising all my experimental work that was conducted in his lab. Last but not the least, my special thanks to Dr. Srdan Simunovic from the Computer Science and Mathematics Division, Oak Ridge National Laboratory, for giving me the opportunity to work on this project on Crash Worthiness. I owe Dr. Fellers, Dr. Starbuck and Dr. Simunovic my sincere gratitude for they are all largely responsible for making my entire stay in Knoxville fruitful and happy. Thank you. Finally, I thank my family for their continuing unconditional love and affection from the day I was born.

Abstract

The energy absorption capability of a composite material is important in developing improved human safety in an automotive crash. In passenger vehicles the ability to absorb impact energy and be survivable for the occupant is called the "crash worthiness" of the structure. The vehicle must be designed such that, in the event of an impact at speeds up to 35 mph with a solid, immovable object, its occupants do not experience a resulting force that produces a net deceleration greater than 20g. Subjection of the occupants to decelerations greater than 20g can cause serious internal injury, particularly brain damage. Energy absorption in these composite materials are dependent on many parameters like fiber type, matrix type, fiber architecture, specimen geometry, processing conditions, fiber volume fraction, and testing speed. Changes in these parameters can cause subsequent changes in the specific energy absorption of composite materials up to a factor of 2. Through ongoing research programs a considerable amount of experimental data on the energy absorption characteristics of polymer composite materials have been generated. They have been found to be efficient energy absorbers and suitable for crash worthy structural applications. But there are a lot of other criteria, in addition to a material being crash worthy, that need to be met before one can begin the use of a particular composite as a crash energy absorber in automobiles. Some of the primary ones being, low costs involved in their manufacture, the raw materials being readily available and many more. Once a composite material is identified to meet the above necessary requirements, one ought to study the effect all the controllable parameters (like fiber volume fraction, specimen geometry etc.) will have on its energy absorption capabilities, in an attempt to design the most crash worthy structure. The

ACC (Automotive Composite Consortium) is interested in investigating the use of chopped fiber reinforced composites as crash energy absorbers primarily due to the low costs involved in their manufacture thus making them cost effective for automotive applications. While many scientists have investigated the energy absorption characteristics in various continuous fiber reinforced composite materials, there is no literature available on the energy absorption and crushing characteristics of chopped fiber reinforced composite materials. Therefore the primary goal of this project was to determine the crash worthiness of a chopped carbon fiber composite material system and to see how it compared with that of other fiber resin systems like graphite/epoxy cross-ply laminates, a graphite/epoxy braided material system and a glass-reinforced continuous strand mat (CSM). To meet this goal first an experimental set up was developed for discerning the deformation behavior and damage mechanisms that occur during the progressive crushing of composite materials. The composite material systems studied were chopped carbon fibers reinforced in an epoxy resin system, graphite/epoxy cross-ply laminates, graphite/epoxy triaxial braids with $0/+30^{\circ}/-30^{\circ}$ fiber orientation and glass/polyurethane continuous strand mat. Quasi-static progressive crush tests were then performed on these composite plates to identify and quantify their energy absorbing mechanisms. An attempt was made to understand in great detail the effect of various material (fiber volume fraction, fiber length, fiber tow size) and test (specimen width, loading rate, profile radius, constraint condition) parameters on their energy absorption capability by varying these parameters during testing. After having identified which combination of fiber volume fraction, fiber length, fiber tow size and specimen width will yield the highest energy absorbing material, the quantity of this material needed to ensure

passenger safety in a mid-size car traveling at various velocities was calculated. The specific energy absorption, SEA, of the chopped carbon fiber composite material, CCF, was the highest compared to that of all the other composites investigated herein. The 2 inch wide specimens belonging to panel group CCF5 having fiber tow size 150 gsm (grams per square meter), a fiber length of 1 inch and 50% fiber volume fraction recorded the highest SEA equal to 28.11 kJ/kg when tested at 5 mm/min crushing speed under the tight constraint condition using a profile block of radius 0.635 cm. It was calculated that only 4.27 kg of it would need to be placed at specific places in the car to ensure passenger safety in the event of a crash at 35 mph. This clearly led to an important practical conclusion that only a reasonable amount of this composite material is required to meet the necessary impact performance standard. The CCF composite tested at 5 mm/min crushing speed met both the criteria that need to be satisfied before a material is deemed highly crash worthy: A high magnitude of energy absorption and a safe allowable rate of this energy absorption. All the experimental data and test observations generated from the above work was used to support the modeling efforts conducted by the Computer Science and Mathematics division at ORNL in their pursuit to develop analytical material damage models.

Table of Contents

Chapter 1 Introduction 1

1.1 Material Performance Requirements 3

1.2 Test Methodologies 6

1.2.1 Quasi-static Testing 6

1.2.2 Impact Testing 8

1.3 Crushing Modes and Mechanisms 9

1.3.1 Catastrophic Failure Modes 9

1.3.2 Progressive Failure Modes 10

1.3.2.1 Transverse Shearing or Fragmentation Mode 10

1.3.2.2 Lamina Bending or Splaying Mode 12

1.3.2.3 Brittle Fracturing 12

1.3.2.4 Local Buckling or Progressive Folding 12

1.4 Calculation of Specific Energy Absorption SEA 16

1.5 Literature Survey 18

1.5.1 The Effect of Reinforcing Fiber on the Energy Absorption Capability of a Composite Material 30

1.5.2 The Effect of the Matrix on the Energy Absorption Capability of a Composite Material 37

1.5.3 The Effect of Fiber Architecture on the Energy Absorption Capability of a Composite Material 40

1.5.4 The Effect of Geometry of the Specimen on the Energy Absorption Capability of a Composite Material 45

1.5.5 The Effect of Processing Conditions on the Energy Absorption Capability of a Composite Material 52
1.5.6 The Effect of Fiber Volume Fraction on the Energy Absorption Capability of a Composite Material 56
1.5.7 The Effect of Testing Speed on the Energy Absorption Capability of a Composite Material 60
1.5.8 Summary of Findings 62
1.5.9 The Most Efficient Crashworthy Composite Material 66
1.5.10 Conclusions Reached at after Review of the Existing Literature 67
1.6 Rate Effects 68
1.7 Design for Optimum Work Rate Decay 70
1.8 Conclusion 71
Chapter 2 Experimental 76
2.1 Objective 76
2.2 Material Systems Investigated 76
2.3 Test Fixture Design 81
2.4 Variables Investigated 90
2.4.1 Test Variables 90
2.4.2 Material Variables 90
2.5 Testing Procedure 91
Chapter 3 Results and Discussion 105
3.1 Graphite/Epoxy Cross Ply Laminate: CP#1 105

3.1.1 Effect of Constraint Condition 105

3.2 Graphite/Epoxy Cross Ply Laminate: CP#2 105

3.2.1 Effect of Constraint Condition 112

3.3 Graphite/Epoxy Triaxial Braid with 0/30/-30 Fiber Orientations: O 112

3.3.1 Effect of Constraint Condition 119

3.4 Glass/Polyurethane Continuous Strand Mat: CSM 119

3.4.1 Effect of Constraint 115

3.4.2 Effect of Crushing Speed 131

3.4.2.1 No Constraint Condition 131

3.4.2.2 Loose Constraint Condition 131

3.4.2.3 Tight Constraint Condition 131

3.4.3 Effect of Profile Radius 141

3.5 Chopped Carbon Fiber/Epoxy Material System: CCF 141

3.5.1 Effect of Tow Size 148

3.5.2 Effect of Fiber Volume Fraction 158

3.5.3 Effect of Fiber Length 167

3.5.4 Effect of Profile Radius 176

3.5.5 Effect of Specimen Width 181

3.5.6 Effect of Constraint 185

3.5.7 Highest and Lowest Energy Absorbing Panel Groups 190

3.6 Comparison of all Materials Tested 192

3.7 Material Performance Requirements 192

3.8 Work Rate Decay 194

Chapter 4 Conclusion 199

Chapter 5 Future Work 203

List of References 204

Appendices 211

Appendix A Table of Experimental Data for CCF1 212

Appendix B Table of Experimental Data for CCF2 215

Appendix C Table of Experimental Data for CCF3 219

Appendix D Table of Experimental Data for CCF5 222

Appendix E Table of Experimental Data for CCF6 226

Appendix F Table of Experimental Data for CCF7 230

Appendix G Table of Experimental Data for CCF8 233

Appendix H Table of Experimental Data for CCF9 236

Vita 239

List of Tables

Table 1. Definition of Terms and Parameters Appearing in this Document 4

Table 2. Specific Energy Absorption SEA, and Inter Laminar Fracture Toughness G_{IC}, Values of Materials That Have Been Tested 20

Table 3. List of Composite Materials Investigated 31

Table 4. Effect of Fiber on Specific Energy Absorption SEA (kJ/kg) 38

Table 5. Effect of Matrix on Specific Energy Absorption SEA (kJ/kg) 41

Table 6. Effect of Matrix on Inter-Laminar Fracture Toughness G_{IC} (kJ/m^2) 42

Table 7. Effect of Fiber Architecture on Specific Energy Absorption SEA (kJ/kg) 46

Table 8. Effect of Specimen Geometry on Specific Energy Absorption SEA (kJ/kg) 53

Table 9. Effect of Processing Conditions on Specific Energy Absorption SEA (kJ/kg) 57

Table 10. Effect of Testing Speed on Specific Energy Absorption SEA (kJ/kg) 63

Table 11. A Matrix to help visualize The Number of Experiments Needed to Determine the Effect of One Parameter upon Another 74

Table 12. The Physical Properties of Carbon Fibers 78

Table 13. The Physical Properties of Glass Fibers 79

Table 14. Experimental Data for CP#1 106

Table 15. Experimental Data for CP#2 111

Table 16. Experimental Data for the Triaxial Braid O 114

Table 17. Experimental Data from Tests Conducted with a Profile Block of Radius 0.635 cm and 0.5 cm/min Loading Rate on CSM 126

Table 18. Experimental Data from Tests Conducted with a Profile Block of Radius 0.635 cm at 5cm/min Loading Rate on CSM 128

Table 19. Experimental Data from Tests Conducted in the No Constraint Condition on CSM 132

Table 20. Experimental Data from Tests Conducted in the Loose Constraint Condition on CSM 135

Table 21. Experimental Data from Tests Conducted in the Tight Constraint Condition on CSM 138

Table 22. Experimental Data from Tests Conducted with a Profile Block of Radius 0.635 cm and 1.27 cm at 0.5 in/min Loading Rate in the No Constraint Condition on CSM 142

List of Figures

Figure 1. Graph of Amount of Crash Worthy Material Required to Rate of Work Decay 7

Figure 2. Fragmentation Crushing Mode 11

Figure 3. Splaying Mode 13

Figure 4. Brittle Fracturing Crushing Mode 14

Figure 5. Progressive Folding Crushing Mode 15

Figure 6. Typical Load Displacement Curve for a Progressively Crushed Composite Tube 17

Figure 7. Design for Optimum Work Rate Decay 72

Figure 8. Schematic of Test Fixture Design 83

Figure 9. Roller Ways and Contact Profile Constraint — 1 84

Figure 10. Test Fixture Assembly — 1 85

Figure 11. Roller Ways and Contact Profile Constraint — 2 86

Figure 12. Test Fixture Assembly — 2 87

Figure 13. Constraint Conditions 89

Figure 14. Test Coupons 92

Figure 15. Composite Panel 93

Figure 16. Push Plates 94

Figure 17. Trimmed Specimens 95

Figure 18. CSM Test Specimen 96

Figure19. 407 Controller 99

Figure 20. Load Displacement DAQ 100

Figure 21. Crushing of a CP#2 Specimen 101

Figure 22. Crushing of a CSM Specimen 102

Figure 23. Crushing of a CP#1 Specimen — 1 103

Figure 24. Crushing of a CP#1 Specimen — 2 104

Figure 25. Load Displacement Traces for CP#1 107

Figure 26. Crushed CP#1 Specimen — 1 108

Figure 27. Crushed CP#1 Specimen — 2 109

Figure 28. Variation of SEA with Constraint Condition for CP#1 110

Figure 29. Comparison of Specific Energy Absorptions of CP#1 and CP#2 113

Figure 30. Load Displacement Traces for CP#2 114

Figure 31. Crushed CP#2 Specimen — 1 115

Figure 32. Crushed CP#2 Specimen — 2 116

Figure 33. Variation of SEA with Constraint Condition for CP#2 117

Figure 34. Load Displacement Traces for the Triaxial Braid O 120

Figure 35. Variation of SEA with Constraint Condition for the Triaxial Braid O 121

Figure 36. Load Displacement Traces for CSM 122

Figure 37. Crushed CSM Specimen 124

Figure 38. Specimen Buckling during Crushing of CSM in Loose Constraint Condition 125

Figure 39. Variation of SEA with Constraint Condition at Loading Rate of 0.5 cm/min for CSM 129

Figure 40. Variation of SEA with Constraint Condition at Loading Rate of 5 cm/min for CSM 130

Figure 41. Load Displacement Traces for a Test Conducted on CSM in the No Constraint Condition at Loading Rates of 0.5 and 5 cm/min respectively 133

Figure 42. Variation of SEA with Crushing Speed for CSM in the No Constraint Condition 134

Figure 43. Load Displacement Traces for a Test Conducted on CSM in the Loose Constraint Condition at Loading Rates of 0.5 and 5 cm/min respectively 136

Figure 44. Variation of SEA with Crushing Speed for CSM in the Loose Constraint Condition 137

Figure 45. Load Displacement Traces for a Test Conducted on CSM in the Tight Constraint Condition at Loading Rates of 0.5 and 5 cm/min respectively 139

Figure 46. Variation of SEA with Crushing Speed for CSM in the Tight Constraint Condition 140

Figure 47. Load Displacement Traces for a Test Conducted with a Profile Block of Radius 0.635 cm and 1.27 cm respectively on CSM 143

Figure 48. Variation of SEA with Profile Radius for CSM 144

Figure 49. Crushed CCF Specimen 147

Figure 50. Load Displacement Traces for CCF 149

Figure 51. Load Displacement Traces Representing the Effect of Tow Size on the SEA of CCF with 1 inch Fiber Length 150

Figure 52. Effect of Tow Size on the SEA of CCF with 1 inch F.L. and

50% F.V. 151

Figure 53. Effect of Tow Size on the SEA of CCF with 1 inch F.L. and 40% F.V. 152

Figure 54. Load Displacement Traces Representing the Effect of Tow Size on the SEA of CCF with 2 inch Fiber Length 154

Figure 55. Effect of Tow Size on the SEA of CCF with 2 inch F.L. and 50% F.V. 155

Figure 56. Effect of Tow Size on the SEA of CCF with 2 inch F.L. and 40% F.V. 156

Figure 57. Load Displacement Traces Representing the Effect of Fiber Volume Fraction on the SEA of CCF with 2 inch Fiber Length 159

Figure 58. Effect of F.V. on SEA of CCF with 2 inch F.L. and Tow Size 150 gsm 160

Figure 59. Effect of F.V. on SEA of CCF with 2 inch F.L. and Tow Size 300 gsm 161

Figure 60. Load Displacement Traces Representing the Effect of Fiber Volume Fraction on the SEA of CCF with 1 inch Fiber Length 163

Figure 61. Effect of F.V. on SEA of CCF with 1 inch F.L. and Tow Size 150 gsm 164

Figure 62. Effect of F.V. on SEA of CCF with 1 inch F.L. and Tow Size 300 gsm 165

Figure 63. Load Displacement Traces Representing the Effect of Fiber Length on the SEA of CCF with 150 gsm Tow Size 168

Figure 64. Effect of F.L. on the SEA of CCF with 150 gsm Tow Size and 50% F.V. 169

Figure 65. Effect of F.L. on the SEA of CCF with 150 gsm Tow Size and 40% F.V. 170

Figure 66. Load Displacement Traces Representing the Effect of Fiber Length on the SEA of CCF with 300 gsm Tow Size 172

Figure 67. Effect of F.L. on the SEA of CCF with 300 gsm Tow Size and 50% F.V. 173

Figure 68. Effect of F.L. on the SEA of CCF with 300 gsm Tow Size and 40% F.V. 174

Figure 69. Load Displacement Traces Representing the Effect of Profile Radius on the SEA of CCF 178

Figure 70. Variation of SEA with Profile Radius for CCF 179

Figure 71. Load Displacement Traces Representing the Effect of Specimen Width on the SEA of CCF 182

Figure 72. Variation of SEA with Specimen Width for CCF 183

Figure 73. Load Displacement Traces Representing the Effect of Constraint Condition on the SEA of CCF 187

Figure 74. Variation of SEA with Constraint Condition for CCF 188

Figure 75. Comparison of Composite Material Systems Tested 193

Figure 76. Graph of Amount of Crash Worthy Material Investigated in this Document Required to Rate of Work Decay 195

Chapter 1

Introduction

In passenger vehicles the ability to absorb impact energy and be survivable for the occupant is called the "crash worthiness" of the structure. There is an important difference between crash worthiness and penetration resistance. Crash worthiness is concerned with the absorption of energy through controlled failure mechanisms and modes that enable the maintenance of a gradual decay in the load profile during absorption. However penetration resistance is associated with the total absorption without allowing projectile or fragment penetration.

Current legislation for automobiles requires that vehicles be designed such that, in the event of an impact at speeds up to 35 mph with a solid, immovable object, the occupants of the passenger compartment should not experience a resulting force that produces a net deceleration greater than 20g. US helicopter requirements of safely surviving a descent, under no power; at 15 $msec^{-1}$ is another example of crash worthiness legislation. Crashworthy structures should be designed to absorb impact energy in a controlled manner, thereby bringing the passenger compartment to rest without the occupant being subjected to high decelerations, which can cause serious internal injury, particularly brain damage.

Vehicle size and mass provide a certain degree of protection but can have negative inertial effects. Driven by the need to overcome these negative effects of both size and mass coupled with mandates for increased fuel efficiency, an attempt is being made to use composites in the development of energy dissipating devices. The ability to tailor composites, in addition to their attributes of high stiffness-to-weight and strength-

to-weight ratios, fatigue resistance and corrosion resistance, makes them very attractive in crash worthiness. The challenge is the use of specific features of geometry and materials in enabling greater safety while simultaneously decreasing the weight, without negatively affecting the overall economics of fabrication and production.

To reduce the over all weight and improve the fuel economy of vehicles more and more metal parts are being replaced by polymer composite materials. Contrary to metals, especially in compression, most composites are generally characterized by a brittle rather than ductile response to load. While metal structures collapse under crush or impact by buckling and/or folding in accordion (concertina) type fashion involving extensive plastic deformation, composites fail through a sequence of fracture mechanisms involving fiber fracture, matrix crazing and cracking, fiber-matrix de-bonding, de-lamination and inter-ply separation. The actual mechanisms and sequence of damage are highly dependent on the geometry of the structure, lamina orientation, type of trigger and crush speed, all of which can be suitably designed to develop high energy absorbing mechanisms.

The crash worthiness of a material is expressed in terms of its specific energy absorption, SEA, and inter laminar fracture toughness, G_{IC}, which are characteristic to that particular material. Specific energy absorption is defined as the energy absorbed per unit mass of material. Mathematically $SEA=\bar{\sigma} / \rho$, where ρ is the density of the composite material and σ is the mean crush stress. Inter laminar fracture toughness is defined as the measure of the damage tolerance of a material containing initial flaws or cracks. Mathematically $G_{IC} = \pi K_{IC}^2/E$, Where E is the Young's modulus

and K_{IC} is the fracture toughness parameter [1]. To get a proper command over the parameters and terms used in this document please refer to Table 1.

1.1 Material Performance Requirements

Consider a midsize car of mass 1000 kg (2200 lbs) traveling at a velocity of 15.5 m/sec (35 mph). The kinetic energy of the car is equal to 0.5 m v^2 = $0.5*1000*(15.5)^2$ = 120125 J, where m is the mass of the car = 1000 kg (2200 lbs) and v is the velocity with which it is traveling = 15.5 m/sec (35 mph). In the event of an impact, crash worthy materials would have work done on them to absorb this kinetic energy over a time frame that ensures the deceleration of the car to be less than 20g, above which the passengers will experience irreversible brain damage. Therefore 120 kJ of work needs to be done on the crash worthy material. One can calculate the minimum safe time frame over which this work needs to be done to ensure the safety of the passengers using the basic equation of motion

$$v = u - at \qquad \text{Eq. (1)}$$

where v is the final velocity of the car which is equal to zero since the car comes to rest, u is the initial impact speed and a is the maximum allowable deceleration which is equal to 20g. This minimum time was calculated to be equal to 0.079 seconds. Therefore the maximum allowable rate of work decay that will ensure the safety of the passengers is equal to 120125 / 0.079 = 1521 kJ/sec. So while testing materials in the lab to determine their crash worthiness, it is equally important to determine the rate of energy absorption, as it is to record the magnitude of energy that is being absorbed by the specimen. No discussion of energy absorption rates was found in the literature on crash worthiness. The load increases very rapidly in the initial stages of the load displacement curve for

Table 1. Definition of Terms and Parameters Appearing in this Document.

Parameter	Details
Fiber Type	Names the type of reinforcing fibers used. Their properties can be related directly to the atomic arrangement and the defect content of the reinforcement, which must be controlled in the manufacturing process.
Matrix Type	Matrix may be thermoset or thermoplastic. The choice of the matrix is related to the required properties, the intended application of the composite and the method of manufacture.
Fiber Orientation	A simple convention is often used when describing the stacking sequences. For example, the angle ply laminate [0/+60/-60/0] is abbreviated to $[0/\pm\theta]$ where $\theta = 60^{o}$.
Specimen Geometry and Dimensions	One of the variables, which affect the crushing behavior, is the geometry and dimensions of the specimen. The different cross sectional shapes of the specimen might be square, circular, or rectangular. 'D' refers to the tube diameter and 't' to the tube thickness.
Trigger	A trigger is a stress concentrator that causes failure to initiate at a specific location within the structure. From there on the failure, in a controlled predictable manner, progresses through the body at the loading speed. A number of trigger geometry such as bevels, chamfers, grooves and holes can be used.

Table 1 continued.

Processing Conditions	Materials are known for their cooling rate dependency of mechanical properties. Fabrication can be done using three kinds of cooling rates: Rapid cooling by immersion in chilled water (95.5°C/min), gradual cooling in air (8.2°C/min) and slow cooling in the oven with heater switched off (0.7°C/min).
Fiber Volume Fraction	Most calculations on composite materials are based on volume fractions of the constituents. $F = w \rho_f / (w \rho_f + w_m \rho_m)$ where w and w_m are the weight fractions and ρ_f, ρ_m are the densities of the fiber and the matrix respectively and F is the volume fraction of the fiber.
Test Speed	The response of composite tubes subjected to constant speed, quasi-static crush tests and impact crush tests where the speed decreases from the initial impact speed to rest have been studied.
SEA	Specific energy absorption defined as the energy absorbed per unit mass of material. $SEA=\sigma / \rho$ where ρ is the density of the composite material and σ is the mean crush stress
G_{IC}	Inter laminar fracture toughness defined as the measure of the damage tolerance of a material containing initial flaws or cracks. $G_{IC} = \pi K_{IC}^2/E$, where E is the Young's modulus and K_{IC} is the fracture toughness parameter [1].

materials undergoing crushing to some maximum value after which stable crushing takes place. Now it is in this initial stage of the crash that the work decay rate might exceed the safe allowable limits. So though these materials may record very high-energy absorption values they might still not ensure the much needed passenger safety. It will be in the interest of improved safety to usefully couple these materials with other materials which when crushed have a lower initial peak load but not necessarily a high-energy absorption capability. This will smear the initial peak load response of the coupled material over a wider range which in the process lowers the net initial peak load to a value that is well within the maximum allowable rate of work decay. The specific energy absorption of unidirectional axial carbon/PEEK composites is recorded to be 180 kJ/kg. Therefore to absorb 120 kJ of kinetic energy one will only need 120125 / 180000 = 0.66 kg (1.45 lbs) of the carbon/PEEK composite located in specific places in the car. This clearly leads to an important practical conclusion that only a reasonable amount of composite is required to meet the necessary impact performance standard. Please see Figure 1 which shows the amount of different crash worthy material that will be required in the event of a crash to ensure a safe rate of work decay in a car of mass 1000 kg (2200 lbs) traveling at a particular velocity.

1.2 Test Methodologies

Crush tests can be carried out in two conditions namely quasi-static and impact conditions.

1.2.1 Quasi-static Testing

In quasi-static testing, the tube specimen is crushed at a constant speed. Quasi-static tests may not be a true simulation of the actual crash condition because in an

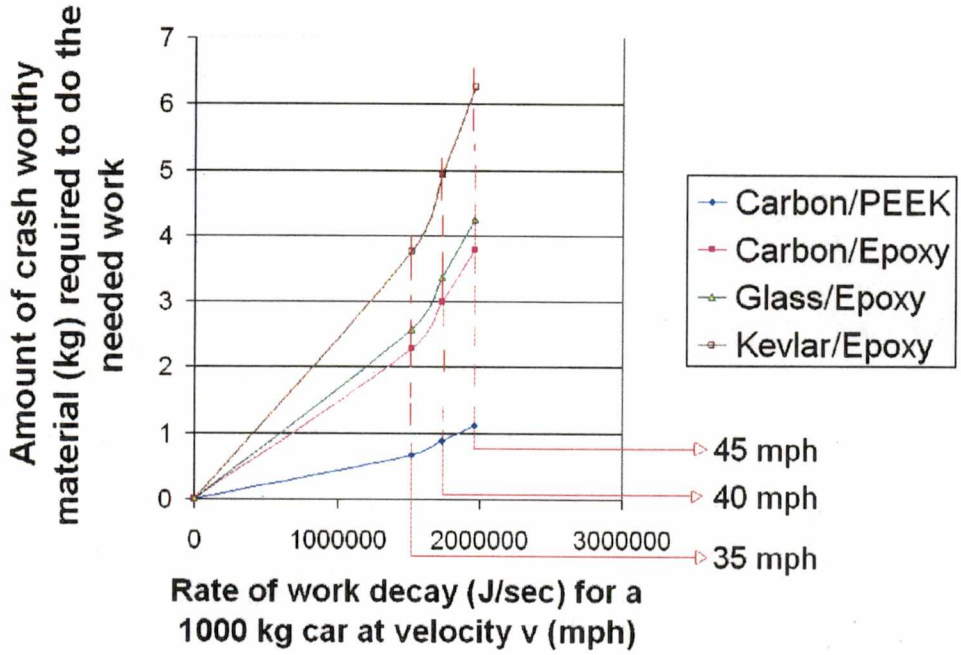

Figure 1. Graph of Amount of Crash Worthy Material Required to Rate of Work Decay.

actual crash condition, the structure is subjected to a decrease in crushing speed, from an initial impact speed, finally to rest. Many materials used in designing crashworthy structures are rate sensitive. That means their energy absorption capability is dependent on the speeds at which they are crushed. So the determination of materials as good energy absorbers after quasi-statically testing them does not ensure their satisfactory performance as crashworthy structures in the event of an actual crash.

The following are some advantages of quasi-static testing.

- Quasi-static tests are simple and easy to control.
- Impact tests require very expensive equipment to follow the crushing process cause the whole crushing takes place in a split second. Hence quasi-static tests are used to study the failure mechanisms in composite tubes, by selection of appropriate crush speeds.

The following is a major disadvantage of quasi-static testing.

- Quasi-static tests may not be a true simulation of the actual crash conditions since certain materials are strain rate sensitive.

1.2.2 Impact Testing

The crushing speed decreases from the initial impact speed to rest as the specimen absorbs the energy.

The following is a major advantage of impact testing

- It is a true simulation of the crash condition since it takes into account the stress rate sensitivity of materials.

The following is a major disadvantage of impact testing.

- In impact testing, the crushing process takes place in a fraction of a second. Therefore it is difficult to study the crushing unless provided with expensive equipment like a high-speed camera.

1.3 Crushing Modes and Mechanisms

1.3.1 Catastrophic Failure Modes

Catastrophic failure modes are not of interest to the design of crashworthy structures. It occurs

- When unstable intra laminar or inter laminar crack growth occurs.
- In long thin walled tubes because of column instability.
- In tubes composed of brittle fiber reinforcement, when the lamina bundles do not bend or fracture due to inter laminar cracks being less than a ply thickness.

The following are the disadvantages of catastrophic failure in the design of crashworthy structures.

- Catastrophic failure is characterized by a sudden increase in load to a peak value followed by a low post failure load. As a result of this the actual magnitude of energy absorbed is much less and the peak load is too high to prevent injury to the passengers.
- Structures designed to react to loads produced by catastrophically failing energy absorbers are heavier than structures designed to react to loads produced by progressively failing energy absorbers.

1.3.2 Progressive Failure Modes

Progressive failure can be achieved by providing a trigger at one end of the tube. A trigger is a stress concentrator that causes failure to initiate at a specific location within the structure. From there on, the failure, in a controlled predictable manner, progresses through the body at the loading speed. A trigger reduces the initial load peak that accompanies failure initiation followed by stable collapse. The most widely used method of triggering is to chamfer one end of the tube. A number of other trigger geometries such as bevels, grooves and holes are also in use.

The following are the advantages of progressive failure in the design of crashworthy structures.

- The energy absorbed in progressive crushing is larger than the energy absorbed in catastrophic failure.
- A structure designed to react to loads produced by progressively failing energy absorbers are lighter than structures designed to react to loads produced by catastrophically failing energy absorbers.

Below are the 4 characteristic types of progressive crushing modes.

1.3.2.1 Transverse Shearing or Fragmentation Mode

- The fragmentation mode is characterized by a wedge shaped laminate cross section with one or multiple short inter laminar and longitudinal cracks that form partial lamina bundles. Please see Figure 2.
- Brittle fiber reinforcement tubes exhibit this crushing mode.
- The main energy absorption mechanisms is fracturing of lamina bundles

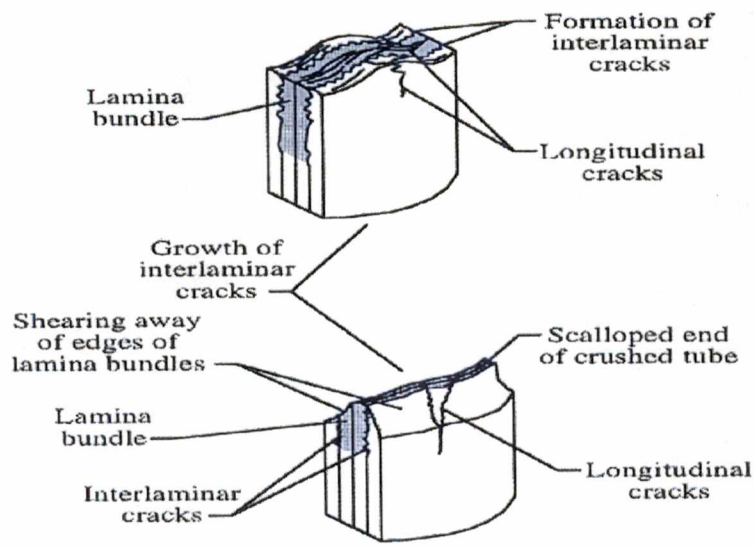

Figure 2. Fragmentation Crushing Mode [51].

- When fragmentation occurs, the length of the longitudinal and inter laminar cracks are less than that of the lamina.
- Mechanisms like inter laminar crack growth and lamina bundles control the crushing process for fragmentation.

1.3.2.2 Lamina Bending or Splaying Mode

- Very long inter laminar, intra laminar, and parallel to fiber cracks characterizes the splaying mode. The lamina bundles do not fracture. Please see Figure 3.
- Brittle fiber reinforcement tubes exhibit this crushing mode.
- The main energy absorbing mechanism is matrix crack growth. Two secondary energy absorption mechanisms related to friction occur in tubes that exhibit splaying mode.
- Mechanisms like inter laminar; intra laminar and parallel to fiber crack growth control the crushing process for splaying.

1.3.2.3 Brittle Fracturing

- The brittle fracturing crushing mode is a combination of fragmentation and splaying crushing modes. Please see Figure 4.
- This crushing mode is exhibited by brittle fiber reinforcement tubes
- The main energy absorption mechanism is fracturing of lamina bundles.
- When brittle fracturing occurs, the lengths of the inter laminar cracks are between 1 and 10 laminate thickness.

1.3.2.4 Local Buckling or Progressive Folding

- The progressive folding mode is characterized by the formation of local buckles. Please see Figure 5.

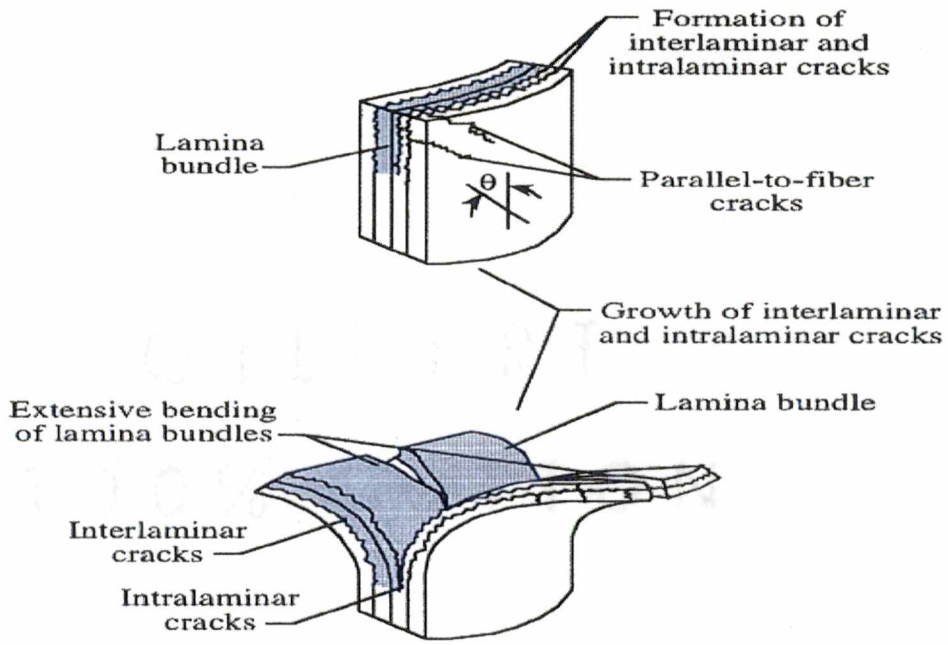

Figure 3. Splaying Crushing Mode [51]

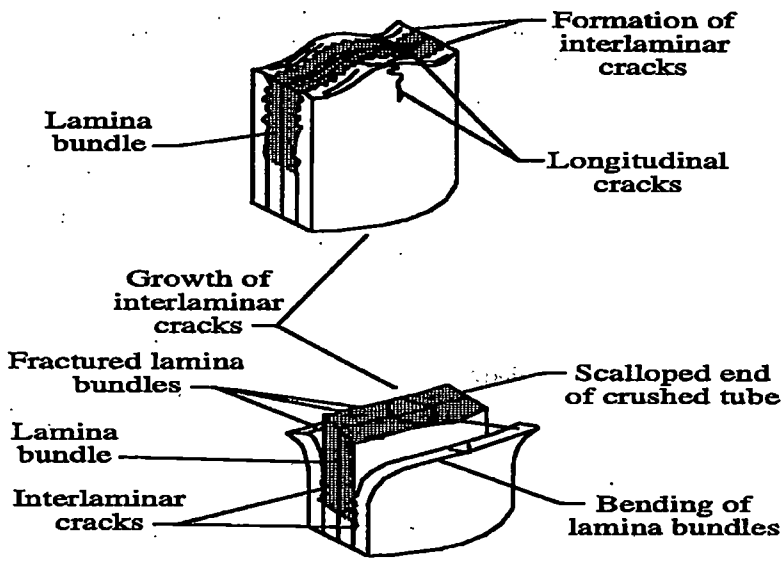

Figure 4. Brittle Fracturing Crushing Mode [51].

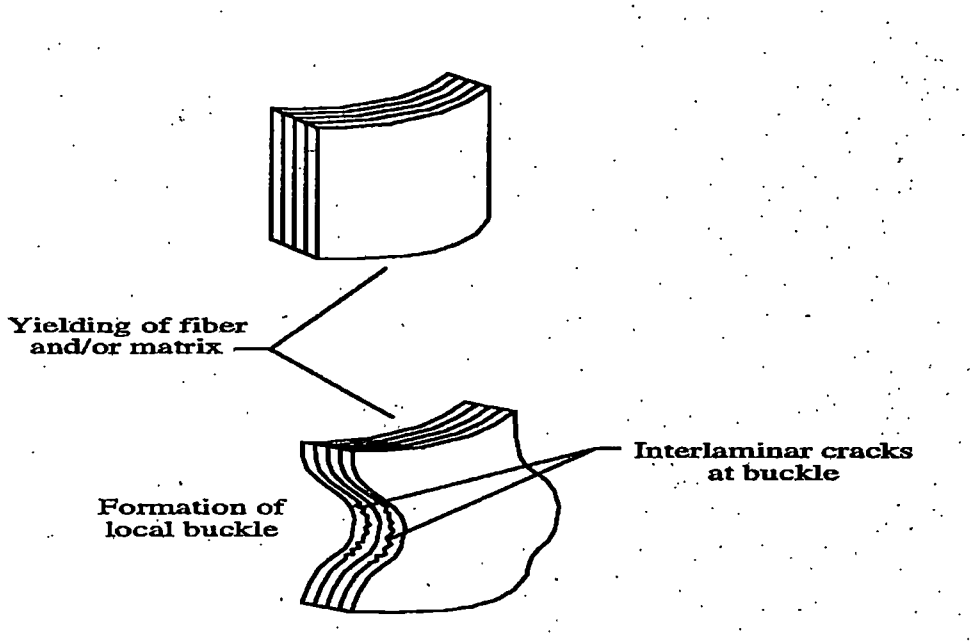

Figure 5. Progressive Folding Crushing Mode [51]

- This mode is exhibited by both brittle and ductile fiber reinforced composite material.
- Mechanisms like plastic yielding of the fiber and/or matrix control the crushing process for progressive folding.

1.4 Calculation of Specific Energy Absorption SEA

Specific energy absorption, SEA, is defined as the energy absorbed per unit mass of material. Figure 6 is a typical load displacement curve obtained from progressive crushing of a composite tube specimen. The area under the load-displacement curve is

$$W = \int_0^{S_b} P dS \qquad \text{Eq. (2)}$$

where W is the total energy absorbed in crushing of the composite tube specimen. A more characteristic property of progressive crushing mode is

$$W = \int_{S_i}^{S_b} P dS = \overline{P}(S_b - S_i) \qquad \text{Eq. (3)}$$

where S_b and S_i are the crush distances as indicated in Figure 6 and $\overline{P}$ is the mean crush load. The specific energy absorption capability, SEA, of a composite material defined as the energy absorbed per unit mass of material is given by

$$SEA = \frac{W}{m} \qquad \text{Eq. (4)}$$

where m is the mass of the composite material.

Combining the above two equations one has

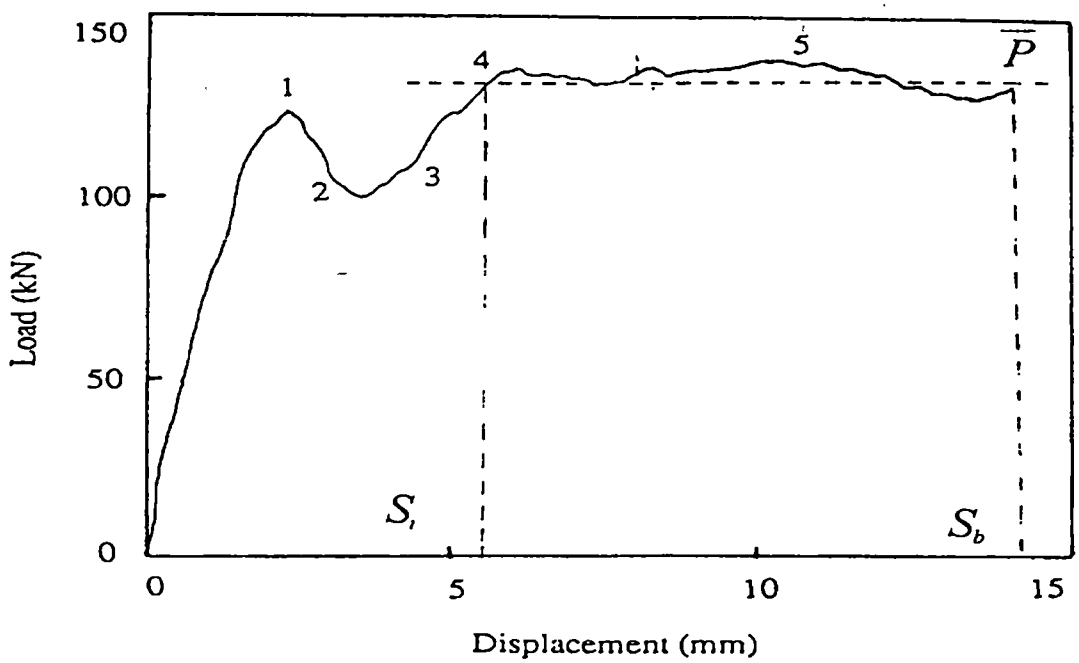

Figure 6. Typical Load Displacement Curve for a Progressively Crushed Composite Tube [35].

$$SEA = \frac{W}{m} = \frac{\overline{P}(S_b - S_i)}{V\rho} \qquad \text{Eq. (5)}$$

where V is the volume of the crushed portion of the composite tube specimen and ρ is the density of the composite material. One can also write

$$SEA = \frac{W}{m} = \frac{\overline{P}(S_b - S_i)}{V\rho} = \frac{\overline{P}(S_b - S_i)}{AL\rho} \qquad \text{Eq. (6)}$$

where A and L are the cross sectional area and length of the crushed portion of the composite tube specimen respectively.

$$SEA = \frac{\overline{P}(S_b - S_i)}{AL\rho} = \frac{\overline{P}S_b}{AL\rho} \qquad \text{Eq. (7)}$$

if S_i is much less than S_b. The ratio (S_b / L) = K is a measure of the capability of the composite tube. Substituting (S_b / L) = K in the above equation one has

$$SEA = \frac{\overline{P}K}{A\rho} = \frac{\overline{\sigma}K}{\rho} \qquad \text{Eq. (8)}$$

where $\overline{\sigma}$ is the mean crush stress. In the case of polymer composites it is rather difficult to determine a specific value for the mean crush load, $\overline{P}$, from the load displacement curve cause more often than not the magnitude of the load varies erratically with the displacement. A common procedure followed for calculating the energy absorbed, W, by polymer composites is to just determine the area under the whole load displacement curve.

1.5 Literature Survey

Several researchers have conducted research on the energy absorption capability of composite materials. Axi-symmetrical tubes, because they are easy to fabricate and close to the geometry of the actual crash worthy structures, have been used

to carry out much of the experimental work on the energy absorption of composite materials. This survey focuses on the experimental work conducted on axi-symmetric tubes. The composite tubes can be designed to absorb impact energy in a controlled manner by providing a trigger to initiate progressive crushing. A trigger is a stress concentrator that causes failure to initiate at a specific location within the structure. From there on, the failure, in a controlled predictable manner, progresses through the body at the loading speed. The most widely used method of triggering is to chamfer one end of the tube. A number of other trigger geometry such as bevels, grooves and holes are also in use.

The energy absorption characteristics of a crashworthy composite structure can be tailored by controlling various parameters like fiber type, matrix type, fiber architecture, specimen geometry, process conditions, fiber volume fraction and testing speed. In this survey care has been taken to group the various research activities that have been conducted to understand the effect of a particular parameter on the energy absorption capability of a composite material.

Table 2 provides a summary view of the range of SEA and G_{IC} values for materials that have been tested. Table 2 ranges over many parameters namely fiber type, matrix type, fiber orientation, specimen dimension, fiber volume fraction, processing conditions, test speed and trigger. Hence one ends up with this large range of values for the specific energy absorption, SEA, and inter laminar fracture toughness, G_{IC}. An exhaustively designed set of experiments to determine the effect of one parameter upon another for a particular composite material would be the square of the number of parameters. Considerable work needs to be done to meet this requirement.

Table 2. Specific Energy Absorption SEA, and Inter Laminar Fracture Toughness G_{IC}, Values of Materials That Have Been Tested.

Material	**Specific Energy Absorption SEA (kJ/kg)**	**Inter Laminar Fracture Toughness G_{IC} (kJ/m^2)**	**Spec.**
Carbon/PEEK	180 Ref. [22]	1.56 - 2.4 Ref. [22]	
Carbon/PEI		1.0 - 1.2 Ref. [19, 20]	
Carbon/PI		0.8 - 0.9 Ref. [19, 20]	
Unidirectional Graphite/ J polymer		2.02 Ref. [20]	
Unidirectional Graphite/Epoxy	53 Ref. [22]	0.21 - 0.26 Ref. [20]	
Unidirectional Graphite/Polyphenylene sulfide		1.37 Ref. [20]	

Table 2 continued.

Unidirectional Graphite/polysulfone		1.13 Ref. [20]	
Knitted Carbon Fiber Fabric/Epoxy	85 Ref. [38, 47, 39, 48, 49]		Carbon fiber volume fraction:22.5%
Braided Glass Fiber Fabric/Epoxy	70 Ref. [50]		Specimen has I cross section with fiber volume fraction 60%
Carbon Fiber/PEEK	226 Ref. [37]		Fibers aligned parallel to the tube axis, rapidly cooled

Table 2 continued.

Carbon Fiber/PEEK	197 Ref. [37]		Fibers aligned parallel to the tube axis, gradually and slow cooled
S. M. C	39 Ref. [40]		13% fiber volume fraction
S. M. C	54 Ref. [40]		18% fiber volume fraction
Pultruded Glass Fiber Reinforced Vinyl ester Resin Tubes	58 Ref. [43]		Bevel trigger, 25*3.1 section size (mm) Initial Vel:0.00021 m/sec

Table 2 continued.

Pultruded Glass Fiber Reinforced Polyester Resin Tubes	41 Ref. [43]		Bevel trigger, 25*3.1 section size (mm) Initial Vel:0.00021 m/sec
Pultruded Glass Fiber Reinforced Vinyl ester Resin Tubes	68 Ref. [43]		Tulip trigger, 25*3.1 section size (mm) Initial Vel:0.00021 m/sec
Pultruded Glass Fiber Reinforced Polyester Resin Tubes	39 Ref. [43]		Tulip trigger, 25*25*3.1 section size (mm) Initial Vel:0.00021 m/sec

Table 2 continued.

Glass Fiber/Polyester Resin Tubes	50 Ref. [8]		Winding angle: 65^0 Crushed at 0.2 mm/sec
Carbon Fiber/Epoxy	110 Ref. [22]		Ratio of hoop to axial fibers of 1 to 3
Glass Fiber Reinforced Thermosetting Resin Composites	50 – 80 Ref. [22]		
Carbon/Epoxy	53 Ref. [22]		Fiber architecture: $\pm 45^0$
Carbon/PEEK	127 Ref. [22]		Fiber architecture: $\pm 30^0$
Graphite-Glass/Epoxy	44 Ref. [4]		Orientation: $[0_{Gr}/\pm 45_{Gl}]$, number of plies:6

Table 2 continued.

Graphite-Kevlar/Epoxy	51 Ref. [4]		Orientation: $[0_{Gr}/\pm45_K]$, number of plies:6
Kevlar-Graphite/Epoxy	35 Ref. [4]		Orientation: $[0_K/\pm45_{Gr}]$, number of plies:6
6061 Aluminum	78 Ref. [4]		Diameter: 2.54 cm
6061 Aluminum	89 Ref. [4]		Diameter: 3.81cm
Glass/Epoxy	31 Ref. [4]		Orientation $[0/\pm\theta]$, $15^0<\theta<45^0$
Glass/Epoxy	47 Ref. [4]		Orientation $[0/\pm\theta]$, $60^0<\theta<90^0$
Kevlar/Epoxy	32 Ref. [4]		Orientation $[0/\pm\theta]$, $\theta=45^0$

Table 2 continued.

Graphite/Epoxy	45 Ref. [4]		Orientation [0/±θ], $\theta=45^0$
Glass cloth/Epoxy	60 Ref. [38]		Mandrel trigger
Glass cloth/Epoxy	62 Ref. [38]		Chamfer trigger
Mono Layer Epoxy Composite Tube With Knitted Carbon Fiber Fabric Reinforcement	25 Ref. [38]		15.75 volume % of fibers. Warp tested tubes
Mono Layer Epoxy Composite Tube With Knitted Carbon Fiber Fabric Reinforcement	15 Ref. [38]		15.75 volume % of fibers. Weft tested tubes
Double Layer Epoxy Composite Tube With Knitted Carbon Fiber Fabric Reinforcement	85 Ref. [38]		22.5 volume % of fibers. Weft tested tubes

Table 2 continued.

Graphite/Epoxy	80 Ref. [15]		0/90 orientation
Glass/Epoxy	60 Ref. [15]		0/90 orientation
Kevlar/Epoxy	63 Ref. [15]		45/45 orientation
Glass Fiber/Polyester Protrusion	38 Ref. [15]		Circular protrusion
Glass Fiber/Polyester Protrusion	20 Ref. [15]		Square protrusion
Graphite/Epoxy	65 Ref. [15]		At Temperatur e = 100 ^{0}C
Glass/Epoxy	40 Ref. [15]		At Temperatur e = 100 ^{0}C
Glass Fiber/Polyester Protrusion	25 Ref. [15]		At Temperatur e = 100 ^{0}C

Table 2 continued.

Graphite/Epoxy	70 Ref. [15]		Compression Rate 10^4 inches/min t/D = 0.035
Glass/epoxy	55 Ref. [15]		Compression Rate 10^4 inches/min t/D = 0.07
Kevlar/Epoxy	14 Ref. [15]		D/t ratio = 25 Inside tube diameter = 3.81 cm, orientation of the fiber $[\pm]_N$
Graphite/Epoxy	63 Ref. [44]		Crushing speed : 10 m/sec Orientation $[\pm 75]_3$.

Table 2 continued.

Kevlar/Epoxy	38 Ref. [44]		Crushing speed : 10 m/sec Orientation $[\pm 75]_3$

Abbreviations used in the Table 2:

- Spec.: Specifications
- PEEK: polyetheretherkeetone.
- PEI: polyetherimide.
- PI: polyimide.
- J polymer: A semi-crystalline polyamide copolymer resin.
- SMC: Sheet-molding compounds based on polyester resins and glass fibers.
- Ref.: Reference.
- kJ: Unit of energy in kilo Joules.
- kg: Unit of mass in kilograms.
- m: Unit of length in meters.
- Vel: Velocity.
- mm: millimeters.
- SEA: Specific energy absorption defined as the energy absorbed per unit mass of material.
- G_{IC}: Inter laminar fracture toughness.

Table 3 provides a summary view of the various composite materials that have been researched to understand the effect of a particular parameter on its energy absorption capability. One can see from Table 3 that the energy absorption capabilities of carbon, glass and kevlar fibers have been investigated the most. Epoxy, polyetheretherkeetone, polyester and vinyl ester are the matrices whose energy absorption capability has been most extensively studied. The succeeding paragraphs report the detailed findings of the various individual studies.

1.5.1 The Effect of Reinforcing Fiber on the Energy Absorption Capability of a Composite Material

The type of reinforcing fiber used in a composite material determines to a very large extent its energy absorption characteristics. The important findings are:

a) Decrease in the density of fiber causes an increase in energy absorption capability of the fiber-reinforced tubes.

b) Higher the strain to failure of the fiber, greater the energy absorption capabilities of the fiber reinforced tubes.

c) When the fiber reinforced tubes crush in similar modes, changes in the fiber stiffness affect the energy absorption capability less than fiber failure strain.

Farley [2, 3, 4, 5, 6], ***Thornton*** and ***Edwards*** [7] and ***Hull*** [8, 9] observed that glass and carbon fiber reinforced thermoset tubes progressively crush in fragmentation and splaying modes. Aramid (Kevlar and Dyneema) fiber reinforced thermoset tubes, on the other hand, crush by a progressive folding mode [2, 10]. Similar results were got when ***Schmuesser*** and ***Wickliffe*** [11] performed impact and static

Table 3. List of Composite Materials Investigated.

Composite Studied	Fiber Type	Matrix Type	Fiber Orientation	Tube Geometry	Testing Speed	Cooling Rate	Fiber Volume Fraction
Kevlar/ Epoxy	X Ref. [11, 4, 5, 15 17]		X Ref. [2]	X Ref. [7, 3, 27, 26, 34]	X Ref. [4, 15, 44, 42, 43, 45]		
Carbon/ Epoxy	X Ref. [11, 2, 4, 5, 15, 16]	X Ref. [22, 21]	X Ref. [2, 8, 10, 23]	X Ref. [7, 3, 27, 26, 28, 36 34, 29]	X Ref. [4, 15, 44, 42, 43, 39]		X Ref. [2, 38, 39, 23]
Glass/ Epoxy	X Ref. [11, 5, 15]		X Ref. [2, 8, 23]	X Ref. [7, 26, 28, 32, 33, 30, 31]	X Ref. [4, 15, 43, 39]		X Ref. [32, 39]

Table 3 continued.

Carbon/ PEEK	X Ref. [12]	X Ref. [18, 22, 21]	X Ref. [18]	X Ref. [30,35]		X Ref. [37]	
Glass/ PEEK	X Ref. [12]						
Carbon/ PEI		X Ref. [18, 21]	X Ref. [18]				
Carbon/ PI		X Ref. [18, 21]	X Ref. [18]				
Carbon/ PAS		X Ref. [18, 21]	X Ref. [18]				
Glass/ Poly-ester		X Ref. [21]	X Ref. [8, 25]	X Ref. [31]	X Ref. [43, 47]		X Ref. [40]
Glass/ Vinyl ester				X Ref. [31]	X Ref. [43]		

Table 3 continued.

Abbreviations used in the Table 3.

- PEEK: polyetheretherkeetone.
- PEI: polyetherimide.
- PI: polyimide.
- PAS: polyarylsulfone
- Ref.: Reference

compression tests on graphite/epoxy, kevlar/epoxy and glass/epoxy composite tube specimens respectively. The graphite/epoxy and glass/epoxy angle-ply tubes exhibited brittle failure modes consisting of fiber splitting and ply delamination, whereas the kevlar/epoxy angle-ply tubes collapsed in an accordion buckling mode. The lower strain to failure of the glass and carbon fibers, which fail at about 1% strain, compared to aramid fibers, which fail at about 8% strain attributes to this difference in behavior. Results of static crushing tests of graphite reinforced composite tubes conducted by ***Farley*** [5] to study the effects of fiber and matrix strain failure on energy absorption helped in drawing the following conclusion: To obtain the maximum energy absorption from a particular fiber, the matrix material in the composite must have a greater strain at failure than the fiber. The graphite/epoxy tubes had specific energy absorption values greater than that of Kevlar/epoxy and glass/epoxy tubes having similar ply constructions. This is attributed to the lower density of carbon fibers compared to glass and kevlar fibers. The theoretical density of carbon is 2.1 g/cm^3. But the actual density of carbon fibers ranges from 1.3 g/cm^3 to 1.9 g/cm^3, which is lower than the theoretical value. This is because in the act of creating the fiber, voids are also generated which causes a decrease in the density of the fibers. Since the difference in energy absorption and crush morphology are attributed to the differences in fiber properties ***Hamada***, ***Ramakrishna***, ***Sato*** and ***Maekawa*** [12] investigated PEEK matrix composite tubes reinforced with AS4 carbon fiber, IM7 carbon fiber and S2 glass fiber respectively. The fibers were aligned parallel to tube axis, i.e. $\theta = 0^o$. The tubes crushed progressively by the splaying mode. The S2/PEEK tubes displayed approximately 20% lower specific energy absorption than the AS4/PEEK and IM7/PEEK tubes though the mean crush stress of S2/PEEK tubes is

comparable to that of AS4/PEEK and IM7/PEEK tubes. This is a direct result of the lower density of carbon fiber reinforced materials than the glass reinforced material, since the specific energy absorption is defined as the ratio of the mean crush stress and density of the composite. Despite AS4 carbon fibers being more ductile than the IM7 carbon fibers, both AS4/PEEK and IM7/PEEK tubes displayed similar specific energies. Hence they concluded, unlike the thermoset tubes, the fiber failure strain has little effect on the energy absorption of the thermoplastic tubes, as the fiber failure strain is much smaller than that of the thermoplastic matrix. Epoxy composite tubes reinforced with low failure strain Thornel-300 carbon fibers and intermediate failure strain Hercules AS-4 carbon fibers was investigated by ***Farley*** [2]. He observed that the tubes having greater energy absorption properties were the ones reinforced with fibers having higher strain to failure. ***Farley*** and ***Jones*** [13] established the modes of crushing and the controlling mechanisms on continuous fiber-reinforced composite tubes. They suggested that the crushing response of the composite tubes could be categorized into three basic modes: transverse shearing, lamina bending, and local buckling. The mechanical properties of the constituent materials and the structure of the specimen influence the mechanisms that control these different crushing modes. In addition, they presented an analysis procedure that can be used to determine the qualitative change in the sustained crushing load due to a change in specimen material properties or geometry. The analysis procedure is similar in form to the equation of buckling load of a column on an elastic foundation. This procedure will be useful in preliminary design and in providing an insight into the crushing behavior of composite tubes. A finite element analysis was also conducted to model the crushing process of continuous-fiber-reinforced tubes by ***Farley*** et al [14].

The analysis is compared with experiments on graphite/epoxy and kevlar/epoxy tubes. The method is based upon a phenomenological mode of the crushing process and obtained a reasonable agreement between the analysis and the experiment. ***Thornton*** et al [15] examined the energy absorption capability in graphite/epoxy, kevlar/epoxy and glass/epoxy composite tubes. The composite tubes collapsed by fracture and folding mechanisms. The load/compression curves for the graphite/epoxy and glass/epoxy tubes had similar characteristics but the Kevlar/epoxy composite tubes collapsed by buckling. For Kevlar composites, the collapse started progressively under essentially a constant load until the collapse was complete, apart from a fine serrated structure superimposed upon the load curve. In addition, they showed that changes in the lay-up that increased the modulus increased the energy absorption of the tube. These tubes made from, or including Kevlar fiber, tended to collapse in an unstable mode by buckling rather than by fracture, which led to low values for specific energy absorption. The fracture collapse mechanism depends upon the geometry. ***Farley*** [4] demonstrated that graphite/epoxy tubes which failed in a brittle mode had negligible post crush integrity, where as Kevlar/epoxy tubes which failed in an accordion buckling mode similar to aluminum tubes exhibited post crush integrity. This characteristic of the kevlar/epoxy tubes can be attributed to fiber splitting and fiber plasticity affects. He observed that longitudinally oriented graphite fibers absorb more energy than longitudinally oriented kevlar or glass fibers. Static crushing tests were conducted by ***Chiu*** et al [16] on 3-D carbon/epoxy and kevlar/epoxy braided composite square tubes to investigate the energy absorption capabilities of these materials. The 3-D carbon braided composite tube displayed higher specific energy absorption than the kevlar tubes. This revealed that carbon tubes in crush

tests are capable of absorbing more energy. However, the kevlar tubes demonstrated good post-crush structural integrity. Another study by ***Chiu*** et al [17] revealed similar results as above where the specific energy absorption of the 3-D braided carbon/epoxy composite square tube was 24% higher than that of the 3- braided kevlar/epoxy composite square tube.

To visualize how much of specific energy absorption, SEA, is really attributable to fiber type, please refer to Table 4.

1.5.2 The Effect of the Matrix on the Energy Absorption Capability of a Composite Material

The following comments tell us about what was found with respect to matrix type:

a) Higher inter laminar fracture toughness, (G_{IC}), of the thermoplastic matrix material causes an increase in energy absorption capability of the composite material.

b) An increase in matrix failure strain causes greater energy absorption capabilities in brittle fiber reinforcements. Conversely, the energy absorption in ductile fiber reinforcements decreases with increasing matrix failure strain.

c) Changes in matrix stiffness have very little effect on the energy absorption capability of composite materials with ductile fiber reinforcement.

d) Further studies are essential to understand clearly the role of

Table 4. Effect of Fiber on Specific Energy Absorption SEA (kJ/kg)

Matrix Material: polyetheretherkeetone, fibers are aligned parallel to the tube axis.

Fiber Material	**Specific Energy Absorption SEA (kJ/kg)**	**Reference**
AS4 Carbon	194	[12]
IM7 Carbon	202	[12]
S2 Glass	143	[12]

thermosetting resin matrices in the energy absorption capability of the composite material.

Carbon fiber reinforced composite tubes with different kinds of thermoplastic matrices were studied by ***Ramakrishna*** et al [18]. Among all types of tubes investigated carbon fiber/PEEK tubes exhibited the highest specific energy owing to its higher fracture toughness (1.6 ~ 2.4 kJ/m^2). These were in comparison to that of carbon fiber/PEI (1.0 ~ 1.2 kJ/m^2) and carbon fiber/PI (1.0 ~ 1.2 kJ/m^2) composite materials [19, 20]. The carbon fiber/PAS tubes displayed the lowest energy absorption capability. The specific energy of thermoplastic tubes follow the order PAS< PI< PEI< PEEK. In a similar study ***Satoh*** et al [21] investigated the energy absorption of carbon/polyetherimide (C/PEI), carbon/polyimide (C/PI), carbon/polyarylsulfone (C/PAS), carbon/polyetheretherkeetone (C/PEEK), and compared it with that carbon/epoxy and glass/polyester. Carbon/thermoplastic tubes demonstrated superior energy absorbing capabilities (SEA = 128 ~ 194 kJ/kg) than carbon/epoxy (SEA = 110 kJ/kg) or glass/polyester (SEA = 80 kJ/kg) structures. Carbon/PEEK crushed progressively and recorded a specific energy absorption value of 194 kJ/kg. The energy absorption capability of carbon/epoxy and carbon/PEEK composite tubes made from unidirectional prepreg materials was investigated by ***Hamada*** et al [22] by conducting axial compressive tests on them. The superior energy absorption capability of carbon fiber/PEEK tubes (180 kJ/ Kg) is attributed to the higher inter laminar fracture toughness, (G_{IC}), of the thermoplastic PEEK matrix composite (1.56 to 2.4 kJ/m^2). The carbon/epoxy tube having an inter laminar fracture toughness in the range 0.12 to 0.18 kJ/m^2 absorbed only 53 kJ/Kg specific energy. ***Farley*** [6] based upon observation and a

general understanding of the crushing process concluded the following: The energy absorption of materials that fails by transverse shearing or brittle fracturing is little affected by matrix stiffness. However, materials that fail by lamina bending can be more significantly affected by matrix stiffness. A change in matrix stiffness can cause brittle fiber composites to fail in a different mode. However, changes in matrix stiffness have very little effect on the energy absorption of ductile fiber reinforcements.

To visualize how much of specific energy absorption, SEA, and inter laminar fracture toughness, G_{IC}, is really assignable to matrix type, please refer to Table 5 and Table 6 respectively.

1.5.3 The Effect of Fiber Architecture on the Energy Absorption Capability of a Composite Material

The following comments tell us what was found with respect to fiber orientation.

The fiber orientations that enhance the energy absorption capability of the composite material requires them to:

a) Increase the number of fractured fibers.

b) Increase the material deformation.

c) Increase the axial stiffness of the composite material.

d) Increase the lateral support to the axial fibers.

Work by ***Farley*** [2] on glass/epoxy, carbon/epoxy and Kevlar/epoxy composite tubes with fiber architecture $[0\pm\theta]_4$, where θ varied from 0° to 90°, showed significant differences in the energy absorption trends for these materials. The difference in trends can be explained by examination of crushing modes. The specific energy of the

Table 5. Effect of Matrix on Specific Energy Absorption SEA (kJ/kg).

Fiber type: Carbon, axial compression at a constant rate of 1 mm/min, fiber orientation: 0° to the axis of the tube.

Matrix Material	**Specific Energy Absorption SEA (kJ/kg)**	**Reference**
Polyetheretherkeetone	194	[21]
Polyetherimide	155	[21]
Polyimide	131	[21]
Polyarylsulfone	128	[21]
Epoxy	110	[21]

Table 6. Effect of Matrix on Inter-Laminar Fracture Toughness G_{IC} (kJ/m^2).

Fiber Type: Unidirectional carbon (AS-4) fiber, fiber volume fraction: 60%.

Matrix Material	**Inter-laminar Fracture Toughness G_{IC} (kJ/m^2)**	**Reference**
Polyetheretherkeetone	1.6	[19]
Polyphenylenesulfide	0.9	[19]
Polyetherimide	1.2	[19]
Epoxy	0.2	[19]

glass/epoxy and kevlar/epoxy tubes remained constant with increasing θ up to 45° and above this value it increased. This trend is not consistent with the general mechanical response of composites. The glass/epoxy and kevlar/epoxy specimen crushed in a lamina bending and local buckling mode respectively. This increase in energy is attributed to the increased lateral support to the axial fibers with increasing θ. On the other hand, the specific energy of the carbon/epoxy tubes initially decreased with increasing θ up to 45° and then remained constant. The carbon/epoxy specimens crushed in brittle fracturing mode. This initial decrease in the energy absorption is attributed to the reduction in axial stiffness of the composite material with increasing θ. ***Farley*** and ***Jones*** [23] in a later study quasi-statically crushed carbon/epoxy and glass/epoxy tube specimens with fiber architecture $[0\pm\theta]_S$, to determine the influence of ply orientation on the energy absorption capability. As θ increases, the energy absorption capability of the carbon/epoxy tube decreases nonlinearly. The crushing mode is primarily brittle fracture. The energy absorption capability of the glass/epoxy tube increases nonlinearly with θ. The crushing mode of the glass/epoxy tube is lamina bending. ***Hull*** [8, 24] studied the effect of fiber arrangement on progressive crushing in carbon fiber/epoxy unidirectional laminate tubes, woven glass cloth/epoxy tubes, filament-wound angle ply glass fiber/polyester tubes and in plane random chopped glass fiber polyester tubes. The filament wound glass/polyester tubes were made by conventional filament winding with winding angles ϕ between $\pm 35^{o}$ and 90°. Here ϕ is the angle between the direction and the longitudinal axis of the tube. The tube had 4 layers of fibers and the volume fraction of the fibers was about 0.45. The tubes were 50 mm in diameter and the wall thickness was about 3-4 mm. All tests were

conducted at a crushing speed of 0.2 mm/s with a servo-hydraulic testing machine having a maximum static loading capacity of 180 kN. A 300 mm stroke was used for all the compression tests. The specific energy increased with increasing ϕ up to $\pm 65^{\circ}$ and after that it decreased. Hence the maximum value of specific energy occurred at $\phi = \pm 65^{\circ}$ and there was systematic changes in the load displacement curves and crush zone morphology with winding angle ϕ. These changes in crush zone morphology (when $\phi = \pm 35^{\circ}$ to $\pm 55^{\circ}$, tubes crush in splaying mode and when $\phi > \pm 65^{\circ}$, tubes crush in fragmentation mode) cause the changes in specific energy. The tube with axially aligned fibers showed very little progressive crushing before complete failure by the formation and growth of longitudinal cracks. ***Hamada*** et al [10] studied the effect of fiber architecture on the energy absorption capability of hybrid composite tubes reinforced with both carbon and dyneema (polyethylene) fibers. The resin fibers used were that of epoxy. It was seen that the energy absorption capability decreased with increasing fiber orientation with respect to the longitudinal axis of the tube. ***Berry*** [25] investigated woven glass fabric/polyester tubes by varying the angle of the lay-up. The energy absorption of the tubes with the warp and weft directions at 45° to the tube axis is observed to be 30% less than that for similar tubes with warp and weft direction parallel to the axial (0°) and hoop (90°) directions respectively. This increase in the energy absorption is due to more material deformation and fracture in the case of the latter tubes. Carbon fiber reinforced composite tubes with different thermoplastic matrices: polyetheretherkeetone (PEEK), polyetherimide (PEI), polyimide (PI) and polyarylsulfone (PAS) were studied by ***Ramakrishna*** et al [18]. Fiber orientations of 0°, $\pm 5^{\circ}$, $\pm 10^{\circ}$, $\pm 15^{\circ}$, $\pm 20^{\circ}$, $\pm 25^{\circ}$ and $\pm 30^{\circ}$ with respect to the axis of the tube were used. The specific energy absorption capability

of the progressively crushed tubes was found to be a function of the θ value. In general, as θ increases, the length of the longitudinal cracks decrease. This is due to the increase of fracture toughness with increasing θ. This improved fracture toughness offers more resistance to the crack growth process, thus resulting in an increased specific energy absorption value for the composite material. Microfracture processes such as fiber fracture and frond (splaying of the fiber matrix structure) splits were observed to increase with increasing θ. Hence it was concluded that this increase in microfracture processes is what causes an increase in the total energy absorbed.

To visualize how much of specific energy absorption, SEA, is really assignable to fiber architecture, please refer to Table 7.

1.5.4 The Effect of Geometry of the Specimen on the Energy Absorption Capability of a Composite Material

The important findings are:

a) It is crush zone fracture mechanisms that determine the overall energy absorption capability of a composite material and tube dimensions largely influence these fracture mechanisms.

b) The specific energy absorption, SEA, follows the order: circular> square> rectangle, for a given fiber lay up and tube geometry.

Thornton and ***Edwards*** [7] conducted a study investigating the geometrical effects in energy absorption of circular, square, and rectangular cross section tubes. Although the range of geometrical parameters was large, the actual number of test conditions was limited. The limited number of tests made it difficult to precisely define certain trends. They concluded that for a given fiber lay up and tube geometry, the

Table 7. Effect of Fiber architecture on Specific Energy Absorption SEA (kJ/kg).

Carbon fiber polyetheretherkeetone tubes, outer diameter: 55 mm, wall thickness: 2.65 mm, length: 55 mm, trigger: 45° chamfer.

Fiber Architecture	**Specific Energy Absorption SEA (kJ/kg)**	**Reference**
0°	194.1	[18]
±5°	205.3	[18]
±10°	225.3	[18]
±15°	226.8	[18]
±20°	202.3	[18]
±25°	181.1	[18]

Carbon fiber polyetherimide tubes, outer diameter: 55 mm, wall thickness: 2.65 mm, length: 55 mm, trigger: 45° chamfer.

Fiber Architecture	**Specific Energy Absorption SEA (kJ/kg)**	**Reference**
0°	155.4	[18]
±5°	162.4	[18]
±10°	187.9	[18]
±15°	167.5	[18]
±20°	162.4	[18]
±25°	135.6	[18]

Table 7 continued.

Carbon fiber polyimide tubes, outer diameter: 55 mm, wall thickness: 2.65 mm, length: 55 mm, trigger: 45° chamfer.

Fiber Architecture	**Specific Energy Absorption SEA (kJ/kg)**	**Reference**
0°	131.4	[18]
±5°	151.1	[18]
±10°	160.7	[18]
±15°	162.3	[18]
±20°	167.9	[18]

Carbon fiber polyarylsulfone tubes, outer diameter: 55 mm, wall thickness: 2.65 mm, length: 55 mm, trigger: 45° chamfer.

Fiber Architecture	**Specific Energy Absorption SEA (kJ/kg)**	**Reference**
0°	128.1	[18]
±5°	148.4	[18]
±10°	147.2	[18]
±15°	147.7	[18]

specific energy follow the order, circular > square > rectangle. Specimens were fabricated with graphite, Kevlar, glass, and hybrid combinations of these reinforcements in an epoxy matrix. Tape and fabric prepregs were utilized to fabricate tubes with ply orientations of [±45] and [0/90]. The tubes made from glass or graphite fibers collapsed by fracture mode. Stable collapse with high-energy absorption occurred over a critical range of tube geometry. Kevlar and Kevlar hybrid composites were found to generally be unsuitable energy absorbers because of unstable crushing behavior, resulting in large undulations in the crushing load. These results are in contrast with results for crushable beams reported by ***Farley*** [26]. ***Farley*** found Kevlar reinforced beams to consistently crush in a stable manner and graphite tubes of reference [7] exhibited combined brittle fracturing and lamina bending crushing modes. Crushing loads of glass and graphite composite tubes were more uniform than the crushing loads for the Kevlar reinforced composite tubes. ***Farley*** [3] investigated the geometrical scalability of graphite/epoxy (Gr/E) and Kevlar/epoxy (K/E) $[\pm 45]_N$ tubes by quasi-statically crush testing them. This ply orientation is used in typical sub floor beam structures. In that study, the tube inside diameter varied between 1.27 cm to 10.16 cm, the number of plies (N) varied between 2 and 24 and the tube inside diameter to wall thickness ratio (D/t) varied between 1.4 and 125. All circular cross section graphite/epoxy tubes exhibited a progressive brittle fracturing mode. All kevlar/epoxy tubes when crushed exhibited the characteristic local buckling crushing mode. The buckle wavelength varied with tube diameter. Tube inside diameter to wall thickness ratio (D/t) was determined to significantly affect the energy absorption capability of the composite materials. Energy absorption was found to be a decreasing nonlinear function of tube D/t ratio. That is, a reduction in D/t ratio results in

an increase in the specific energy. This increase is due to reduction in inter laminar cracking in the crush region of the tube. Kevlar/epoxy tubes are reported to exhibit similar trends. Their energy absorption capability is geometrically scalable but that of graphite/epoxy tubes are not. ***Farley*** and ***Jones*** [27] reported carbon/epoxy and kevlar/epoxy tubes with elliptical cross section to also exhibit similar trends. When statically crushed, the energy absorption capability was determined to be a decreasing nonlinear function of the ratio of tube internal diameter to wall thickness (D/t). ***Thornton*** et al [28] studied the effect of tube dimensions. It was found that carbon/epoxy exhibited large changes in their energy absorption characteristics with a range of values of tube diameter (D), tube wall thickness (t) and (D/t) ratio. Relative density, defined as the ratio of the volume of the tube to that of a solid of the same external dimensions, was varied in the range 0.01 to 1.0. The tube crush length is unstable and the critical size of the tube is dependent on the fiber type and fiber architecture, below a relative density value of 0.025 for carbon/epoxy and 0.045 for glass/epoxy. The specific energy is essentially independent of tube dimensions for the tubes that crushed in a stable manner. A total of 28 graphite/epoxy flat plate specimens and 6 graphite/epoxy tube specimens were crushed by ***Dubey*** and ***Vizzini*** [29] under quasi-static conditions to provide a basis for the comparison of the measured energy absorbency of these two geometries. The tube and flat plate specimens crushed in similar failure modes with the flat plates absorbing 12% less energy per unit mass. It is concluded that flat specimens can be used as a lower cost alternative to tube specimens or in test programs requiring simpler geometry. Glass cloth/epoxy tubes and carbon fiber/PEEK tubes with cross sectional shapes full circle, three quarter circle, half circle and quarter circle were investigated by ***Hamada*** et al [30].

Two types of glass cloth/epoxy composite tubes were tested. One type of tubes contained glass cloth treated with an aminosilane-coupling agent and the other type of tubes used glass cloth treated with acrylsilane-coupling agent. Quasi-static tests were performed by axial compression between two flat platens. All the specimens crushed progressively from the chamfered end. One of the important results of this study is that the mode of progressive crushing is independent of the cross sectional shape of the composite tubes. The constituent materials in the composite mainly determine it. The aminosilane-treated glass cloth/epoxy specimens, owing to the good interfacial bonding of its fiber to the resin matrix, crush by splaying mode whereas the acrylsilane-treated glass cloth/epoxy specimens, due to the presence of higher frictional forces in the crush zone, crush by fragmentation mode. The carbon/PEEK specimens crush progressively by the splaying mode, mainly due to the orientation of carbon fibers parallel to the tube axis. Another important result of this study was that the cross-sectional shape of the tube influences the specific energy absorption capability of composite tubes. In the case of the glass cloth/epoxy specimens, the specific energy decreased by 20% with the change in tube cross section from full circle to quarter circle. The specific energy of carbon fiber/PEEK tube specimens decreased by only 5% for the same change in cross sectional shape. Square tubes, circular tubes and circular cones made of glass fiber, polyester or vinylester resin were tested by ***Mamalis*** et al [31] under static and dynamic crushing conditions in a speed range of 18 - 24 m/sec. It was found that for specimens showing stable crushing, greater thickness tends to reduce the specific energy absorption, square tubes have less specific energy absorption than circular tubes, and greater cone angle results in lower specific energy absorption. ***Fairfull*** [32] and ***Fairfull*** and ***Hull*** [33] studied the effects

of specimen dimensions on the specific energy of glass cloth/epoxy tubes. Five sets of tubes with D ranging from 16 mm to 50 mm were studied. The specific energy decreased with increasing D. The specific energy, for a given D, initially increased with decreasing D/t ratio up to 5 below which, it decreased. It was concluded that there could not be a universal relationship to predict energy absorption capability because the reason for this variation of energy could not be clearly identified. Static crushing tests were conducted by ***Farley*** [34] on graphite/epoxy and kevlar/epoxy square cross section tubes to study the influence of specimen geometry on the energy absorption capability and scalability of composite materials. Tube ply orientations were $[\pm 45]_N$. The square cross section tube widths were between 1.27 cm and 7.62 cm. The width to wall thickness ratios (w/t) was between 6 and 125. These tube geometry and materials are representative of helicopter sub floor beam structure applications. The tube inside width to wall thickness ratio (w/t) was determined to affect the energy absorption capability of composite materials. The energy absorption capabilities of graphite/epoxy and kevlar/epoxy tubes are non-linear functions of tube ratios (w/t). Energy absorption generally increased with decreasing w/t ratio. For graphite/epoxy tubes having w/t ratios in the range of 20 and 50, changes in crushing mode occurred, resulting in a decrease in energy absorption capability as w/t ratio decreased. Both graphite/epoxy tubes and kevlar/epoxy tubes crushed in a progressive and stable manner. All graphite/epoxy tubes exhibited a lamina bending crushing mode while kevlar/epoxy tubes exhibited a local buckling crushing mode. The test results suggest that kevlar/epoxy tubes are geometrically scalable where as that of graphite/epoxy are not. ***Hamada*** and ***Ramakrishna*** [35] studied the crushing performance of carbon fiber/PEEK tubes with different thickness t and diameter D

values. When t is in the range of 2mm and 3mm all the types of tube display their highest specific energies. With increasing t up to this critical range, the specific energy increased, above which it decreased. Changes in the crush zone morphology were the cause of specific energy variation. Microfracture processes in the crush zone varied with the thickness t though the tubes crushed progressively by splaying mode. With increasing t up to critical range both the frond splits and fractured fibers increased. It was confirmed after the above investigation that in the case of thermoplastic composite tubes, the energy absorption characteristics are mainly influenced by the absolute value of t rather than the (D/t) ratio. Static energy absorption tests were conducted on different geometry of 6 ply T300/934, graphite/epoxy sine web by ***Hanagud*** et al [36]. They reported that the sine web composite material exhibit good energy absorption capabilities when crushed in the web direction. They demonstrated that the energy absorption efficiency of the web specimens with 180° included angle is equal to corresponding tube specimens. By reducing the included angle of the sine web from 90°-60°, the crushing mode changed abruptly from stable progressive crushing to unstable global buckling.

To visualize how much of specific energy absorption, SEA, is really assignable to specimen geometry, please refer to Table 8.

1.5.5 The Effect of Processing Conditions on the Energy Absorption Capability of a Composite Material

The following comments tell us what was found with respect to processing conditions:

a) The cause for variation in energy absorption capability with cooling rate

Table 8. Effect of Specimen Geometry on Specific Energy Absorption SEA (kJ/kg).

Aminosilane treated glass cloth/epoxy tubes, fiber volume fraction: 43%, internal diameter: 50 mm, wall thickness: 2.5 mm, trigger: 45° chamfer.

Sectional Shape	**Specific Energy Absorption SEA (kJ/kg)**	**Reference**
Full Circle	66.6	[30]
¾ Circle	60.6	[30]
½ Circle	60.1	[30]
¼ Circle	53.5	[30]

Acrylsilane treated glass cloth/epoxy tubes, fiber volume fraction: 43%, internal diameter: 50 mm, wall thickness: 2.5 mm, trigger: 45° chamfer.

Sectional shape	**Specific Energy Absorption SEA (kJ/kg)**	**Reference**
Full Circle	53.0	[30]
¾ Circle	41.3	[30]
½ Circle	41.8	[30]
¼ Circle	40.7	[30]

Table 8 continued.

Carbon fiber/polyetheretherkeetone, fiber volume fraction: 65%, outer diameter: 55 mm, wall thickness: 2.65 mm, length: 55 mm, trigger: 45° chamfer.

Sectional shape	**Specific Energy Absorption SEA (kJ/kg)**	**Reference**
Full Circle	194.1	[30]
¾ Circle	192.9	[30]
½ Circle	190.6	[30]
¼ Circle	187.1	[30]

Carbon fiber/polyetheretherkeetone composite tubes.

Diameter D (mm)	**Thickness t (mm)**	**t/D**	**Specific Energy Absorption SEA (kJ/kg)**	**Reference**
35.5	*0.80*	0.023	171.7	[35]
35.5	*1.04*	0.029	172.3	[35]
35.5	*2.20*	0.062	205.9	[35]
35.5	*3.44*	0.097	207.1	[35]
35.5	*4.58*	0.130	154.9	[35]
35.5	*6.33*	0.178	140.6	[35]
55.0	*1.09*	0.020	189.0	[35]

Table 8 continued.

55.0	*2.09*	0.038	218.4	[35]
55.0	*2.66*	0.048	228.3	[35]
55.0	*5.27*	0.096	186.7	[35]
55.0	*6.43*	0.117	186.0	[35]
55.0	*10.47*	0.190	113.7	[35]
96.0	*1.64*	0.017	194.0	[35]
96.0	*1.91*	0.020	215.2	[35]
96.0	*2.14*	0.022	195.6	[35]
96.0	*5.68*	0.059	156.9	[35]
96.0	*10.54*	0.110	147.8	[35]

is the cooling rate dependence of fracture toughness of thermoplastic composite materials. Fracture toughness increases with an increase in cooling rate and hence causes an increase in the energy absorption capability of the thermoplastic composite material.

b) There has been no systematic study reported in the literature on the effect of processing conditions on the energy absorption characteristics of thermoset composite tubes.

Hamada et al [37] investigated the effect of processing conditions on the energy absorption capabilities of carbon fiber/PEEK composite tubes. The thermoplastic tubes having the carbon fibers aligned parallel to the tube axis were fabricated using a thermally expandable PTFE mandrel technique. Three cooling rates were used: rapid cooling by immersion in chilled water (95.5°C/min.), gradual cooling in air (8.2°C/min.) and slow cooling in the oven with heater switched off (0.7°C/min). All the tubes crush progressively by splaying mode when quasi-statically crush tested. The rapidly cooled tubes have specific energy absorption of 226 kJ/kg, the highest recorded for any material, which is 15% higher than the 197 kJ/kg, the specific energy absorbed by the gradually and slow cooled tubes.

To visualize how much of specific energy absorption, SEA, is really assignable to processing conditions, please refer to Table 9.

1.5.6 The Effect of Fiber Volume Fraction on the Energy Absorption Capability of a Composite Material

The following comments tell us what was found with respect to fiber volume fraction:

Table 9. Effect of Processing Conditions on Specific Energy Absorption. SEA (kJ/kg).

Carbon fiber/polyetheretherkeetone composite tube with fibers aligned parallel to the tube axis, tubes tested at a constant speed of 1 mm/min, outer diameter: 55 mm, wall thickness: 2.7 mm for rapidly cooled tubes and 2.8 mm for gradual and slow cooled tubes, trigger: 45° chamfer.

Processing Condition	**Specific Energy Absorption SEA (kJ/kg)**	**Reference**
Rapidly Cooled (95.5 °C/min)	226	[37]
Gradually Cooled (8.2 °C/min)	197	[37]
Slow Cooled (0.7 °C/min)	196	[37]

a) The effect of fiber volume fraction on the energy absorption has been less extensively studied.

b) It is not always true, as one would normally think that an increase in the fiber content would necessarily improve the specific energy absorption capability of a composite material. A possible explanation for the above statement is that as the fiber volume fraction increases, the volume of the matrix between the fibers decrease. This causes an increase in the matrix density. This further leads to a decrease in the inter laminar strength of the composite. As inter laminar strength decreases, inter laminar cracks form at lower loads, resulting in a reduction in the energy absorption capability. So what actually determines the changes in the energy absorption trends with fiber content is the crushing response of the composite material.

Ramakrishna and ***Hull*** [38] investigated the specific energy absorption capability of knitted carbon fiber-fabric/epoxy tubes tested under axial compressive load. Tubes with lower fiber content crushed irregularly where as progressive crushing took place in tubes having fiber content above 15%. The specific energy absorption capability increased with fiber content. ***Ramakrishna*** [39], a couple of years later, again investigated the effect of fiber content on the specific energy absorption capability of knitted carbon fiber fabric/epoxy and knitted glass fiber fabric/epoxy composite tubes. The specific energy of both types of composite tubes increased with increasing fiber content. One possible explanation for this is that a higher tube loading is associated with generation of larger surfaces due to fiber/matrix debonding which results in increased

energy absorption capability. Contrary to the above finding, ***Farley*** [2] reported a decrease in specific energy of carbon fiber/epoxy composite material with the increase in fiber volume fraction from 40% to 70%. The decrease in specific energy is attributed to the decrease in inter laminar shear strength of the composite with increasing fiber content. In a later study ***Farley*** and ***Jones*** [29] again investigated carbon/epoxy composite tubes with fiber volume fractions in the range 40% to 55% to get similar results. They reported some specimens exhibit a large decrease in energy absorption capability with increasing fiber volume fraction, where as other specimens exhibit a slight decrease. Hence, it should be concluded that an increase in the fiber content might not always necessarily improve the specific energy absorption capability. The crushing response is what determines the energy absorption trends. Work by ***Hull*** and ***Snowdon*** [40] on sheet molding compounds based on polyester resins and glass fibers (SMC) showed an increase in specific energy with an increase in fiber volume fraction. The tube specimens made by hot press molding of SMC were subjected to axial compression at speeds up to 15 m/sec (33 mph). ***Thornton*** et al [41] investigated glass fiber/vinyl ester rods with fiber volume fraction in the range 10% to 50%. He reported an increase in specific energy with increase in fiber volume fraction. ***Wess*** et al [32] reported an increase in specific energy of glass fiber/epoxy composite material with increasing fiber volume fraction from 10 to 50% above which it remained constant.

1.5.7 The Effect of Testing Speed on the Energy Absorption Capability of a Composite Material

The important findings are:

a) The energy absorption capability is a function of testing speed when the mechanical response of the crushing mechanisms is a function of strain rate. The rate at which the structure is loaded has an effect on both the material's behavior and also the structural response of the target.

b) The strain energy absorbing capabilities of the fibers and the geometrical configuration of the target are very important factors that determine the impact resistance of composites at low rates of strain.

c) The strain energy absorbing capabilities of the fibers and the geometrical configuration of the structure is less important at very high rates of strain since the structure responds in a local mode. What is important is the magnitude of energy dissipated in delamination, debonding and fiber pull out.

Bannerman and ***Kindervater*** [42] while investigating carbon/epoxy and Kevlar/epoxy tubular and beam specimens reported an increase in energy absorption with crushing speed. ***Thornton*** [15] reported very little change in the specific energy absorption of 0/90 graphite/epoxy, kevlar/epoxy and glass/epoxy composite tubes over a wide range of compression rates (10^{-1} to $2*10^{4}$ inches/min). ***Thornton*** [43] also investigated the energy absorption behavior of Pultruded glass/polyester and glass/vinyl ester tubes in the crushing speed range from 2.1 X 10^{-4} m/s to 15 m/s. He reported a 10% decrease with increasing test speed in the case of glass/vinyl ester tubes and a 20%

increase in energy absorption in the case of glass/polyester tubes. This can be attributed to the higher tensile strength and modulus of the vinylester. ***Thornton*** et al [41] later investigated glass fiber/vinyl ester rods with testing speed in the range 0.13 to 2.54 mm/min. The specific energy was seen to increase essentially linearly with log (testing rate). ***Farley*** [4] investigated kevlar/epoxy, carbon/epoxy, and glass/epoxy and composite tubes with fiber architecture $[0\pm\theta]_4$ at speeds of quasi-static and 7.6 m/sec impact and found specific energy to be independent of crushing speed. When ***Farley*** [44] investigated carbon/epoxy and kevlar/epoxy tubes with $[\pm\theta]_3$ fiber architecture he found a 35% increase in specific energy with the change in the crushing condition from quasi-static to impact. The magnitude of effects of crushing speed on specific energy was determined to be a function of the mechanism that controls the crushing process. Static and dynamic crushing tests in a speed range of 18 – 24 m/sec were conducted by ***Mamalis*** et al [31] on three different composite materials. Two of the composite materials consisted of fiberglass and vinyl ester resins. The third was made up of fiberglass and polyester resin. The specimens under investigation had different geometry: square, circular and circular cone. The specific energy of thin walled circular conical specimen made of polyester resin and random chopped strand mat of glass fiber were reduced by 35% under a crushing speed of about 21 m/sec. It was hence concluded that crush speed interacts with cone angle and wall thickness of the specimen. Reduction in specific energy caused by the increase of crush speed becomes more significant when wall thickness or cone angle is larger. However the crushing speed was not observed to have a significant effect on the specific energy absorption of thin walled circular or square tubes made of the three kinds of composite materials. In another investigation

Kindervater [45] observed little difference between the quasi-static and dynamic energy absorption of kevlar/epoxy tubes. ***Schmueser*** and ***Wickliffe*** [43] reported a decrease of up to 30% in energy absorption of impacted carbon/epoxy, glass/epoxy and Kevlar/epoxy tubes with fiber architecture $[0_2/\pm45]_s$, as compared to static test results. ***Ramakrishna*** [39] studied the effect of testing speed on the specific energy absorption capability of knitted glass fiber/epoxy and knitted carbon fiber fabric/epoxy composite tubes. The specific energy of both types of composite tubes decreased by 20% with change in testing condition from quasi-static to impact. This is attributed to the decrease in fracture toughness, (G_{IC}), of composite materials with increasing test speeds. Decreased fracture toughness means less resistance to the longitudinal cracking of the tube wall and therefore lower energy absorption.

To visualize how much of specific energy absorption, SEA, is really assignable to testing speed, please refer to Table 10. Note that of the two systems reported, the SEA for the glass/polyester system goes up with an increase in the testing speed while the SEA for the glass/vinyl ester goes down with a similar increase in testing speed.

1.5 8 Summary of Findings

The effect of a particular parameter (such as fiber type, matrix type, fiber orientation, specimen geometry, processing conditions, fiber content, test speed and test temperature) on the energy absorption of a composite material is summarized below.

The density of the **reinforced fibers** has a lot to do with the energy absorption characteristics of a composite material. As the density of the fiber decreased from a higher to a lower value, the specific energy of the fiber reinforced tubes increased

Table 10. Effect of Testing Speed on Specific Energy Absorption SEA (kJ/kg).

*Section size of the test specimen: 25 mm * 3.1 mm.*

Composite	**Initial Velocity**	**Specific Energy Absorption SEA (kJ/kg)**	**Reference**
Pultruded Glass Fiber Reinforced Vinyl ester Resin Tube	$2.1 * 10^{-4}$ m/sec	57.5	[43]
	12 m/sec	53.5	
Pultruded Glass Fiber Reinforced Polyester Resin Tube	$2.1 * 10^{-4}$ m/sec	40.5	[43]
	12 m/sec	47.5	

from a lower to a higher value respectively. Tubes reinforced with fibers having higher strain to failure result in greater energy absorption properties. Changes in fiber stiffness affect energy absorption capability less than changes in fiber failure strain, provided the different materials crush in the same mode. If one is restricted to discussing the energy absorption capability of a reinforced fiber **thermoplastic matrix** material it could be concluded that higher inter laminar fracture toughness, G_{IC}, of the thermoplastic matrix material would increase the energy absorption capability of the composite material. Also an increase in matrix failure strain causes greater energy absorption capabilities in brittle fiber reinforcements. Conversely, the energy absorption in ductile fiber reinforcements decreases with increasing matrix failure strain. The role of **thermosetting resin matrices** in energy absorption is not clear and further studies are essential.

Regarding the effects of **fiber orientation** on the energy absorption capability of a composite material, the fiber orientations that enhance the energy absorption capability of the composite material requires them to:

a) Increase the number of fractured fibers.

b) Increase the material deformation.

c) Increase the axial stiffness of the composite material.

d) Increase the lateral support to the axial fibers.

Studying the effect of **tube dimensions** it can be said that the tube dimensions influence the crush zone fracture mechanism and these fracture mechanisms determine the overall energy absorption capability of the composite tubes. For a given fiber lay up and tube geometry, the specific energy follows the order, circular> square> rectangle. The **cooling rate** dependence of fracture toughness of thermoplastic

composite materials is the cause for variation in energy absorption capability with cooling rate. Fracture toughness increases with increase in cooling rate and hence causes an increase in the energy absorption capability. There has been no systematic study reported in literature on the effect of **processing conditions** on the energy absorption characteristics of thermoset composite tubes. The same could be said about the studies on the effect of **fiber volume fraction** on the energy absorption of composites. It should be noted that an increase in the fiber content might not always necessarily improve the specific energy absorption capability. As the fiber volume fraction increases, the volume of the matrix between the fibers decreases. This causes the inter laminar strength of the composite to decrease. As inter laminar strength decreases, inter laminar cracks form at lower loads, resulting in a reduction in the energy absorption capability. Also, as fiber volume fraction increases, the density of the composite increases which results in a lower energy absorption capability. Upon reviewing the literature there seems to be a lack of consensus about the influence of **test speed** on the energy absorption. However it is known that energy absorption capability is a function of testing speed when the mechanical response of the crushing mechanism is a function of strain rate. The rate at which the structure is loaded has an effect on both the material's behavior and also the structural response of the target. The strain energy absorbing capabilities of the fibers and the geometrical configuration of the target are very important to the impact resistance of composites at low rates of strain. However the strain energy absorbing capabilities of the fibers and the geometrical configuration of the structure is less important at very high rates of strain since the structure responds in a local mode. What is important is the magnitude of energy dissipated in delamination, debonding and fiber pull out.

1.5.9 The Most Efficient Crashworthy Composite Material

Carbon fiber reinforced tubes display higher strength than other fiber-reinforced tubes. Its superior specific energy absorption is a direct result of the lower density of carbon fiber reinforced materials, since energy absorption is defined as the ratio of mean crush stress and density of the composite. The energy absorption capability of the fiber reinforced thermoplastic PEEK tubes is higher than the other fiber reinforced matrix materials due to its superior inter laminar fracture toughness (1.56–2.4 kJ/m^2) compared to other matrix materials. Because of their high strains to failure, they are the only matrices presently available that allow the new intermediate modulus, high strength (and strain) carbon fibers to use this full strain potential in the composite. The PEEK resin in carbon/PEEK is believed to have three phases: an amorphous phase, a trans-crystalline growth from fiber surfaces and a sphere shaped crystal. The bond strength of the carbon fibers to the matrix is enhanced by this kind of crystallinity. Therefore one can conclude that the specific energy absorption (180 kJ/kg) of the semi crystalline 0° carbon fiber/PEEK tube should be much higher than other composite tubes. The damages they incur while absorbing energy are in very small amounts. The superior performance of carbon fiber/PEEK tubes is attributed to mainly to:

a) Higher fracture toughness of PEEK matrix composites (Carbon fiber/PEEK composites exhibit excellent static and dynamic toughness).
b) Splitting of fronds.
c) Large number of fiber fractures.
d) The PEEK matrix allows rapid repair using fusion techniques. For example, if we adopt the hot press technique, simply treating the

component to a temperature above the melting point of the matrix, reforming and cooling can reduce the impact damage.

The PEEK matrix leads to a much higher resistance to crack growth between the fibers. This ensures that the tube does not fail before the onset of progressive crushing mode. Measurements of the inter laminar Mode I fracture toughness, (G_{IC}), parallel to the fibers of the unidirectional materials gave values of G_{IC} in the range 1.56 to 2.4 kJ/m^2 for carbon fiber/PEEK.

The success of the PEEK matrix as a superior energy absorbing material suggests the high potential in thermoplastic matrix materials to be good energy absorbers. The role of a thermoplastic resin matrix in energy absorption is extensively reported in the literature. However the same cannot be said with regard to thermosetting resin matrices. Their role in energy absorption, the effect of processing conditions on their energy absorption characteristics etc. is not clear. Considering the large number of cost efficient, low temperature processing methods available to industry more work towards understanding the energy absorption characteristics of these matrices is currently needed.

1.5.10 Conclusions Reached at after Review of the Existing Literature

•Only a reasonable amount of composite is required to meet the necessary impact performance standard.

•There is no literature available on the energy absorption characteristics of chopped carbon fiber composites. Future testing demands the investigation of the progressive crush behavior of chopped fiber composite material systems.

•While conducting impact tests on a composite material, it is equally important to determine the rate of energy absorption, as it is to record the magnitude of the energy being absorbed by the specimen.

•It is important when one reports the magnitude of energy absorbed in a particular material when quasi-statically or impact tested, he also reports the speed at which the testing was done.

•Concept of coupling of different materials is in the interest of improved safety of passengers.

1.6 Rate Effects

The ability of a structure to absorb impact energy and be survivable for the occupant is called the "crash worthiness" of the structure. From this definition it is understood that an ideal crashworthy material used in a car, in the event of a crash, must do the following. One, absorb the kinetic energy of the car and two, dissipate this energy over a time frame that ensures the deceleration of the car to be less than a critical value, above which the passengers will experience irreversible brain damage. So while testing specimens in the lab to determine their crashworthiness before using them in cars one needs to measure the magnitude of the energy that it is capable of absorbing and the length of time over which this energy will be absorbed. Both the magnitude and the rate of energy absorption is characteristic to a particular material. If there were two different types of materials with similar energy absorption capabilities, the material that dissipated this energy over a longer period of time would be considered more crashworthy. So in the course of evaluating the crash worthiness of a material, measurement of time is important. The magnitude of the energy absorbed by the crash elements in a car is the

area under the load displacement curve where load is nothing but the product of the mass of the car and its deceleration after impact. The rate of energy absorption in the car is dependent on the constituent materials the car is made of.

Both quasi-static and impact testing can be carried out in the lab. Impact testing is a true simulation of the actual crash condition. The magnitude of energy absorbed by a material when impact tested and the rate at which this energy is dissipated can be used to accurately interpret the material behavior in the event of an actual crash. Here again the magnitude of energy absorbed by the specimen is the area under the load displacement curve where load is the product of the mass of the impactor and its deceleration after impact. The rate of energy transformation is solely a material property.

In quasi-static testing the tube specimen is crushed at a constant speed. Here the energy absorbed is the area under the load displacement curve. However load in this case is just the specimen's reaction to it being crushed. It does not have a deceleration term because the crushing process is taking place at a constant speed. The measurement of the time quantity is not worthwhile because one actually controls the rate of energy absorption rather than it being a material property as in the case of impact testing. Hence it is inferred that quasi-static testing is not a true simulation of the actual crash conditions. It can however be used to study the failure mechanisms that take place during the crushing of a tube.

One can conclude from the above thoughts the following: 1) While conducting impact tests on a composite material, it is equally important to determine the rate of energy transformation as it is to record the magnitude of the energy being absorbed by the specimen. 2) It is important that when one reports the magnitude of

energy absorbed by a particular material when quasi-statically or impact tested, the speed at which the testing was done be also reported. Many materials are rate sensitive and can absorb different magnitudes of energies at different testing speeds. 3) Quasi-static testing is not a true simulation of real crash conditions and is used to study the failure mechanisms that take place when composite tubes are crushed. However if a sample is progressively crushed, its load displacement curve is characterized by the load rising to some peak value followed by an initial failure and then a sustained crushing load (Mean Crush Load) that cycles about some average value suggested to be at least 75% of the peak load. Hence in this special case, the mean crush load is independent of the change in displacement and time. The magnitude of the specific energy absorbed will give a clear measure of its crash worthiness. Hence there is no need to calculate the rate of energy absorption. But not all materials when crush tested exhibit ideal progressive crushing. Therefore there is a need to measure the rate of energy absorption for these materials in addition to recording the magnitude of energy they absorb before determining their crash worthiness.

1.7 Design for Optimum Work Rate Decay

The load increases very rapidly in the initial stages of the load displacement curve for most materials undergoing crushing to some maximum value after which stable crushing takes place. Though these materials might be on the whole good energy absorbers, it is in the interest of passenger safety that the deceleration in this stage of the crash not exceed the critical range above which the passengers will experience irreversible brain damage. To safe guard the interest of the passengers but still use these high energy absorbing materials as crash elements why not couple them with other

materials which have a lower peak load but not necessarily a high energy absorption capability? This will smear the initial peak load response of the coupled material system over a wider range which in the process will lower the net initial peak load to a value that is well within the safe deceleration range that the passengers are allowed to experience. Hence by stretching the duration of energy absorption the crash worthiness of the structure has been improved. Please see Figure 7.

$$W_{Vehicle} + W_{Structure} = 0 \qquad \text{Eq. (9)}$$

This expression will always be true: The sum of the work done by the vehicle and work done by the structure is always zero. Here $W_{Vehicle}$ is the work done by the vehicle moving at a particular velocity v having a kinetic energy of 0.5 m v^2. During the crash event the structure does work to absorb this kinetic energy. It will be desirable that this energy be absorbed over a large period of time rather than in a short time duration. That is, the rate of work done by the structure is as low as possible. This can be accomplished by coupling different material types as mentioned above.

1.8 Conclusion

There are a lot of criteria, in addition to a material being crash worthy, that need to be met before one can begin the use of a particular composite as a crash energy absorber in automobiles. Some of the primary ones being, low costs involved in its manufacture, the raw materials being readily available and many more. Once a composite material is identified to meet the above necessary requirements, one ought to know the effect all the controllable parameters (like fiber arrangement, specimen geometry etc.) will have on its energy absorption capabilities, in an attempt to design the most crash worthy structure. Though in the past several researchers have investigated the

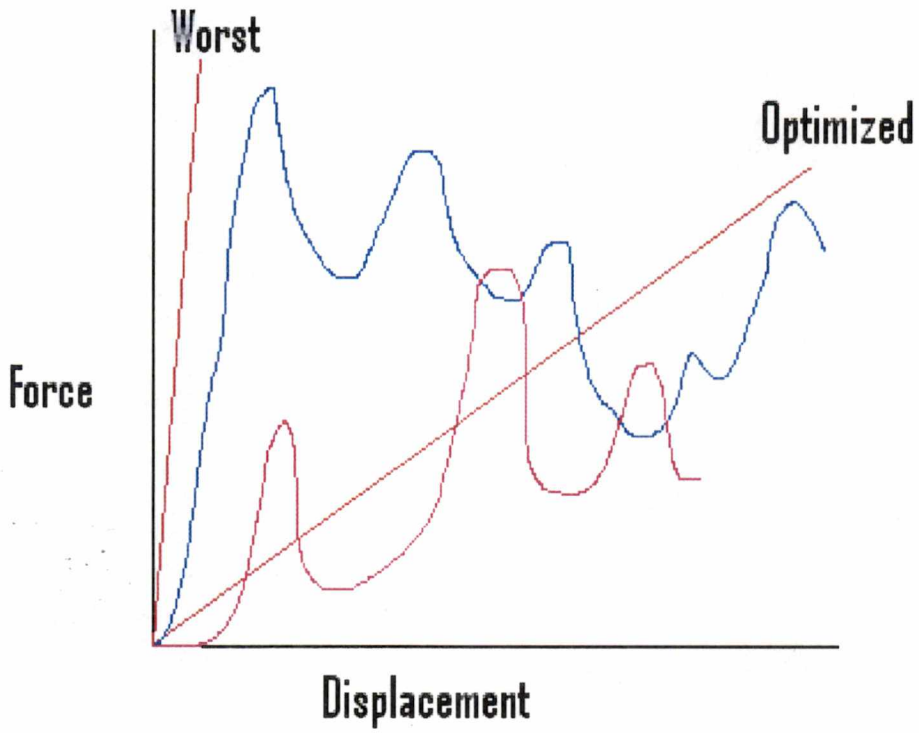

Figure 7. Design for Optimum Work Rate Decay.

energy absorption capabilities of composite materials, it is now time that we have in the literature enough data to understand the effect of all the parameters on the energy absorption characteristics of every composite material presently imaginable. It will also be of interest to create a database on the specific energy of various composite materials for the designer's reference. A lot of this experimental data can be used to support the analytical modeling efforts being conducted by several U.S. national laboratories [46].

From Table 2 one sees a range of values for the specific energy absorption, SEA, and Inter laminar fracture toughness, G_{IC}. This is because Table 2 ranges over all the parameters namely fiber type, matrix type, fiber orientation, specimen dimensions, volume fraction, processing condition, test speed and trigger. Consider Table 11 to help visualize how many experiments are needed to determine the effect of one parameter upon another.

An exhaustively designed set of experiments to determine the effect of each parameter on the energy absorption capability of the composite material, would thus be the number of parameters plus one. The number of experiments required to explore the effect of one parameter upon another, would be the square of the number of parameters. This helps to show just how complicated the task is.

Crash worthiness has been enhanced by the long standing use of seat belts and the recent introduction of air bags in the steering wheel activated by a detector in the event of a crash. Optimizing crash worthiness could be helped by the use of appropriate sensors to initiate the breaking system, adjusted to an optimized stopping capacity, in an emergency situation. This would minimize both the intensity and the extent of damage.

Table 11. A Matrix to help visualize The Number of Experiments Needed to Determine the Effect of One Parameter upon Another.

Para-meter	**1st Exp.**	**2nd Exp.**	**3rd Exp.**	**4th Exp.**	**5th Exp.**	**6th Exp.**	**7th Exp.**	**8th Exp.**	**9th Exp.**
Fiber Type	Kevlar	Carbon	kevlar	Kevlar	kevlar	kevlar	kevlar	kevlar	kevlar
Resin Type	Epoxy	Epoxy	PEEK	Epoxy	epoxy	epoxy	epoxy	epoxy	epoxy
Fiber Arch.	$[\pm 45^{o}]$	$[\pm 45^{o}]$	$[\pm 45^{o}]$	$[\pm 55^{o}]$	$[\pm 45^{o}]$	$[\pm 45^{o}]$	$[\pm 45^{o}]$	$[\pm 45^{o}]$	$[\pm 45^{o}]$
Vol. Fract.	15.7%	15.7%	15.7%	15.7%	22.7%	15.7%	15.7%	15.7%	15.7%
Proc. Cond.	Slow cooled	slow cooled	slow cooled	Slow cooled	slow cooled	rapid cooled	slow cooled	slow cooled	slow cooled
Test Speed	10 m/sec	10 m/sec	10 m/sec	10 m/sec	10 m/sec	10 m/sec	15 m/sec	10 m/sec	10 m/sec
Trigg-er	chamf.	chamf.	chamf.	Chamf.	chamf.	chamf.	chamf.	Bevel	chamf.
Spec. Dim.	D/t=2	D/t=2	D/t=2	D/t=2	D/t=2	D/t=2	D/t=2	D/t=2	D/t=5

Table 11 continued.

SEA (kJ/ kg)	80	90	70	75	76	67	78	65	78
G_{IC} (J/m^2)	1130	1150	1230	1300	1430	1234	1342	1432	1236

Chapter 2

Experimental

2.1 Objective

The primary objective was to determine the crash worthiness of chopped carbon fibers reinforced in an epoxy resin system and too see how it compared with that of other fiber resin systems like graphite/epoxy cross-ply laminates, a graphite epoxy braided material system and a glass-reinforced continuous strand mat (CSM). To meet this objective first an experimental set up was developed for discerning the deformation behavior and damage mechanisms that occur during the progressive crushing of composite materials. Quasi-static progressive crush tests were then performed on these composite plates to identify and quantify the energy absorbing mechanisms. An attempt was made to understand in great detail the effect of various material (fiber volume fraction, fiber length, fiber tow size) and test (specimen width, loading rate, profile radius, constraint condition) parameters on their energy absorption capability by varying these parameters during testing. After having identified which combination of fiber volume fraction, fiber length, fiber tow size and specimen width will yield the highest energy absorbing material, the quantity of this material needed to ensure passenger safety in a mid-size car traveling at various velocities was estimated.

2.2 Material Systems Investigated

The ACC (Automotive Composite Consortium) was interested in investigating the use of carbon and glass fibers in chopped fiber reinforced composite materials. Carbon fiber reinforced tubes display higher specific energy absorption than other fiber-reinforced tubes. This is a direct result of the lower density of the carbon

fiber thus also contributing to the lightweight of the structures they are used in. Glass fibers are cheap to buy and this makes them cost effective for automotive applications. Table 12 and Table 13 lists the physical properties of carbon and glass fibers respectively

Polyurethane and Epoxy were the resin matrices of interest to the ACC. Polyurethane was favored from its cost stand point as there are a large number of low temperature processing techniques for polyurethane resins available to the industry that makes it very cost efficient to manufacture them. Polyurethane resins, due to their low viscosity wet the fiber better thus strengthening the interfacial bonding between the matrix and reinforcement. Good interfacial bonding prevents the formation of instabilities around the fibers that cause the formation of micro cracks and initiate failure. For polyurethane resins, adjusting its molecular structure can vary the glass transition temperature Tg. The energy absorption capability of a test specimen would be greatest if its glass transition temperature is near the test temperature. This is because the viscous response time of the specimen is in tune to the rate of energy absorption near its glass transition temperature. We can therefore smear T_g over a wide range of temperature by combining polyurethanes of different molecular structures. Hence we can expect to have high-energy absorption capabilities for the composite. Epoxy on the other hand is more expensive than polyurethane but is regarded as a standard resin, which frequently finds use in most composites.

The material systems that were tested included a graphite/epoxy cross-ply laminate, a graphite epoxy braided material, a glass-reinforced continuous strand mat (CSM) and a chopped carbon fiber/epoxy resin system. The cross ply laminate was fabricated using the hand lay-up process and Akzo Fortafil Prepreg #602. There were

Table 12. The Physical Properties of Carbon Fibers.

Density	**2.1 g/cm^3**
Tensile Strength	**100 Gpa**
Tensile Modulus	**1000 Gpa**

Table 13. The physical Properties of Glass Fibers.

Density	**2.54 g/cm^3**
Tensile Strength	**2068 Mpa**
Tensile Modulus	**82 Gpa**

two plates fabricated, designated as CP#1 and CP#2, where the CP#2 plate was not adequately consolidated because of loosing vacuum pressure partially through the cure cycle. The graphite/epoxy braided specimens were fabricated using Akzo #556 carbon fiber with Ashland Hetron 922 epoxy vinyl ester. The lay up was a triaxial braid with $0/+30^{o}/-30^{o}$ fiber orientations and the panel designation was 'O'. The CSM specimens were machined from plates that were fabricated using glass-fiber reinforcement in a Baydur polyurethane resin. The chopped carbon fiber composites (CCF) were fabricated using Toray T700 carbon fiber with YLA RS-35 epoxy resin. YLA supplied the molding compound and CCS compression molded the plates. Below is the detailed procedure that was employed to make the chopped carbon fiber panels for testing.

Making of the molding compound:

1. Fiber: Upwards of 200 creels of fiber was loaded into the feed rack on the prepreg machine.
2. Resin: On a separate machine, the resin system was mixed and transformed into a film of uniform thickness.
3. Prepreg: The fiber tows were spread to a very accurate FAW (fiber aerial weight defined as the weight per unit area of the fiber) and then mated with the resin film.
4. Prepreg: The impregnated fibers were then rolled up at the end of the line.
5. Molding Compound: After a few days (These days are given for some chemical reaction to complete) the prepreg was then slit and chopped to a specified width and length.
6. Stock: The material was then freezer stored while it awaited a molding requirement.

Part molding:

7 Tooling: A master mold base was loaded into a press. A core and cavity die set was installed onto the master base. The ejector system was installed into the assembly. The heating and temperature controls were also installed into the assembly. The system was heated up and a shear edge check was performed. Finally, the tool was released, and was ready to go.

8 Charge Prep: The material charge was weighed and placed into the preheat mold.

9 Preheat: The material was preheated at 150 °F in an oven for 30 minutes.

10 Load Tool: The material was then pulled from the preheat tool and placed into the molding tool. The tool was rapidly closed to a "trigger point", where the LP pump transitions to the HP pump.

11 Pressing the Part: The process cycle then involved applying "pinch" pressure onto the material for a fixed condition of about 100 psi, for 15 to 60 seconds. The process then was automatically switched to full pressure for the full cure cycle. This was at a molding pressure of 2000 psi, for 30 minutes, at a temperature of 295 °F.

12 Ejection: The part was then ejected with a 5 point ejection system, and it was then placed in a cool down clamp fixture for about 10 minutes.

13 The edges were then deflashed and the post weight was recorded in the logbook.

It must be noted that the hand lay up process used to fabricate the graphite/epoxy cross-ply laminates is far more expensive than the above compression molding process that is used to manufacture the chopped carbon fiber epoxy panels.

2.3 Test Fixture Design

A new test fixture design was developed for determining the deformation behavior and damage mechanisms that occur during progressive crushing of composite

materials. The fixture was designed to isolate the damage modes associated with the frond formation (splaying mode) in composite tubes by testing plate geometries. The fixture can be used in conventional screw driven or hydraulically actuated load frames and is intended for quasi-static loading but may be adaptable to conducting dynamic tests with minor modifications. The design of the test fixture can accommodate different plate widths (up to 50 mm), plate thicknesses (nominally 3mm ± 1.55 mm), contact profile shapes, and contact profile constraints.

The design is a modified version of an existing test fixture used for crush testing of composite plates [52]. Features incorporated into the design include an observable crush zone, long crush length, interchangeable contact profile, frictionless roller for contact constraint, and out of plane roller supports to prevent buckling. A schematic of the test fixture is shown in Figure 8 and photos are shown in Figure 9, Figure 10, Figure 11 and Figure 12.

The primary components of the fixture:

1. Top plate
2. Base plate
3. Profile block
4. Roller plate
5. Grip plate and insert
6. Linear shaft and bearing
7. Load cell
8. Roller way

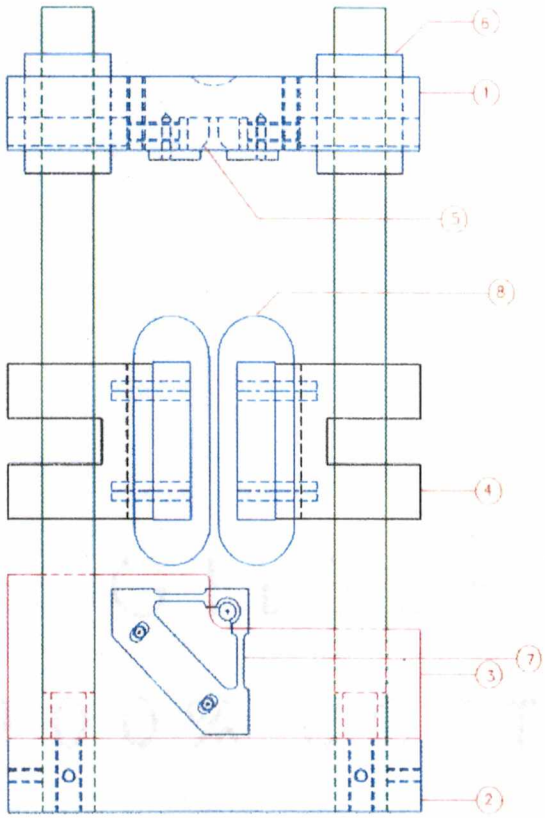

Figure 8. Schematic of Test Fixture Design.

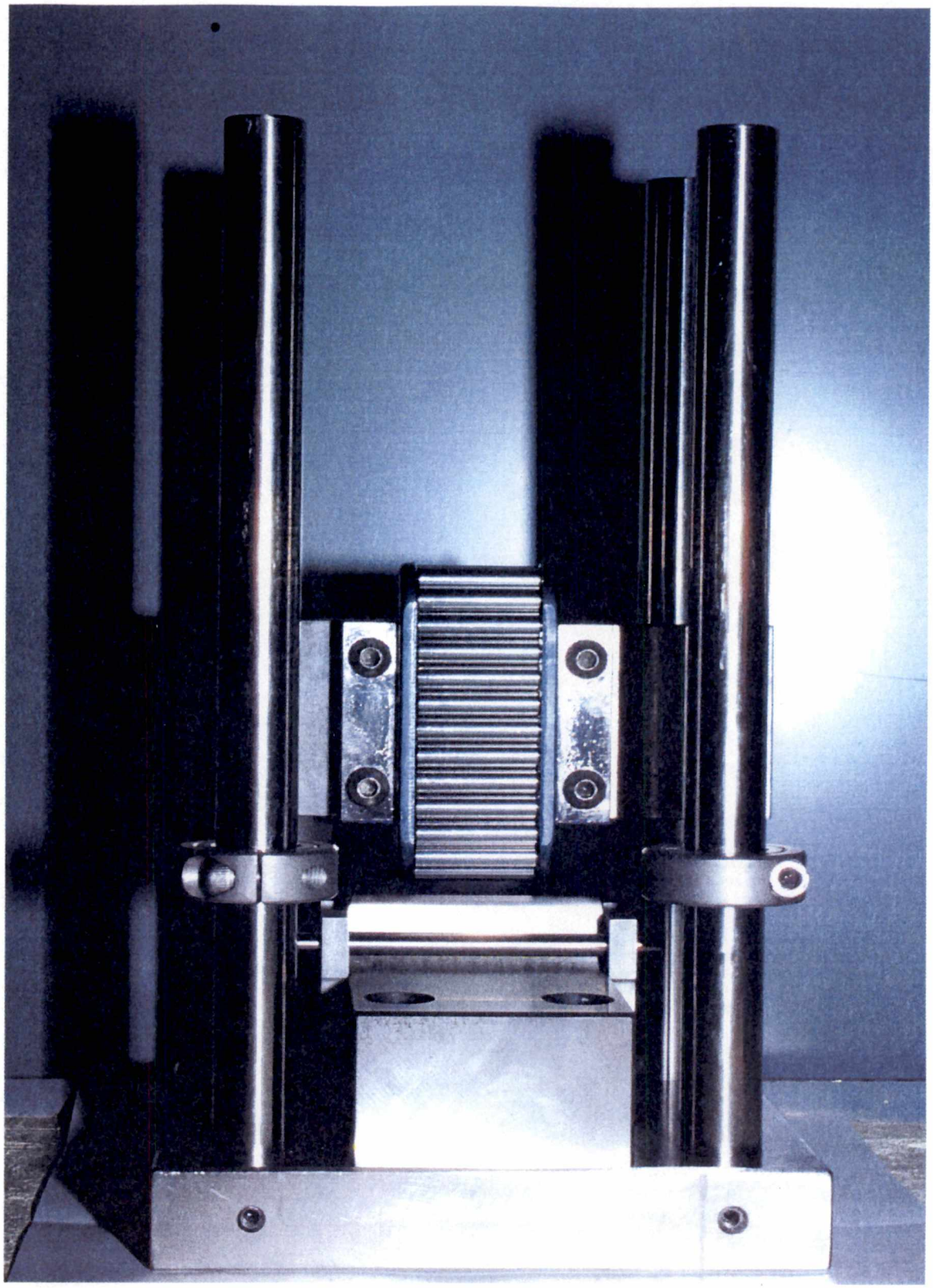

Figure 9. Roller Ways and Contact Profile Constraint — 1.

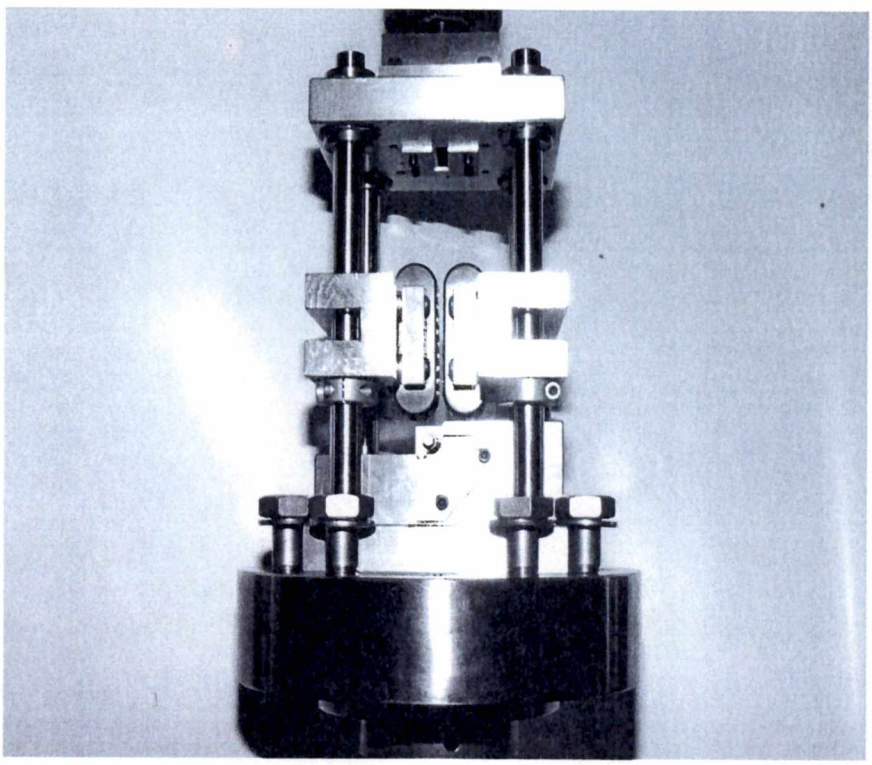

Figure 10. Test Fixture Assembly — 1.

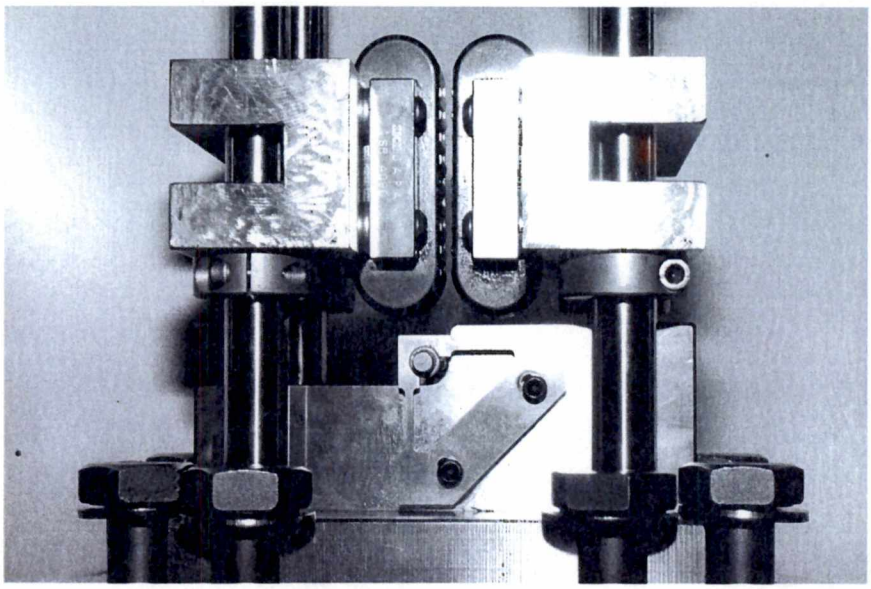

Figure 11. Roller Ways and Contact Profile Constraint — 2.

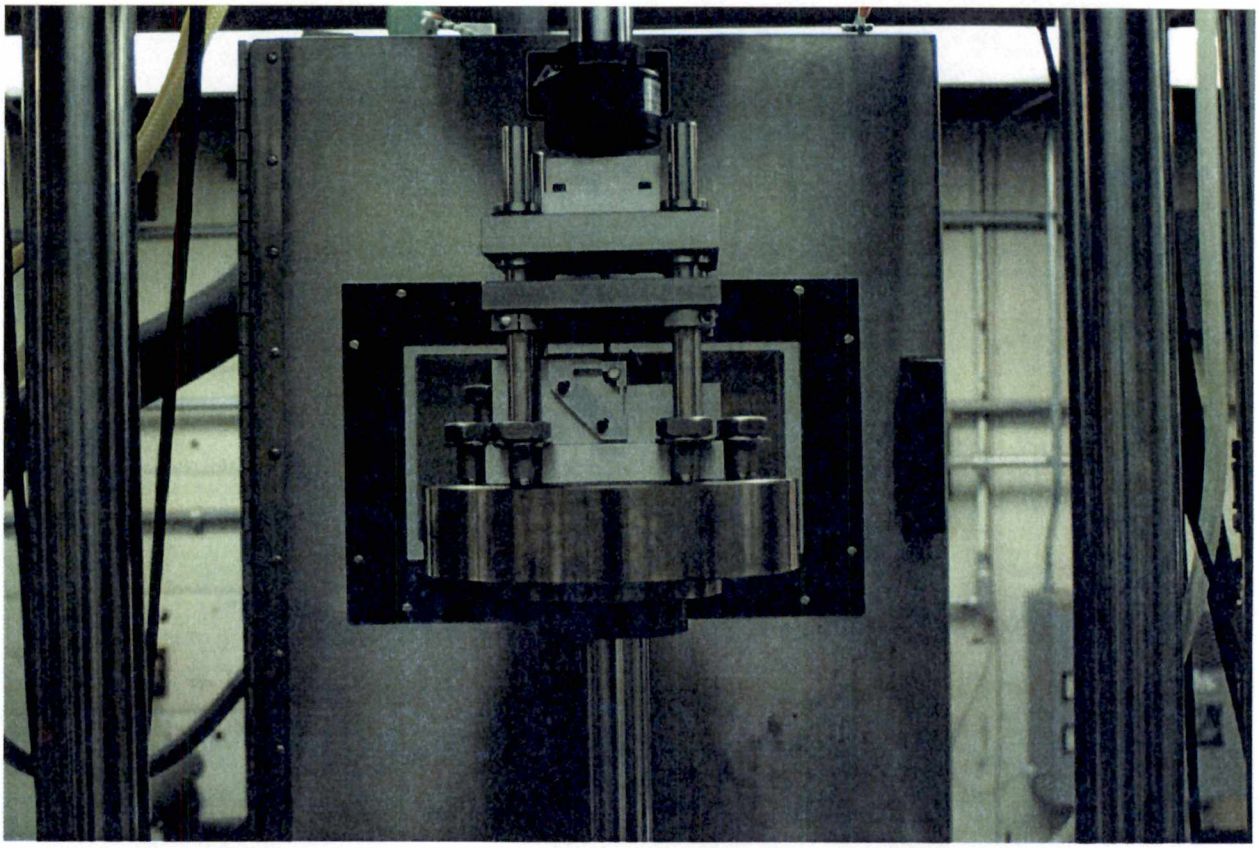

Figure 12. Test Fixture Assembly — 2.

The composite plate specimen is clamped in the top plate by the grip inserts. The specimen is the loaded in compression and crushed through the contact profile as defined by the profile block via the top plate that is connected to the load train using a shaft coupler. The top plate is displaced downward, relative to the base plate and profile block. Alignment is maintained by using four linear shafts and linear bearings. Attached to the roller plates that are positioned on the linear shafts by shaft collars are the roller ways. The roller ways are used to reduce the unsupported length of the specimen thereby preventing the specimen from buckling. The brackets on either side of the profile plate were designed to serve two functions. The first function is to provide a method of constraining the specimen to deform along the path of the contact profile. Using oil-impregnated bronze sleeve bearings in each bracket and installing a precision ground shaft that acts as a roller accomplish this. The second function is a development effort to measure the vertical and horizontal reaction forces experienced by the specimen during the deformation process. The severity of the contact profile constraint is determined by the position of the load cell brackets and is adjustable using slotted positioning holes. Please see Figure 13. Slotted holes are used throughout the test fixture design to accommodate different plate thicknesses and maintain alignment with the centerline of the load train. Below is a summary of the test fixture features.

- Modified version of existing test fixtures used for crush testing of composite plates
- Observable crush zone
- Long crush length
- Interchangeable contact profile

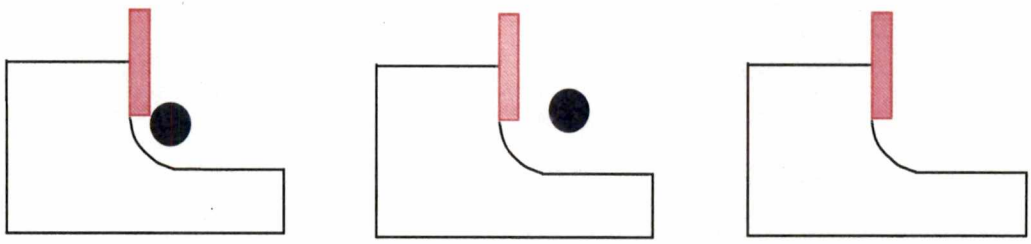

a) Tight constraint b) Loose constraint c) No constraint

Figure 13. Constraint Conditions.

- Out of plane buckling prevented by roller supports
- Frictionless roller for contact profile constraint
- Adaptable for dynamic testing
- Frictionless forces can be quantified

2.4 Variables Investigated

The fixture was designed to study the effects plate width, loading rate, profile constraint and profile shape have on the energy absorbing characteristics of composite plates. Furthermore, the objective of the profile constraint was to determine if different damage mechanisms could be activated depending on the position of the roller. An attempt was also made to understand in great detail the effect various material parameters like fiber volume fraction, fiber length and fiber tow size had on the energy absorption characteristics of chopped carbon fiber composite plates. Below is a summary of the various material and test variables that were investigated.

2.4.1 Test Variables

- Profile Radius: 0.25 and 0.5 inch
- Loading Rate: 0.2, 2, inches/min
- Constraint: None, Loose, Tight
- Plate Width: 0.5, 1, 2 inches

2.4.2 Material Variables

- Fiber and Matrix Type: Carbon/Epoxy and Glass/polyurethane
- Tow Size: 48K (300 gsm), 12K (150 gsm)
- Fiber Volume Fraction: 50%, 40%
- Fiber length: 1, 2 inches

2.5 Testing Procedure

Composite plate specimens are very cheap to fabricate and it has been observed that plate specimens progressively crush in modes very similar to the damage modes that occur during the progressive crushing of composite tubes. Practical considerations related to the cost production of the test specimens were of paramount importance in developing the test methodology to be used in the fixture.

The specimen had a nominal length of 178 mm and a width of 50mm, 25 mm or 13 mm, and a 45° chamfer was used was used as the crush initiator. A diamond cut off wheel was used to the cut the specimens off the composite panel. Please see Figure 14 and Figure 15 for a sketch of the test coupons and the composite panels from which they were cut. No coolant was used during cutting to prevent contamination of the test specimens. In some of the tests a metal push plate needed to be used to reduce the unsupported specimen length. This metal push plate was 76 mm (approximately 3 inches) in length and was bonded to the end of the test specimen using 5-minute epoxy. This called for the test specimens to be trimmed to a length of 100 mm (approximately 4 inches) so that it could accommodate the metal push plate. Please see Figure 16 and Figure 17 for a sketch of the push plates and trimmed specimens used. A loading rate of either 5.0 mm/min or 50 mm/min and a profile block of radius equal to either 6.4 mm or 12.7 mm were used through out the entire testing. Figure 18 shows an uncrushed CSM specimen attached to a steel push plate.

The MTS machine (Model 810, axial/torsional mode) used for testing had a load capacity of 50000 lbs. It was calibrated to second standard in a 5000 lbs range by MTS up to an accuracy of ±0.5%. The machine was designed with Thomson linear



Figure 14. Test Coupons.

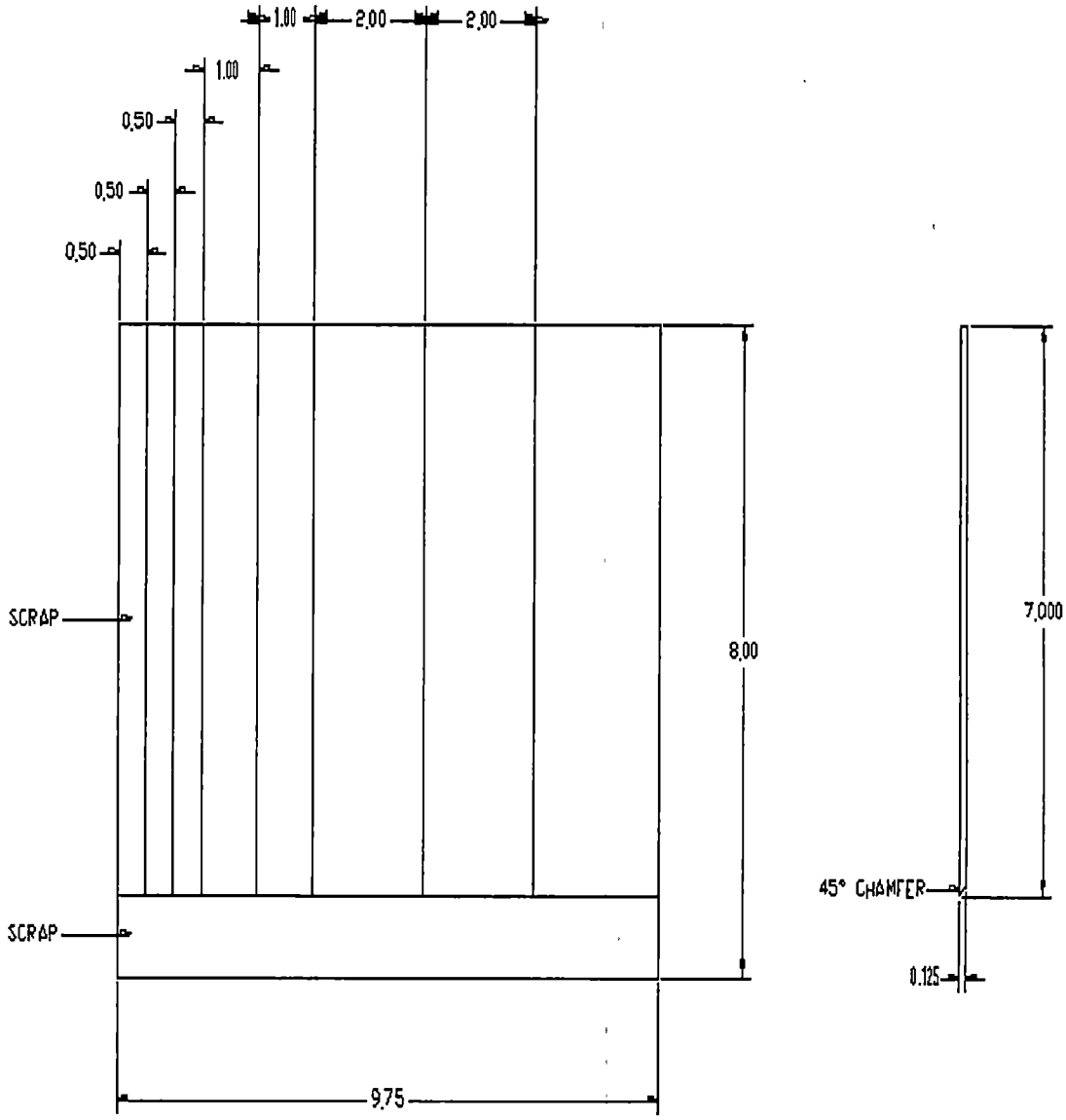

COMPOSITE PANEL

ALL DIMENSIONS ARE IN INCHES

Figure 15. Composite Panel.

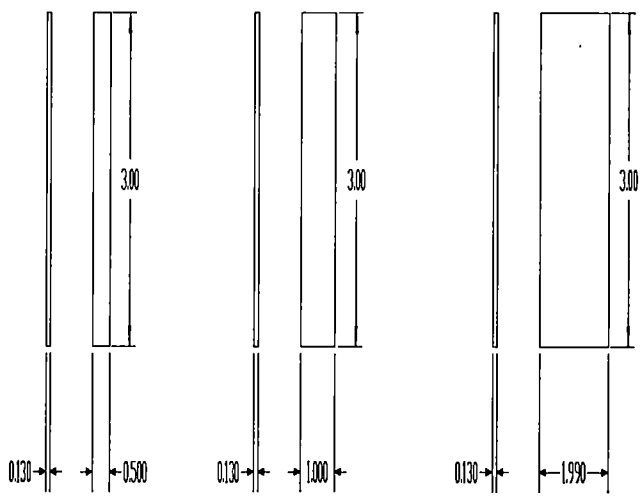

PUSH PLATES

MATERIAL: STEEL

ALL DIMENSIONS ARE IN INCHES

Figure 16. Push Plates.

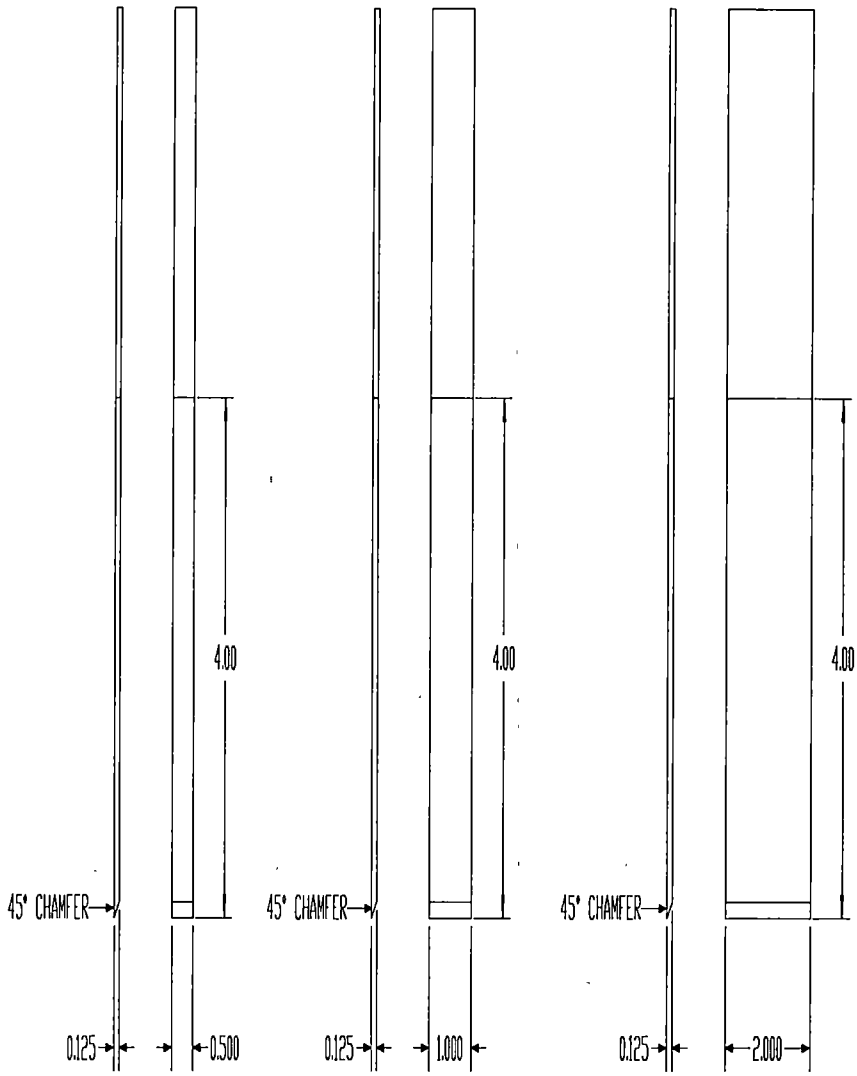

Figure 17. Trimmed Specimens.

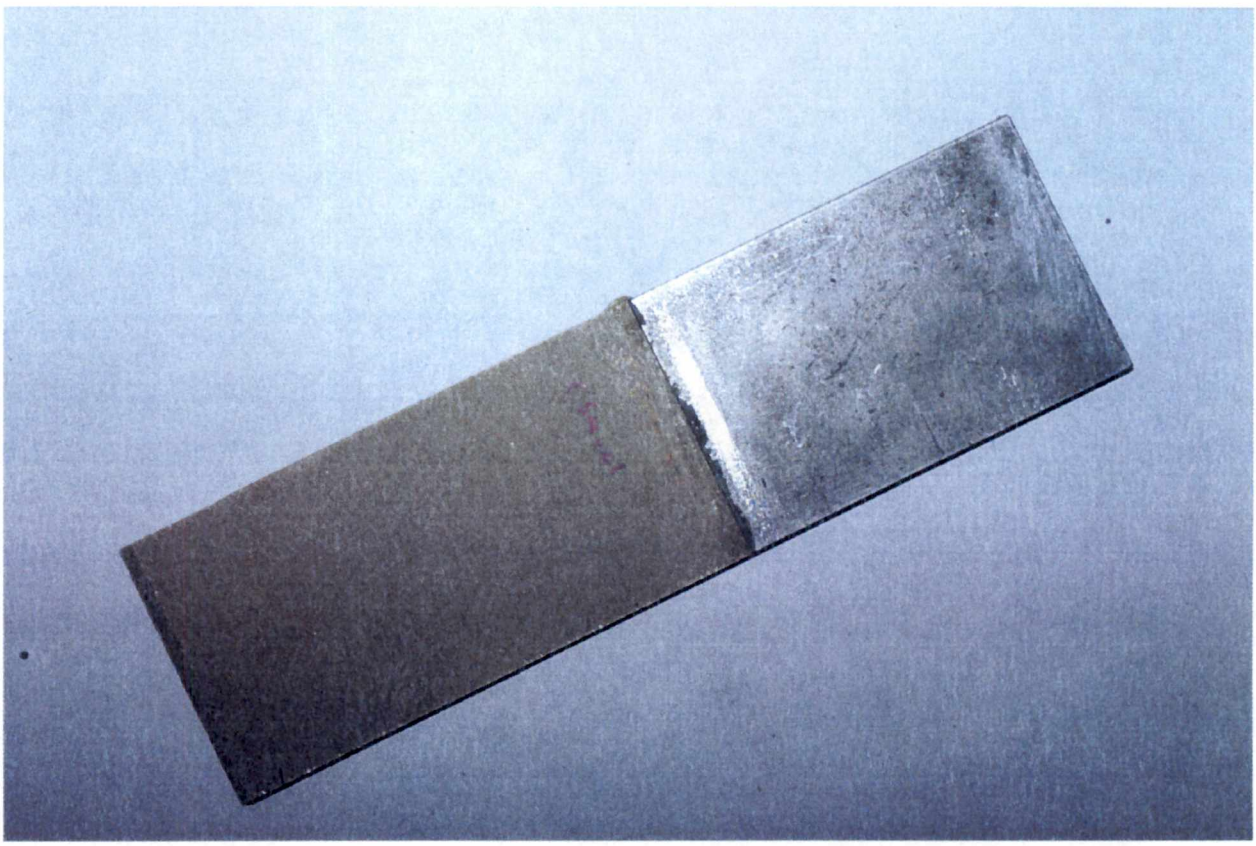

Figure 18. CSM Test Specimen.

bearing and a universal joint provided all the required alignment specifications. The bearings and joints were all connected to the top movable load platen. An MTS model 407 controller which is a single channel, digitally-supervised proportional, integral, derivative, feed forward (PIDF) servo controller, was used to provide complete control of one servo hydraulic channel/station in the MTS testing system. This included ac and dc transducer conditioning, basic function generation (with the capability of accepting externally generated command signals), servo valve drive signal generation, and hydraulic pressure control. Operations were controlled through the 407 controller front panel. An easy to read multi-line display showed the status of the parameter that was currently being adjusted or monitored. A simple scroll-through menu provided quick access to any parameter or function. All parameters were entered through a keypad or adjusted by a single multi-turn knob. The current settings were saved in battery-backed RAM and were automatically recalled at start up. Two conditioner set ups (for each conditioner) could also be stored. In addition to providing the means to adjust and monitor the test parameters, the front panel also provided program control, system hydraulic pressure control, and an emergency stop button that would shut down the system hydraulics in an emergency situation. BNC monitor connectors were also provided to allow connection to easily to external read out devices. The 407 controller provided interlocks for adjustable upper/lower limit, under peak, and error detection for each installed conditioner module, plus an end-of-count interlock. A function generator (with a built in cycle counter) in the 407 controller provided basic sine, square, and triangle command waveforms. The 407 controller provides complete control of the test

system hydraulics. It was used to control a hydraulic power supply to apply low and high hydraulic pressure to the test system. The 407 controller is shown in Figure 19.

The load-deflection response was recorded using a computerized data acquisition system. A 16 bit, 100 kHz National instrument data acquisition card numbered pci6031E was used. The area under the load deflection curve was the total energy absorbed and the initial peak load and sustained crush load were identified. The load-displacement DAQ used is shown in Figure 20.

The specific energy absorption, SEA, of a composite material defined as the energy absorbed per unit mass of the material is equal to W/m where 'W' is the total energy absorbed in crushing of the composite plate specimen which is the area under the load-displacement curve. From SEA=W/m, we can write SEA=W/Vρ, where 'V' is the volume of the crushed portion of the composite plate specimen and 'ρ' is the density of the composite material. One can also write SEA=W/(ALρ), where 'A' and 'L' are the cross sectional area and length of the crushed portion of the composite plate specimen respectively. SEA=W/(ALρ) was used to calculate the specific energy absorption of all the composite plate specimens tested. Figure 21, Figure 22, Figure 23 and Figure 24 show the crushing of the specimen plates when loaded in compression.



Figure 19. 407 Controller

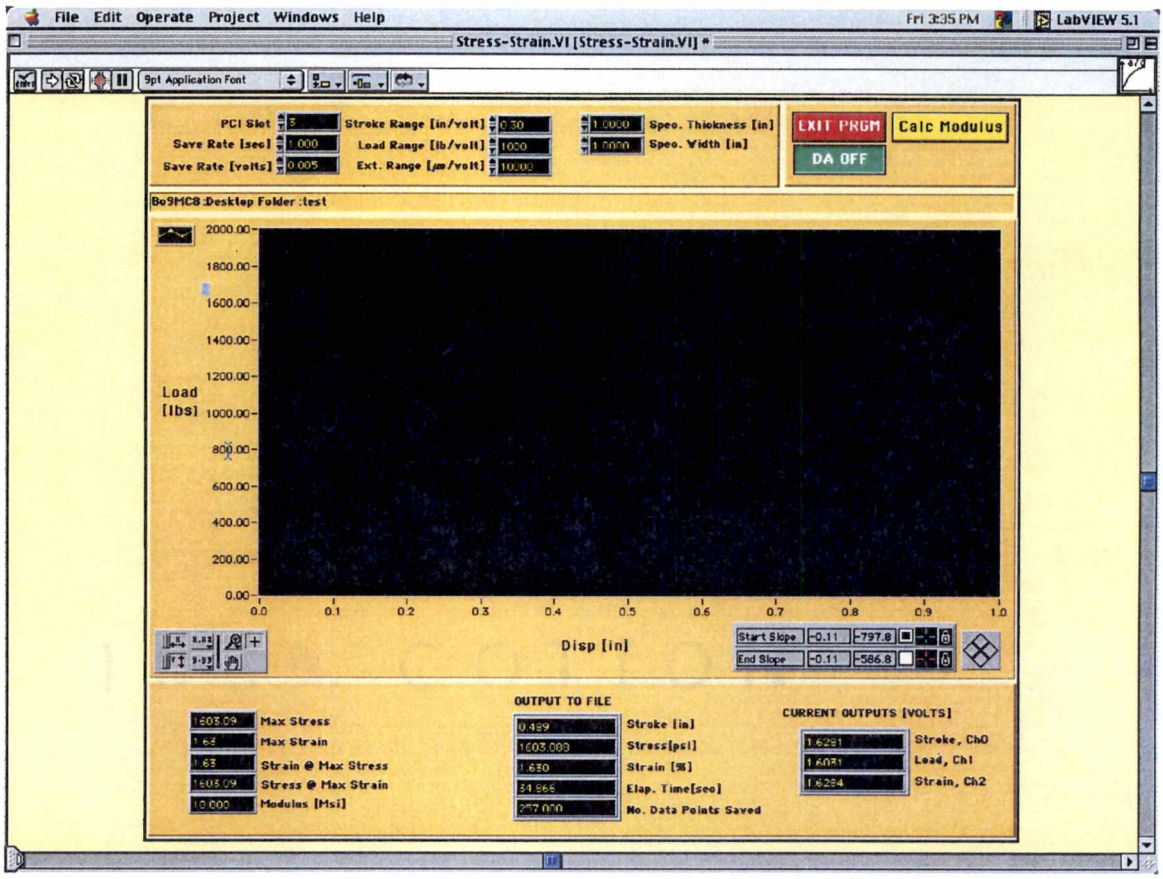

Figure 20. Load Displacement DAQ.

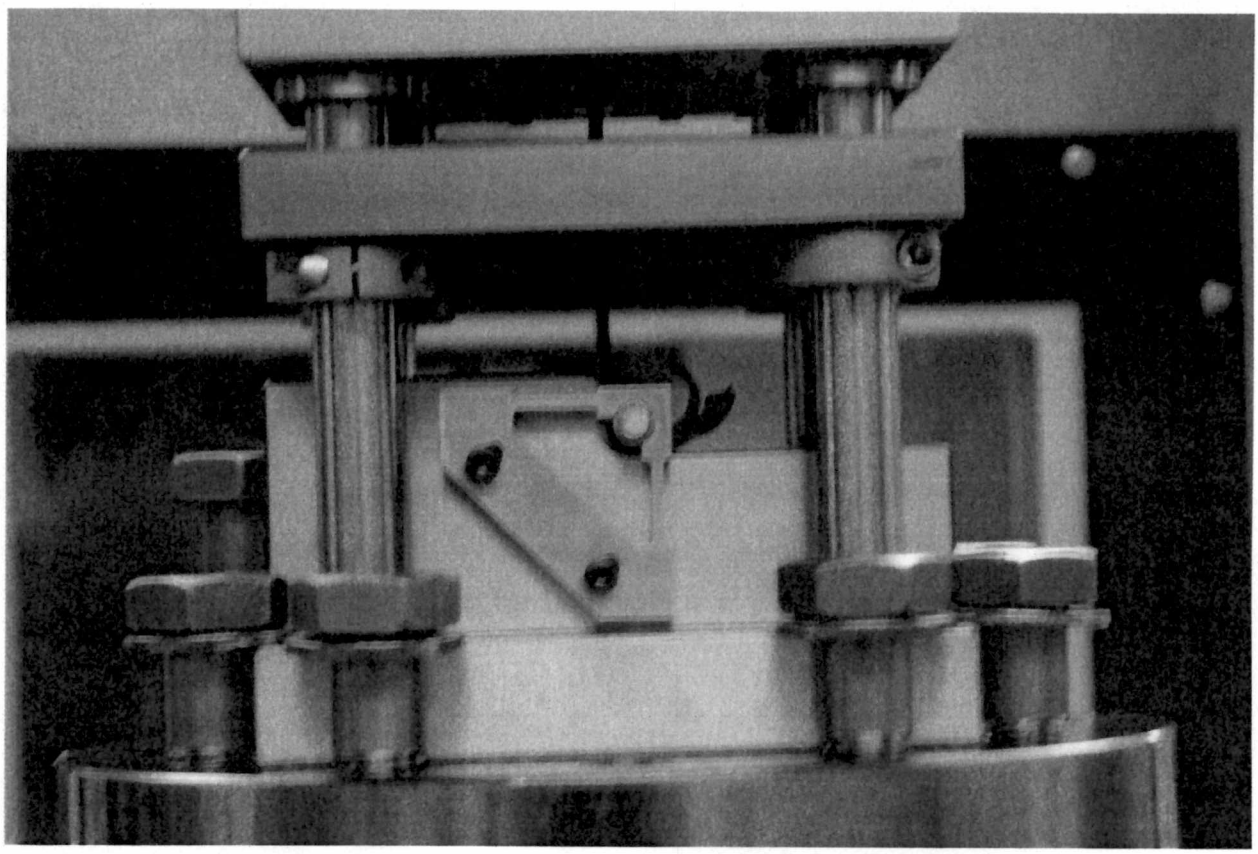

Figure 21. Crushing of a CP#2 Specimen.

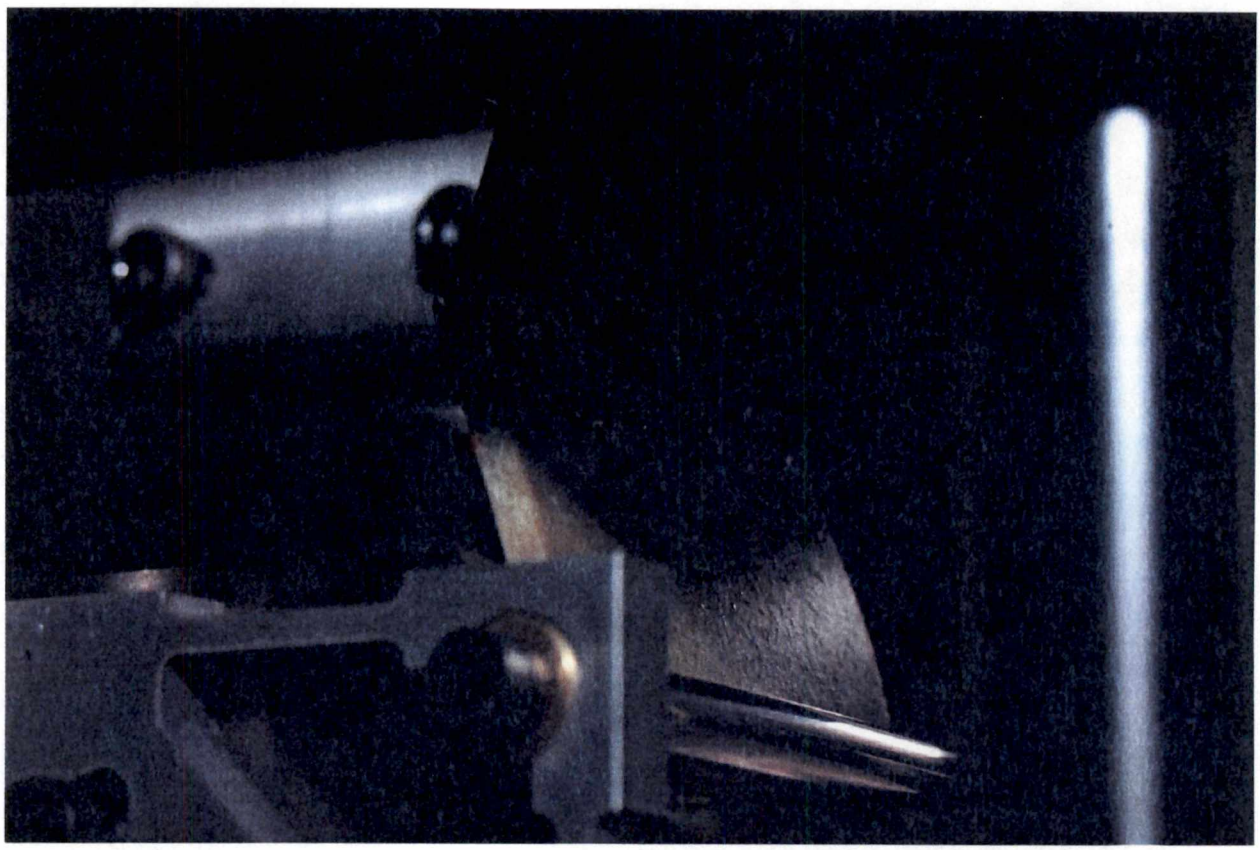

Figure 22. Crushing of a CSM specimen.

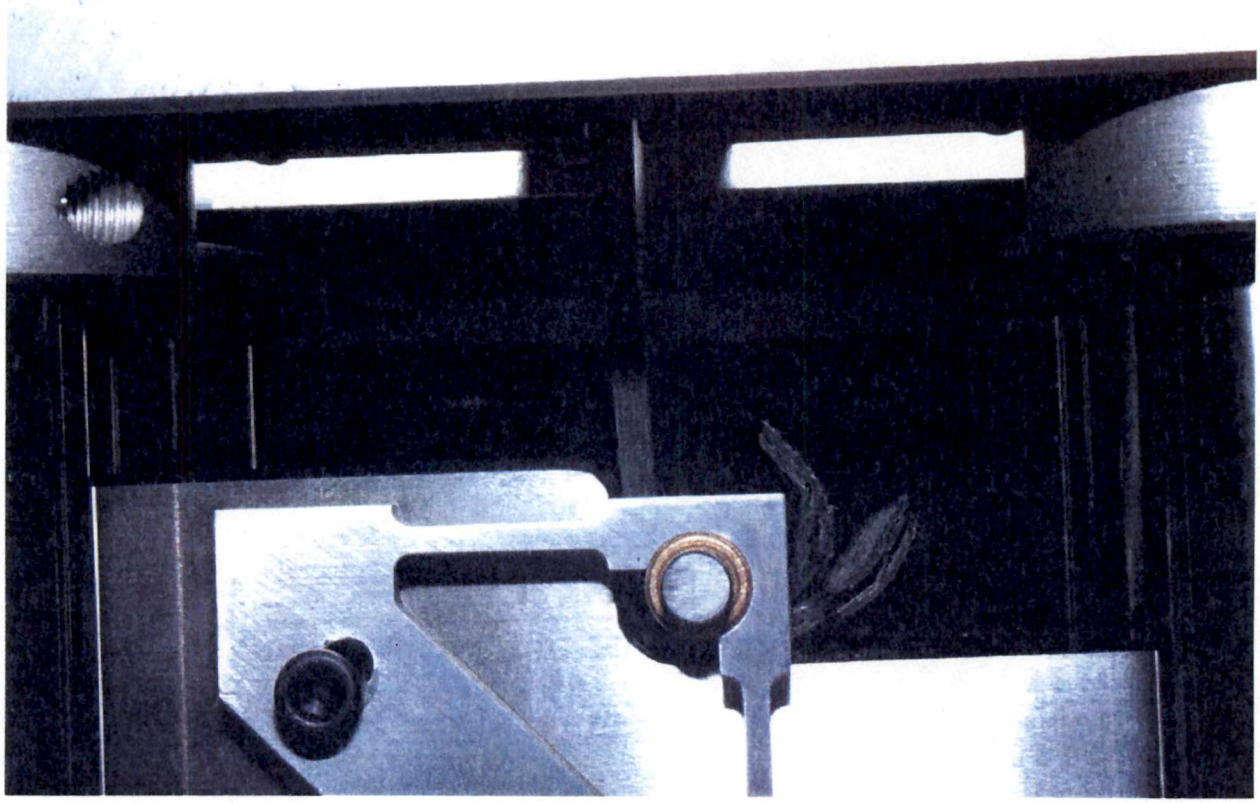

Figure 23. Crushing of a CP#1 Specimen — 1.



Figure 24. Crushing of a CP#1 Specimen — 2.

Chapter 3

Results and Discussion

3.1 Graphite/Epoxy Cross Ply Laminate: CP#1

The experimental data from the measured load-deflection responses are summarized in Table 14.

3.1.1 Effect of Constraint Condition

- For the CP#1 cross-ply panels the no constraint condition resulted in the highest initial peak load and the highest sustained crush load relative to the other constraint conditions. Please see Table 14. For a comparison of the load displacement traces recorded for a test conducted on a specimen in the no constraint, the loose constraint and the tight constraint condition respectively please see Figure 25.
- The predominant damage mechanism for the cross ply plate was delamination. Please see Figure 26 and Figure 27. The constraint condition influenced the damage mechanisms. Tight constraint to loose constraint to the no constraint condition resulted in larger delamination growths, larger number of delaminations, and greater permanent deformations. The plateau in the load deflection responses (see Figure 25) corresponded to complete delamination between all the layers.
- The specific energy absorption, SEA, was highest in the tight constraint condition. No constraint to loose constraint to tight constraint resulted in larger specific energy absorption, SEA (see Table 14). Please look at Figure 28.

3.2 Graphite/Epoxy Cross Ply Laminate: CP#2

The experimental data from the measured load-deflection responses are summarized in Table 15.

Table 14. Experimental Data for CP#1.

Spec. Numb.	Spec. Width (cm)	Profile Radius (cm)	Const-raint	Initial Peak Load (N)	Max. Peak Load (N)	Sustain-ed Crush Load (N)	SEA (J/g)	Avg. SEA (J/g)
CP1-4	5.072	0.635	None	5491.1	7982.2	5280.7	11.12	
CP1-5	5.075	0.635	None	7561.4	7806.0	4372.8	13.65	12.39
CP1-1	5.070	0.635	Loose	4534.2	4975.5	3580.5	19.81	
CP1-2	5.072	0.635	Loose	4615.4	7758.4	4194.8	21.58	18.35
CP1-3	5.075	0.635	Loose	3807.8	5688.2	3505.8	13.65	
CP1-6	5.065	0.635	Tight	4422.2	6238.4	5038.7	25.58	25.58

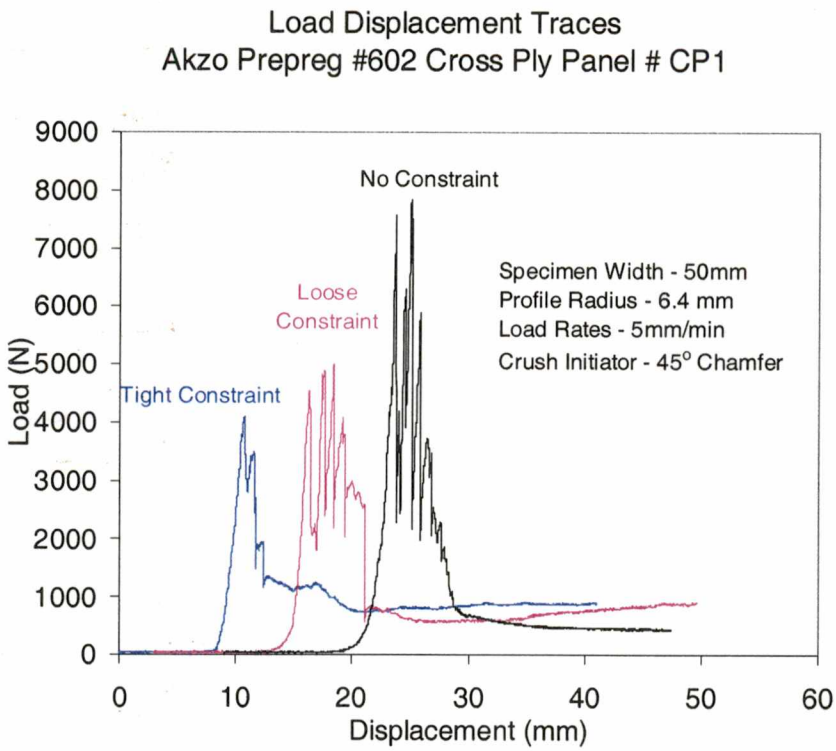

Figure 25. Load Displacement Traces for CP#1.

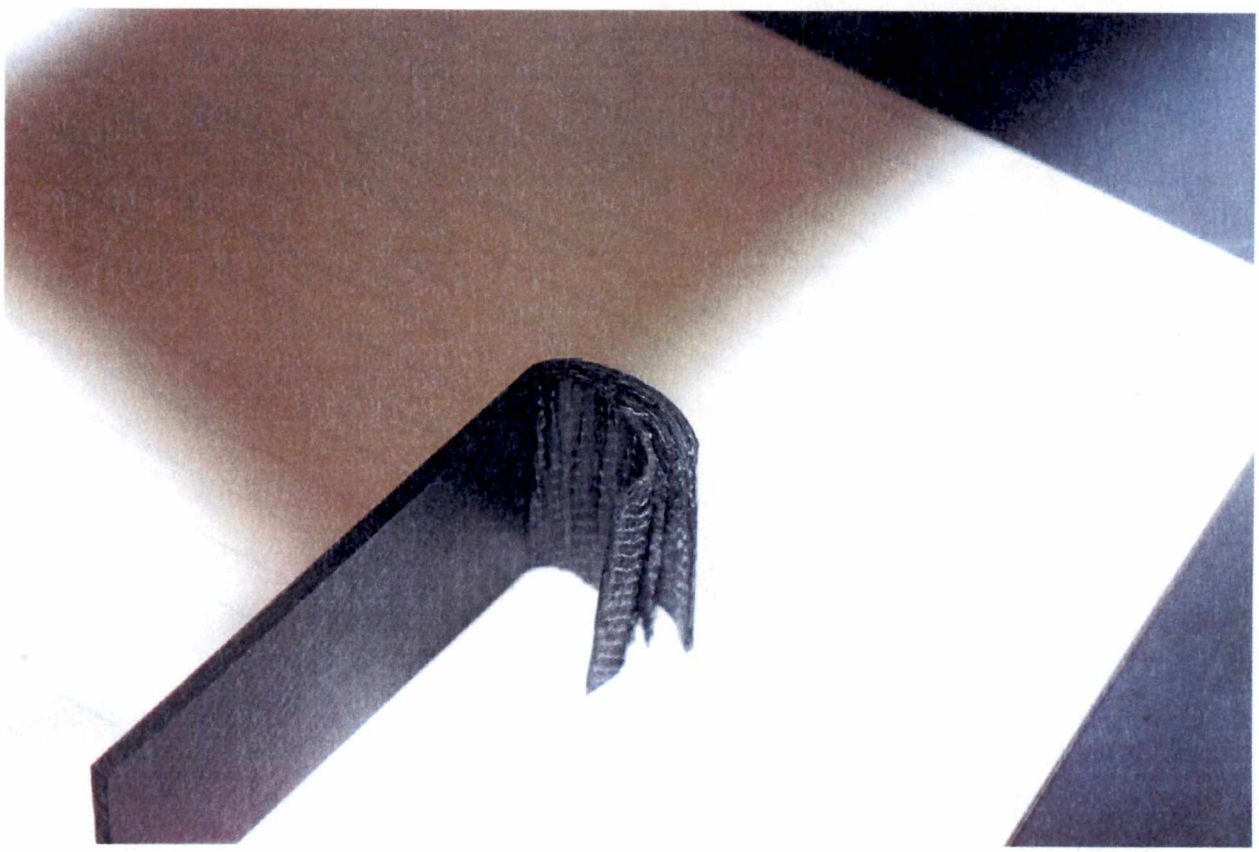

Figure 26. Crushed CP#1 Specimen —1.

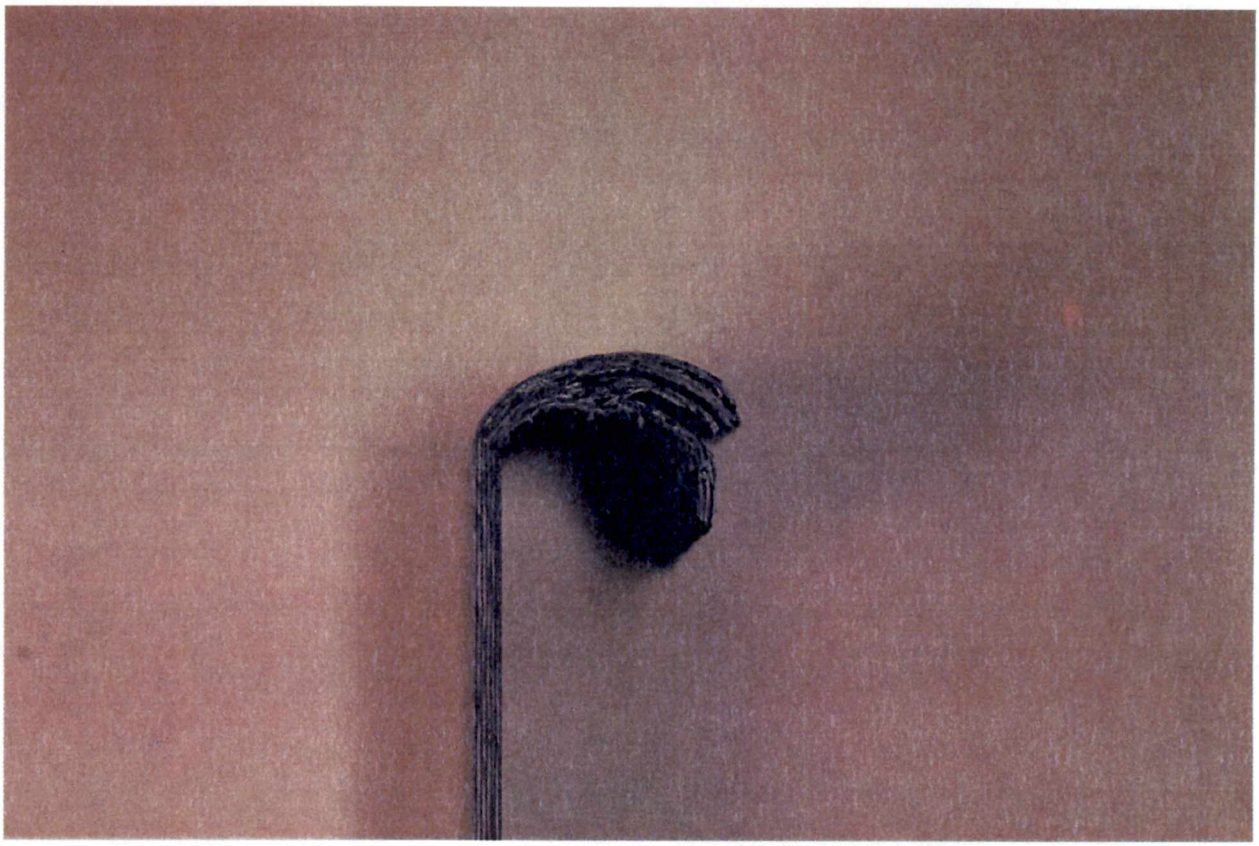

Figure 27. Crushed CP#1 Specimen — 2

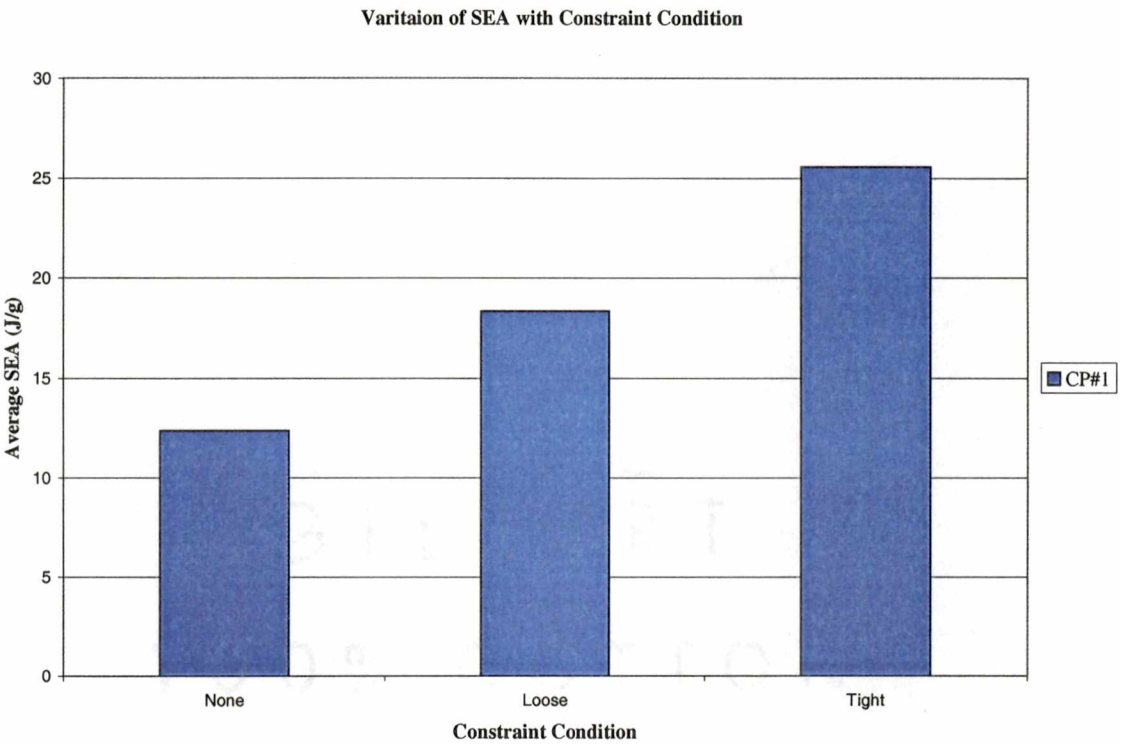

Figure 28. Variation of SEA with Constraint Condition for CP#1.

Table 15. Experimental Data for CP#2.

Spec. Numb.	Spec. Width (cm)	Profile Radius (cm)	Const-raint	Initial Peak Load (N)	Max. Peak Load (N)	Sustain-ed Crush Load (N)	SEA (J/g)	Avg. SEA (J/g)
CP2-1	5.072	0.635	None	5962.1	6103.8	3970.5	7.89	
CP2-2	5.070	0.635	None	4309.9	6721.9	3259.2	7.08	7.49
CP2-3	5.080	0.635	Loose	4594.8	4594.8	2175.5	6.33	
CP2-4	5.055	0.635	Loose	4436.8	4436.8	1463.1	6.86	6.60
CP2-5	5.075	0.635	Tight	4670.1	6000.2	4618.5	20.10	
CP2-6	5.075	0.635	Tight	4582.6	4582.6	3020.1	15.13	17.62

The panel CP#2 had significantly lower SEA's than panel CP#1. Please see Figure 29. Compared to panel CP#1, the lower specific energy absorption, SEA, in panel CP#2 is attributed to the weaker interfacial bond strength, resulting from poor consolidation, requiring less energy to delaminate.

3.2.1 Effect of Constraint Condition

- For the CP#2 cross-ply panels the no constraint condition resulted in the highest initial peak load relative to the other constraint conditions. Please see Table 14. The constraint condition however had a minimal effect on the sustained crush load. For a comparison of the load displacement traces recorded for a test conducted on a specimen in the no constraint, the loose constraint and the tight constraint condition respectively please see Figure 30.
- The predominant damage mechanism for the cross ply plate was delamination. Please see Figure 31 and Figure 32. The constraint condition influenced the damage mechanisms. Tight constraint to loose constraint to the no constraint condition resulted in larger delamination growths, larger number of delaminations, and greater permanent deformations. The plateau in the load deflection responses (see Figure 30) corresponded to complete delamination between all the layers.
- For the panel CP#2, the specific energy absorption, SEA, was significantly higher for the tight constraint condition (see Table 15). Please look at Figure 33.

3.3 Graphite/Epoxy Triaxial Braid with 0/+30°/-30° Fiber Orientations: O

The experimental data from the measured load-deflection responses are summarized in Table 16.

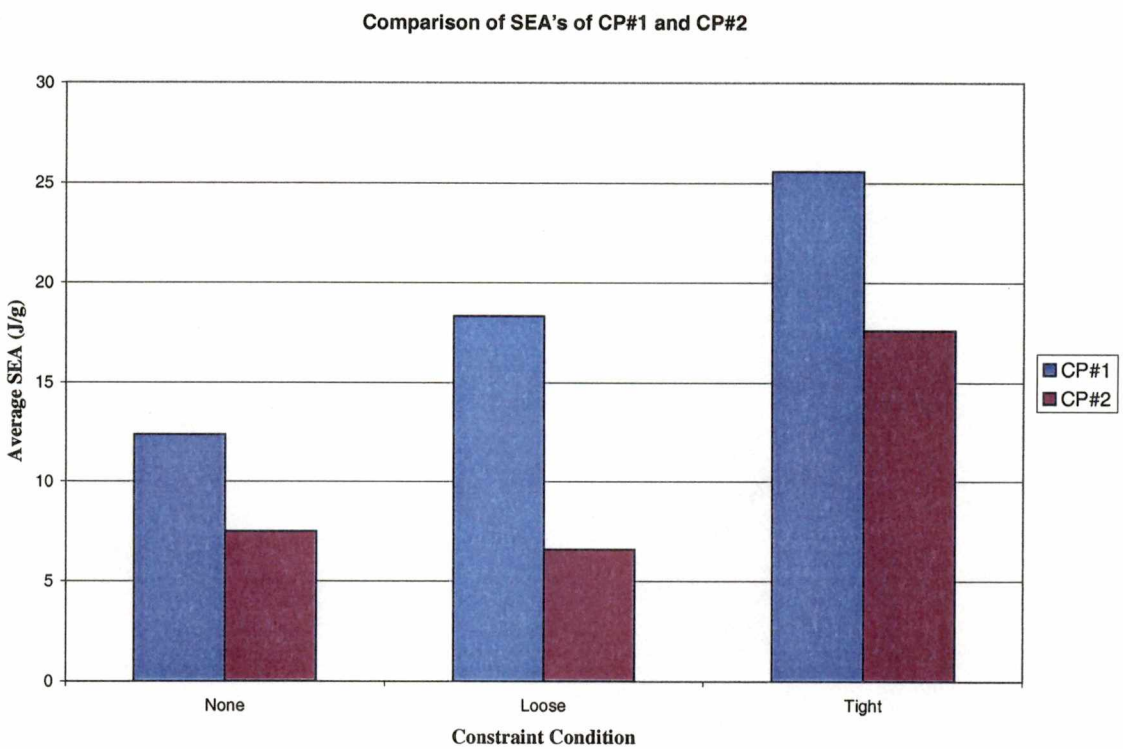

Figure 29. Comparison of Specific Energy Absorptions of CP#1 and CP#2.

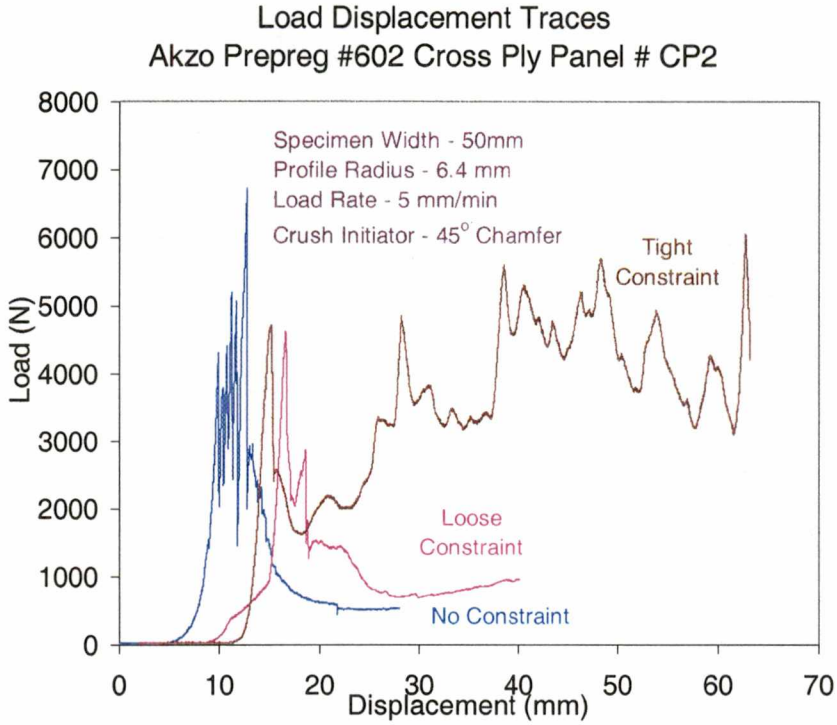

Figure 30. Load Displacement Traces for CP#2.

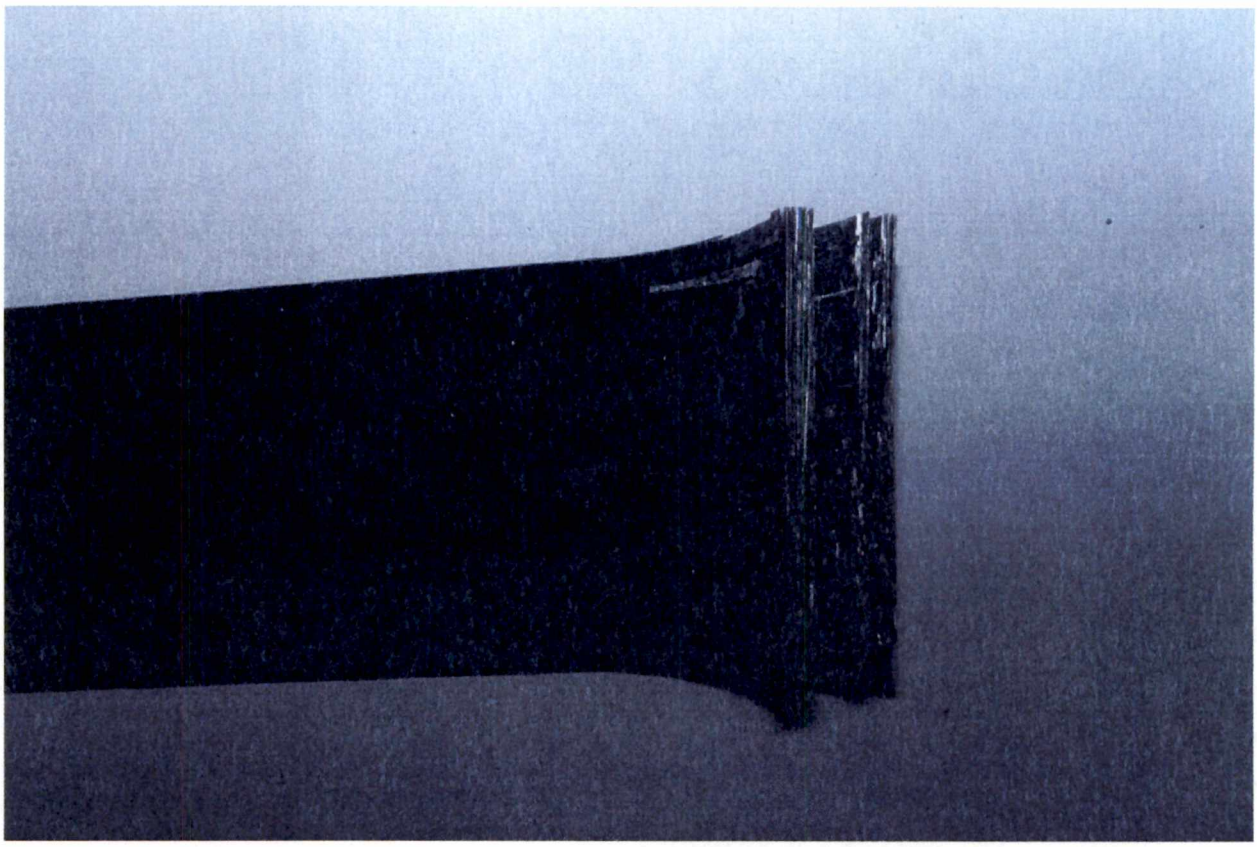

Figure 31. Crushed CP#2 Specimen — 1.

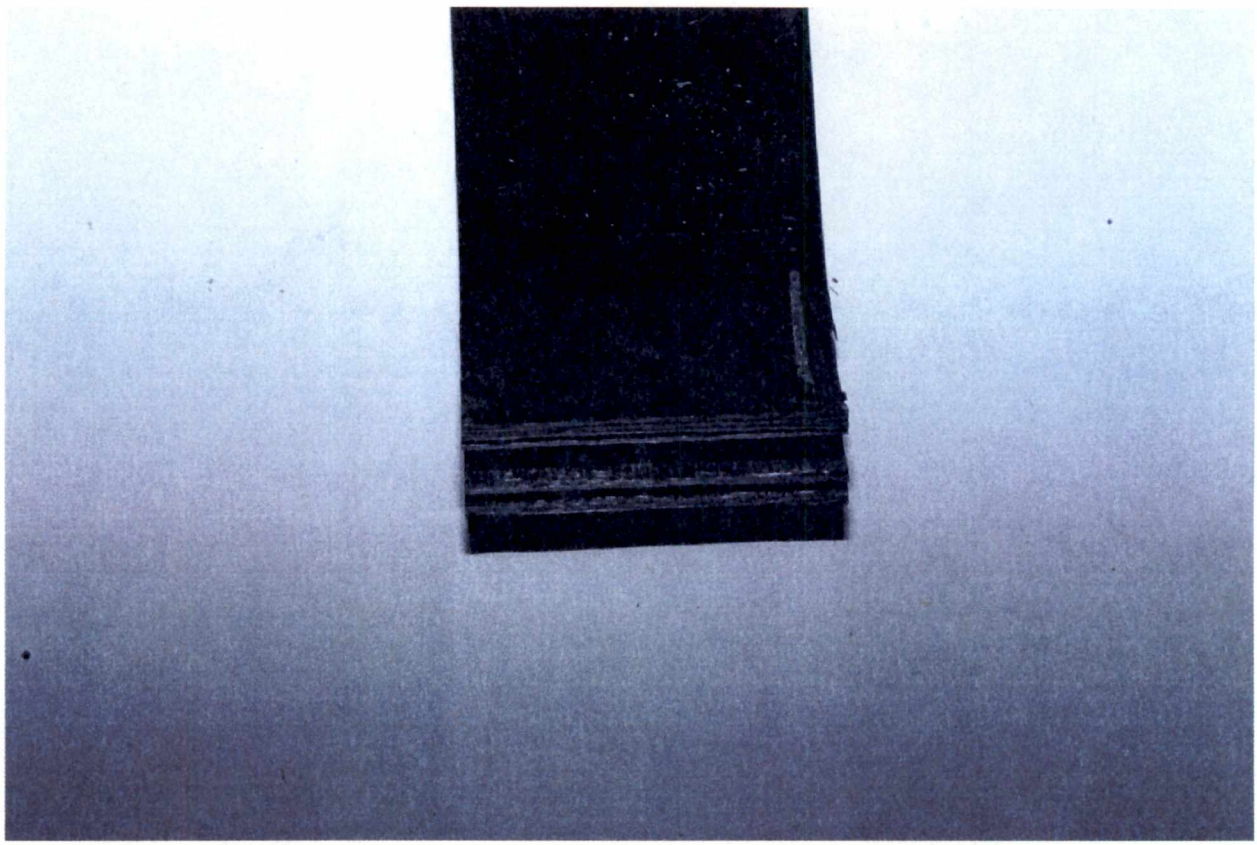

Figure 32. Crushed CP#2 Specimen — 2.

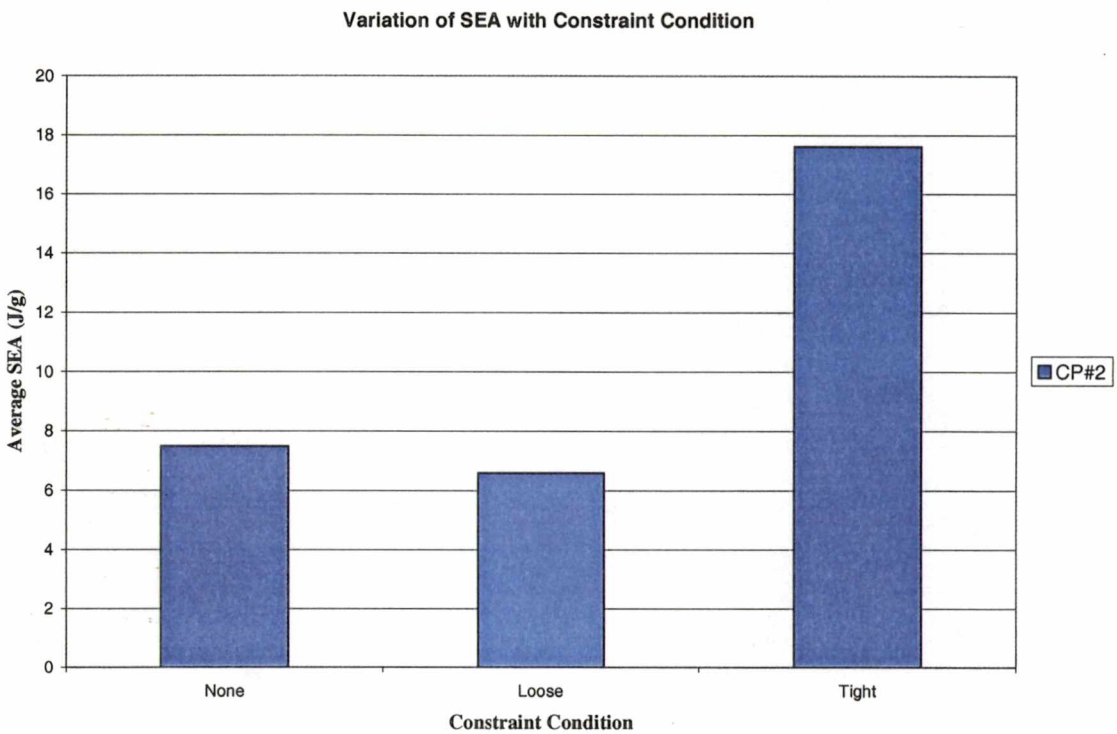

Figure 33. Variation of SEA with Constraint Condition for CP#2.

Table 16. Experimental Data for the Triaxial Braid O.

Spec. Numb.	Spec. Width (cm)	Profile Radius (cm)	Const-raint	Initial Peak Load (N)	Max. Peak Load (N)	Sustain-ed Crush Load (N)	SEA (J/g)	Avg. SEA (J/g)
O-7	3.814	0.635	None	4232.6	4421.1	1916.8	7.36	
O-8	3.810	0.635	None	3673.7	3912.4	1000.9	6.91	
O-10	3.825	0.635	None	4967.0	4967.0	1238.2	7.69	7.32
O-6	3.814	0.635	Loose	3489.8	3489.8	2417.1	14.17	
O-9	3.810	0.635	Loose	3365.7	3650.6	2934.2	20.24	17.21

3.3.1 Effect of Constraint Condition

- For the braided material the no constraint condition resulted in a higher initial peak load relative to the loose constraint condition. The no constraint condition however resulted in a lower sustained crush load relative to the loose constraint condition. Please see Table 16. For a comparison of the load displacement traces recorded for a test conducted on a specimen in the no constraint and the loose constraint condition respectively please see Figure 34.
- For the braided material, the active damage mechanisms were localized crushing, fiber fracture on the tensile side of the specimen, and fiber buckling of the off-axis tows on the compressive side of the specimen. The fiber buckling was more extensive when the no constraint condition was used, where as the fiber fracture was more predominant in the loose constraint tests.
- The results of the braided material show higher specific energy absorption, SEA, when the loose condition was used compared to no constraint (see Table 16). Please see Figure 35. The loose constraint condition produced a nearly ideal response for progressive crushing as can be seen in Figure 34.

3.4 Glass/Polyurethane Continuous Strand Mat: CSM

In the CSM specimens, finite length fractures across the entire width were observed. For a comparison of the load displacement traces recorded for a test conducted on a specimen in the no constraint and the loose constraint condition respectively please see Figure 36.

For tests conducted in the no and loose constraint condition, load would monotonically increase until fracture occurred and then the load would drop to almost

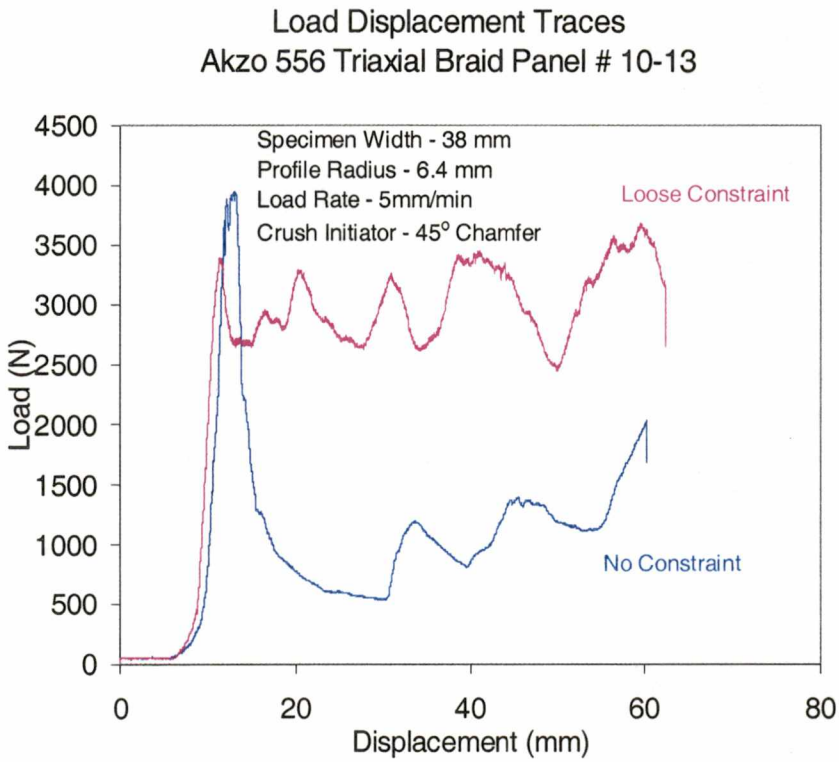

Figure 34. Load Displacement Traces for the Triaxial Braid O.

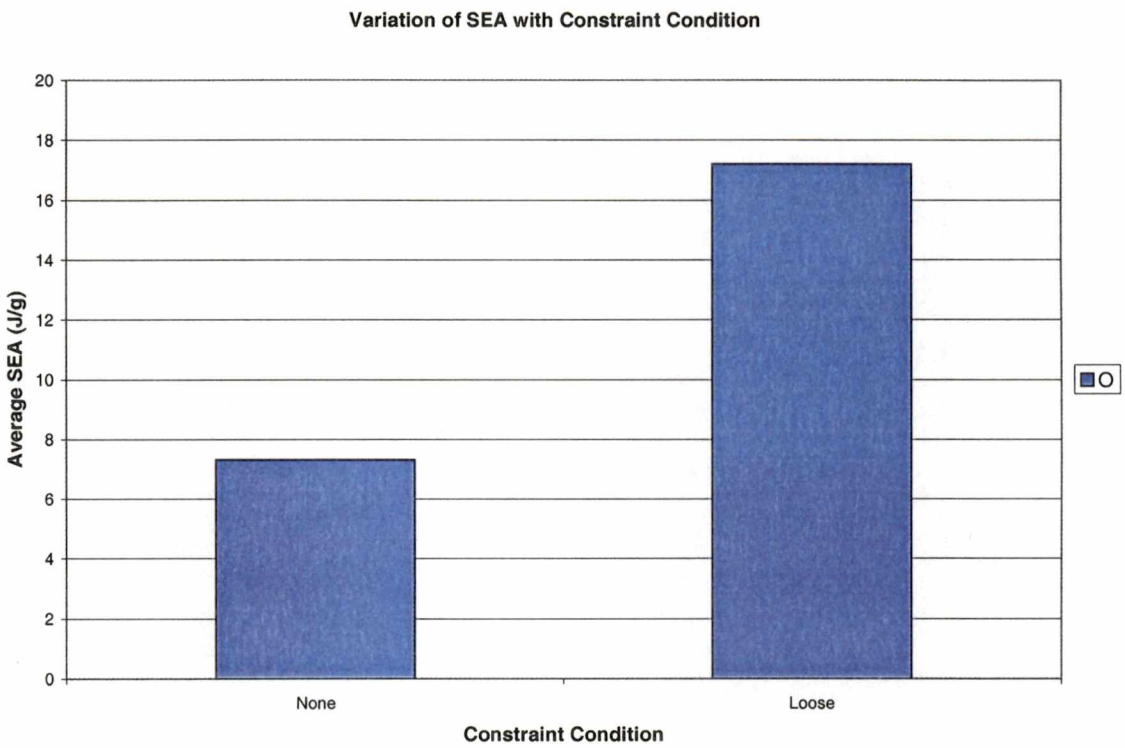

Figure 35. Variation of SEA with Constraint Condition for the Triaxial Braid O.

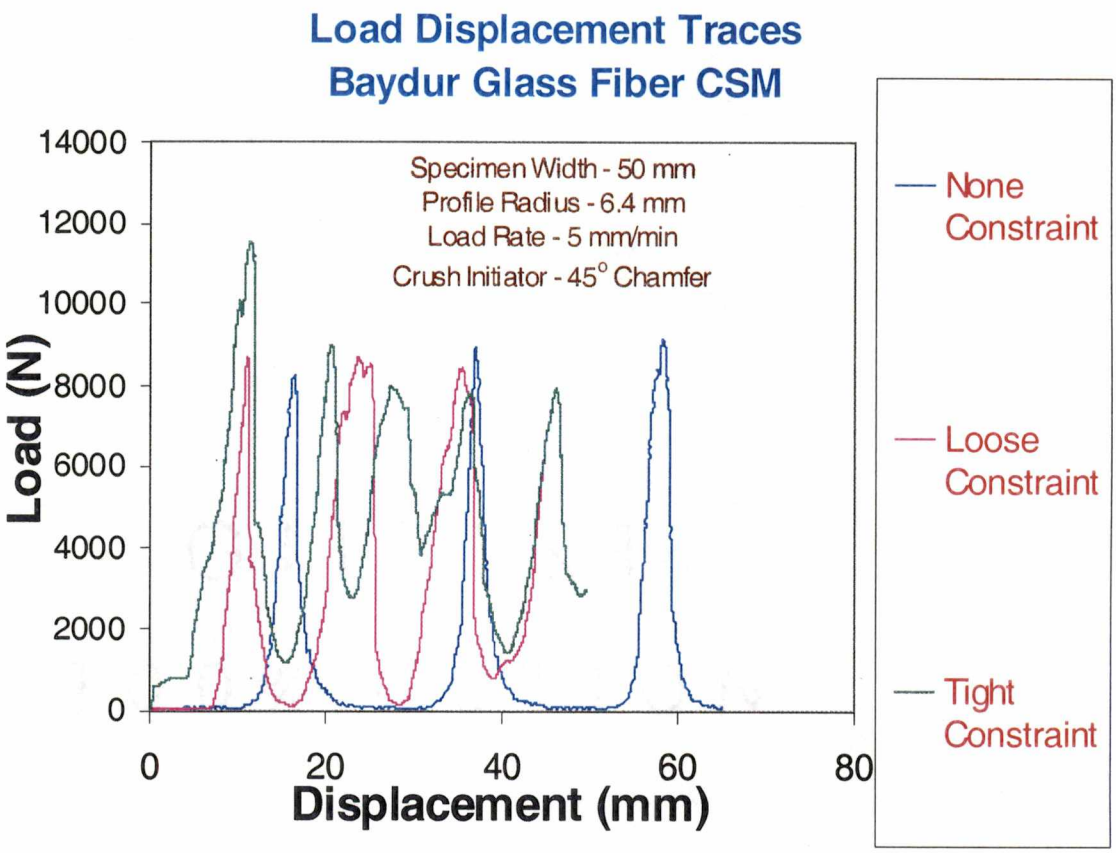

Figure 36. Load Displacement Traces for CSM.

zero (see Figure 36). Approximately the same magnitude of load was measured at each of the fracture points and fracture lengths were approximately the same. Please see Figure 37.

3.4.1 Effect of Constraint

- The tests conducted on the CSM material were only successful when the roller was positioned in the no constraint condition. When the loose or tight constraint condition was attempted the initial peak load increased and the CSM specimens buckled between the top plate and roller ways. Figure 38 shows specimen buckling when a test was conducted on the CSM material in the loose constraint condition. The roller ways were unsuccessful in preventing out-of-plane buckling in the CSM material because of its low buckling strength. This resulted in having to use a metal push plate to reduce the unsupported specimen length. The metal plate was 76 mm in length and was bonded to the end of the CSM specimens using 5-minute epoxy. This specimen configuration was successful when the roller was positioned in the loose and tight constraint condition.
- The specific energy absorption, SEA, was highest in the tight constraint condition. Tight constraint to loose constraint to no constraint condition resulted in lower specific energy absorption, SEA. Please see Table 17 and Table 18. In Table 17, the data for CSM4 and CSM5 corresponds to an erroneous test where in the specimen buckled between the top plate and the roller ways. Please see Figure 39 and Figure 40.

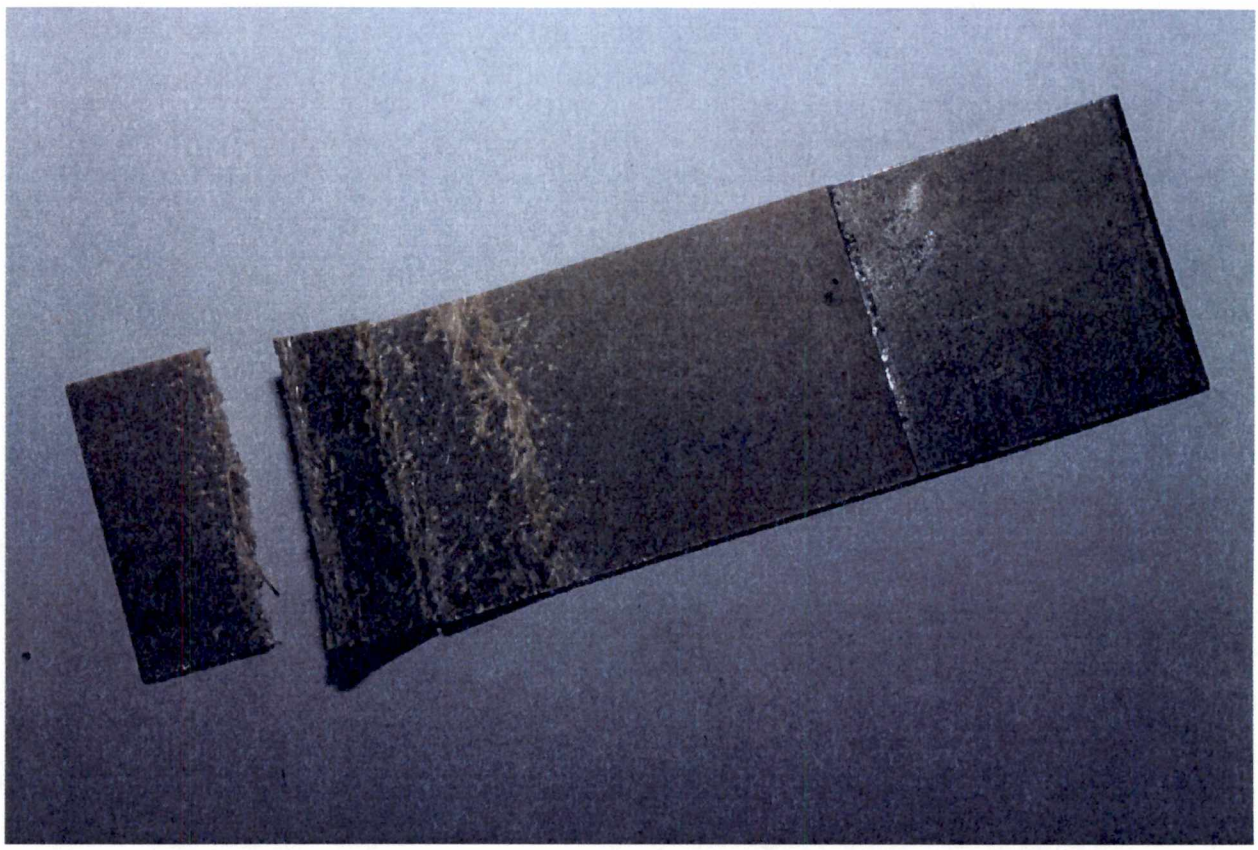

Figure 37. Crushed CSM Specimen.

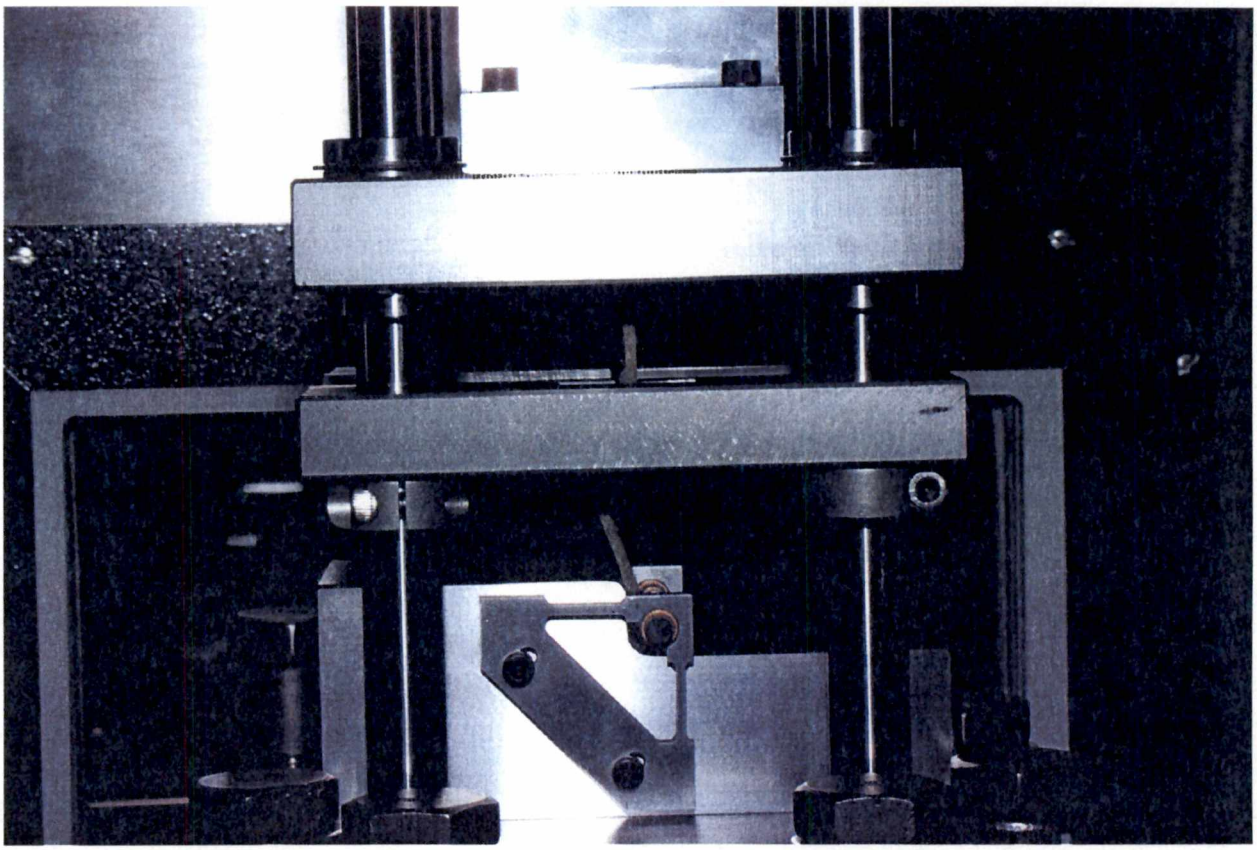

Figure 38. Specimen Buckling during Crushing of CSM in Loose Constraint Condition.

Table 17. Experimental Data from Tests Conducted with a Profile Block of Radius 0.635 cm at 0.5 cm/min Loading Rate on CSM.

Spec. Numb.	Spec. Width (cm)	Profile Radius (cm)	Const-raint	Load Rate (cm/ min)	Initial Peak Load (N)	Max. Peak Load (N)	Sustai-ned Crush Load (N)	SEA (J/g)	Avg. SEA (J/g)
CSM-1	5.070	0.635	None	0.5	7478.2	9556.5	4829.1	10.79	
CSM-3	5.073	0.635	None	0.5	8157.8	9064.7	4443.9	9.71	
CSM-6	5.070	0.635	None	0.5	8334.2	9460.9	4560.6	10.10	10.20
CSM-5	5.078	0.635	Loose	0.5	9209.2	9209.2	6081.3	16.96	
CSM-4	5.074	0.635	Loose	0.5	10611. 2	10611. 2	5400.6	38.64	
CSM-7	5.116	0.635	Loose	0.5	11852. 5	11852. 5	4652.1	21.80	
CSM-8	5.100	0.635	Loose	0.5	10932. 8	10932. 8	3950.1	16.39	
CSM-9	5.157	0.635	Loose	0.5	8679.9	8679.9	4238.7	19.95	19.38
CSM-10	5.096	0.635	Tight	0.5	9922.8	11412. 3	5892.7	26.39	
CSM-11	5.086	0.635	Tight	0.5	6774.8	8688.3	5838.4	29.37	

Table 17 continued.

CSM-12	5.106	0.635	Tight	0.5	7568.4	7568.4	4193.9	23.74	26.50

Table 18. Experimental Data from Tests Conducted with a Profile Block of Radius 0.635 cm at 5 cm/min Loading Rate on CSM.

Spec. Numb.	Spec. Width (cm)	Profile Radius (cm)	Const-raint	Load Rate (cm/ min)	Initial Peak Load (N)	Max. Peak Load (N)	Sustai-ned Crush Load (N)	SEA (J/g)	Avg. SEA (J/g)
CSM-14	5.114	0.635	None	5	8313.2	10046.9	4542.5	11.10	
CSM-15	5.110	0.635	None	5	8319.3	8749.3	4413.3	10.79	10.95
CSM-16	5.098	0.635	Loose	5	8968.4	8968.4	4700.9	16.54	
CSM-17	5.111	0.635	Loose	5	9827.1	9827.1	3929.7	16.36	16.45
CSM-18	5.103	0.635	Tight	5	8575.7	9143.4	5720.8	22.68	22.68

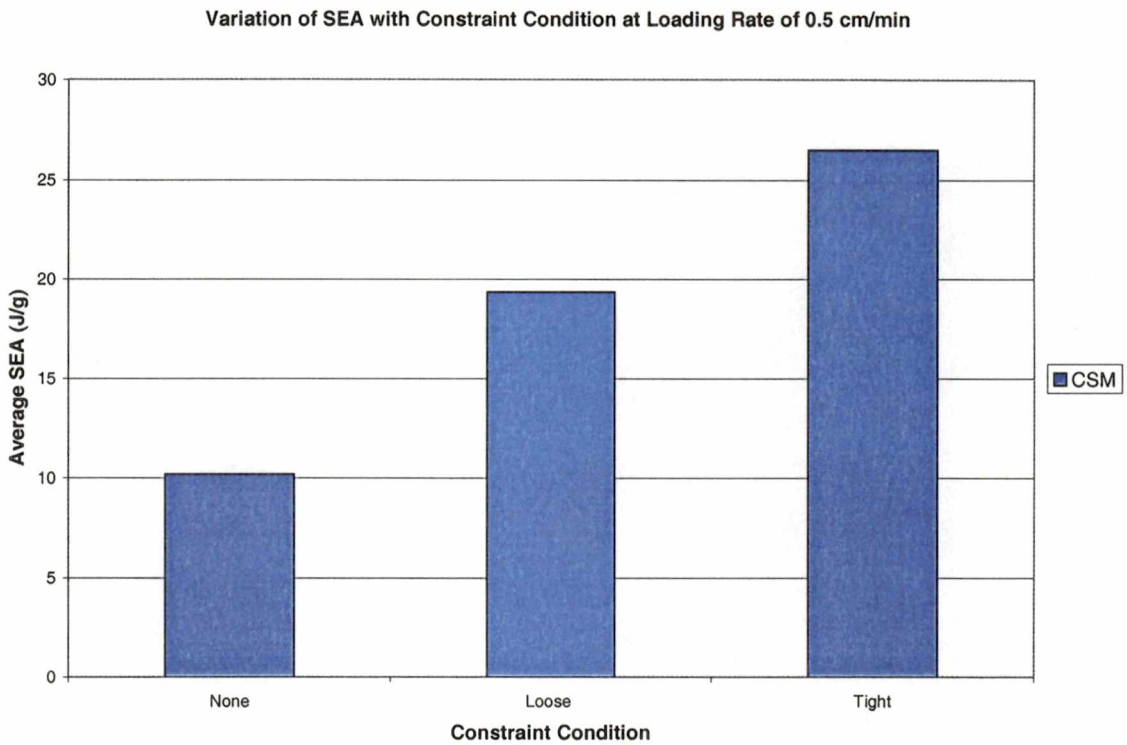

Figure 39. Variation of SEA with Constraint Condition at Loading Rate of 0.5 cm/min for CSM.

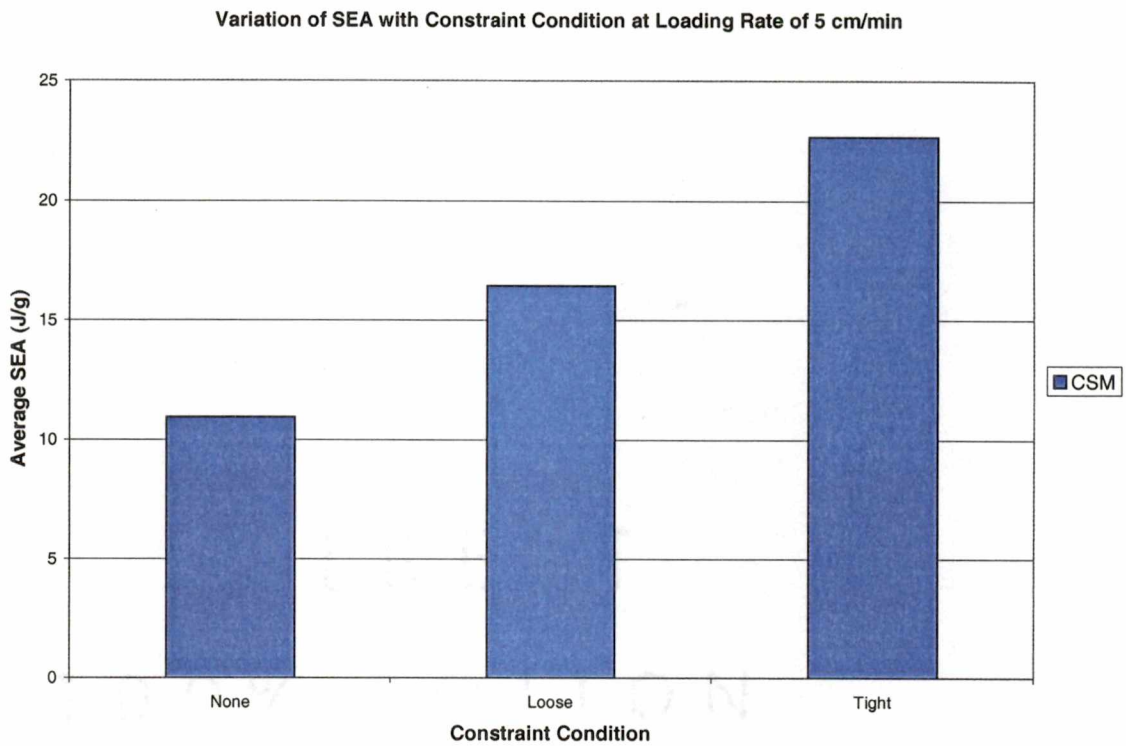

Figure 40. Variation of SEA with Constraint Condition at Loading Rate of 5 cm/min for CSM.

3.4.2 Effect of Crushing Speed

3.4.2.1 No Constraint Condition

The specific energy absorption, SEA, was independent of changes in crushing speed when the tests were conducted in the no constraint condition. See Table 19.

For a comparison of the load displacement traces recorded for a test conducted on a specimen in the no constraint condition at loading rates of 0.5 and 5 cm/min respectively please see Figure 41. Please see Figure 42.

3.4.2.2 Loose Constraint Condition

An increase in the crushing speed caused a decrease in the specific energy absorption, SEA, when the tests were conducted in the loose constraint condition. See Table 20. The data for CSM4 and CSM5 in Table 20 corresponds to an erroneous test where in the specimen buckled between the top plate and the roller ways.

For a comparison of the load displacement traces recorded for a test conducted on a specimen in the loose constraint condition at loading rates of 0.5 and 5 cm/min respectively please see Figure 43. Please see Figure 44.

3.4.2.3 Tight Constraint Condition

An increase in the crushing speed caused a decrease in the specific energy absorption, SEA, when the tests were conducted in the tight constraint condition. See Table 21.

For a comparison of the load displacement traces recorded for a test conducted on a specimen in the tight constraint condition at loading rates of 0.5 and 5 cm/min respectively please see Figure 45. Please see Figure 46.

Table 19. Experimental Data from Tests Conducted in the No Constraint Condition on CSM.

Spec. Numb.	Spec. Width (cm)	Profile Radius (cm)	Const-raint	Load Rate (cm /min)	Initial Peak Load (N)	Max. Peak Load (N)	Sustai-ned Crush Load (N)	SEA (J/g)	Avg. SEA (J/g)
CSM-1	5.070	0.635	None	0.5	7478.2	9556.5	4829.1	10.79	
CSM-3	5.073	0.635	None	0.5	8157.8	9064.7	4443.9	9.71	
CSM-6	5.070	0.635	None	0.5	8334.2	9460.9	4560.6	10.10	10.20
CSM-14	5.114	0.635	None	5	8313.2	10046.9	4542.5	11.10	
CSM-15	5.110	0.635	None	5	8319.3	8749.3	4413.3	10.79	10.95

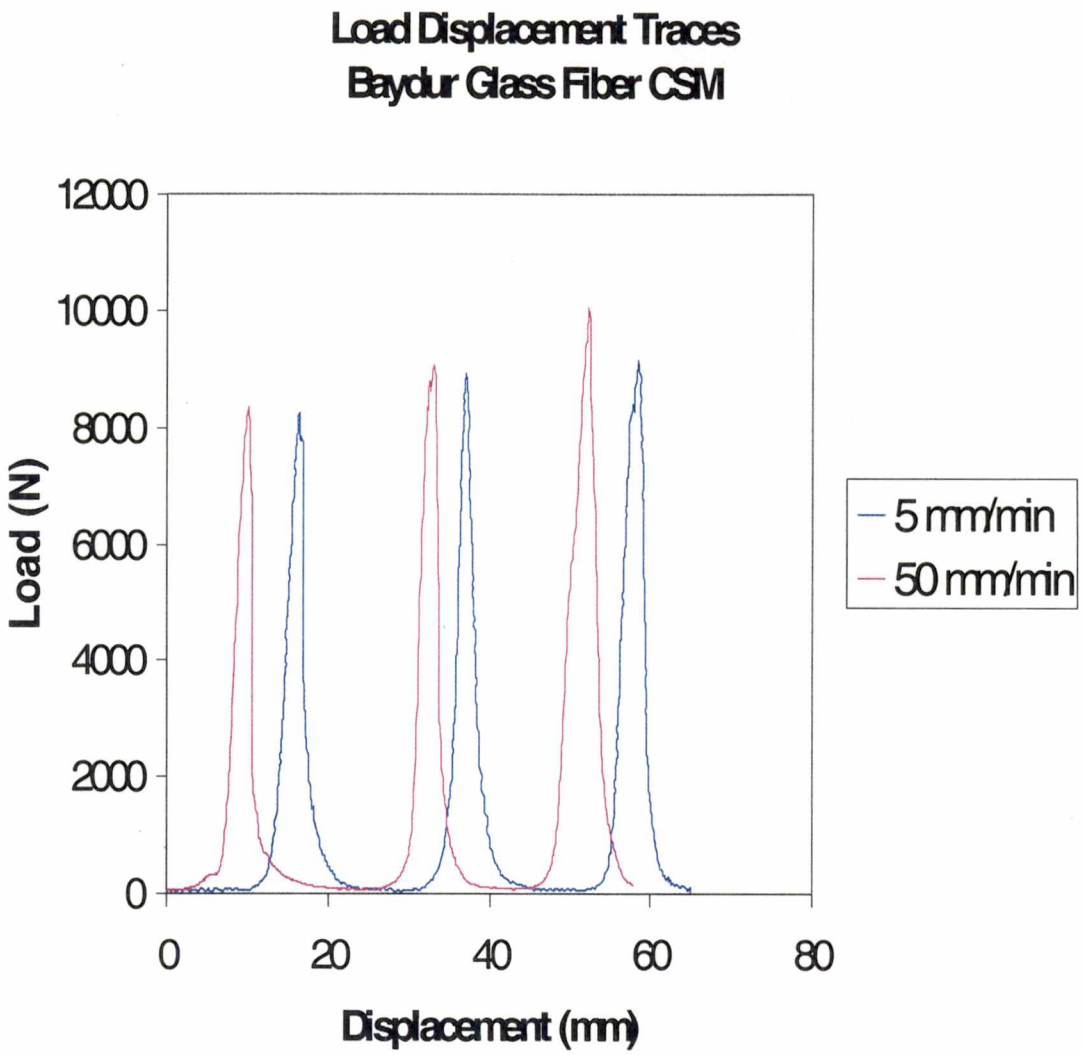

Figure 41. Load Displacement Traces for a Test Conducted on CSM in the No Constraint Condition at Loading Rates of 0.5 and 5 cm/min respectively.

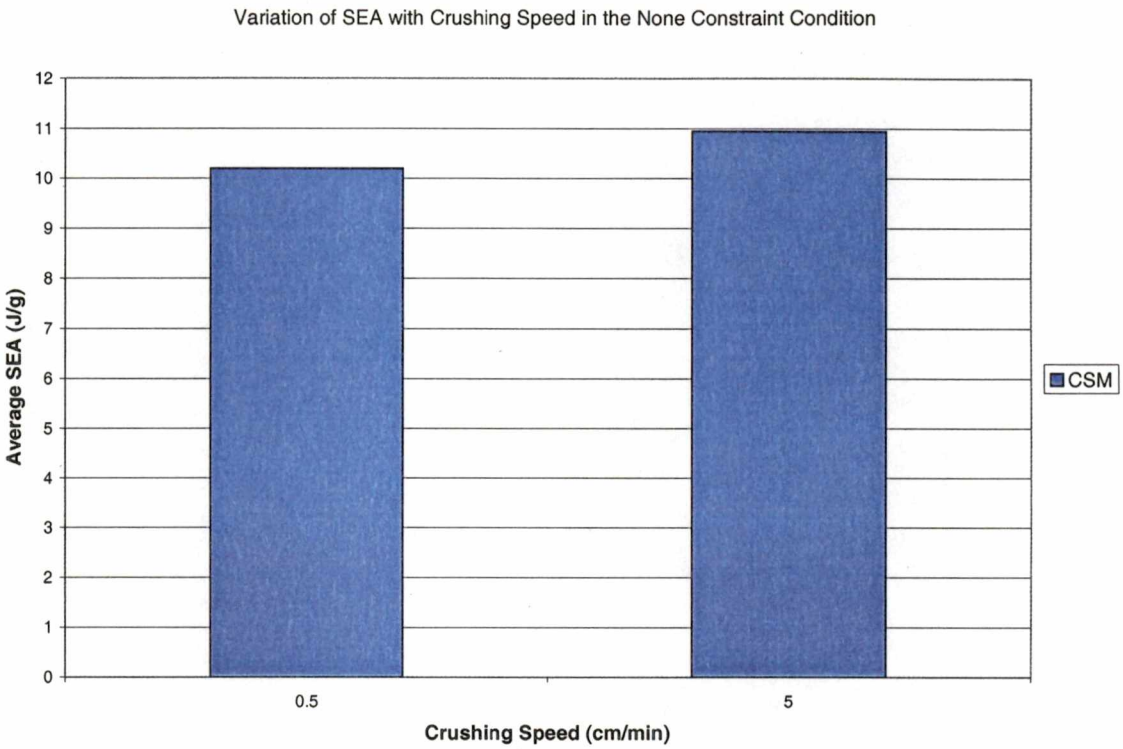

Figure 42. Variation of SEA with Crushing Speed for CSM in the No Constraint Condition.

Table 20. Experimental Data from Tests Conducted in the Loose Constraint Condition on CSM.

Spec. Numb.	Spec. Width (cm)	Profile Radius (cm)	Const-raint	Load Rate (cm/ min)	Initial Peak Load (N)	Max. Peak Load (N)	Sustai-ned Crush Load (N)	SEA (J/g)	Avg. SEA (J/g)
CSM-5	5.078	0.635	Loose	0.5	9209.2	9209.2	6081.3	16.96	
CSM-4	5.074	0.635	Loose	0.5	10611.2	10611.2	5400.6	38.64	
CSM-7	5.116	0.635	Loose	0.5	11852.5	11852.5	4652.1	21.80	
CSM-8	5.100	0.635	Loose	0.5	10932.8	10932.8	3950.1	16.39	
CSM-9	5.157	0.635	Loose	0.5	8679.9	8679.9	4238.7	19.95	19.38
CSM-16	5.098	0.635	Loose	5	8968.4	8968.4	4700.9	16.54	
CSM-17	5.111	0.635	Loose	5	9827.1	9827.1	3929.7	16.36	16.45

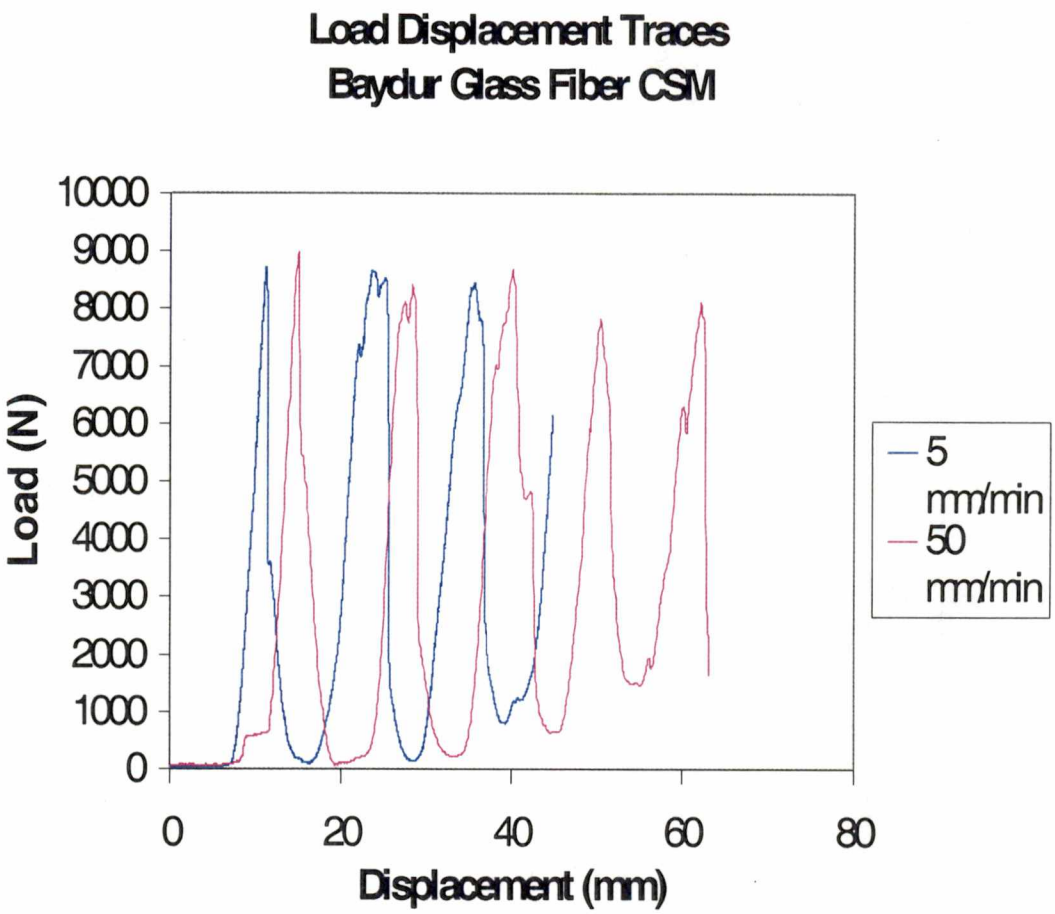

Figure 43. Load Displacement Traces for a Test Conducted on CSM in the Loose Constraint Condition at Loading Rates of 0.5 and 5 cm/min respectively.

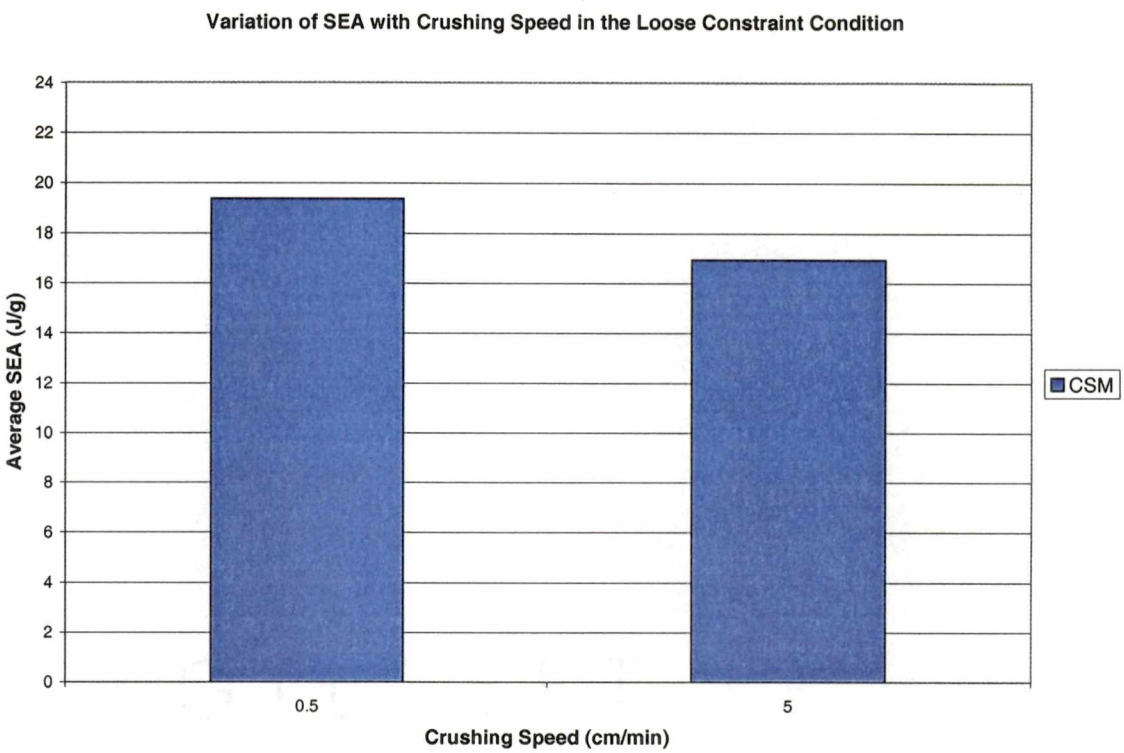

Figure 44. Variation of SEA with Crushing Speed for CSM in the Loose Constraint Condition.

Table 21. Experimental Data from Tests Conducted in the Tight Constraint Condition on CSM.

Spec. Numb.	Spec. Width (cm)	Profile Radius (cm)	Const-raint	Load Rate (cm/ min)	Initial Peak Load (N)	Max. Peak Load (N)	Sustai-ned Crush Load (N)	SEA (J/g)	Avg. SEA (J/g)
CSM-10	5.096	0.635	Tight	0.5	9922.8	11412.3	5892.7	26.39	
CSM-11	5.086	0.635	Tight	0.5	6774.8	8688.3	5838.4	29.37	
CSM-12	5.106	0.635	Tight	0.5	7568.4	7568.4	4193.9	23.74	26.50
CSM-18	5.103	0.635	Tight	5	8575.7	9143.4	5720.8	22.68	22.68

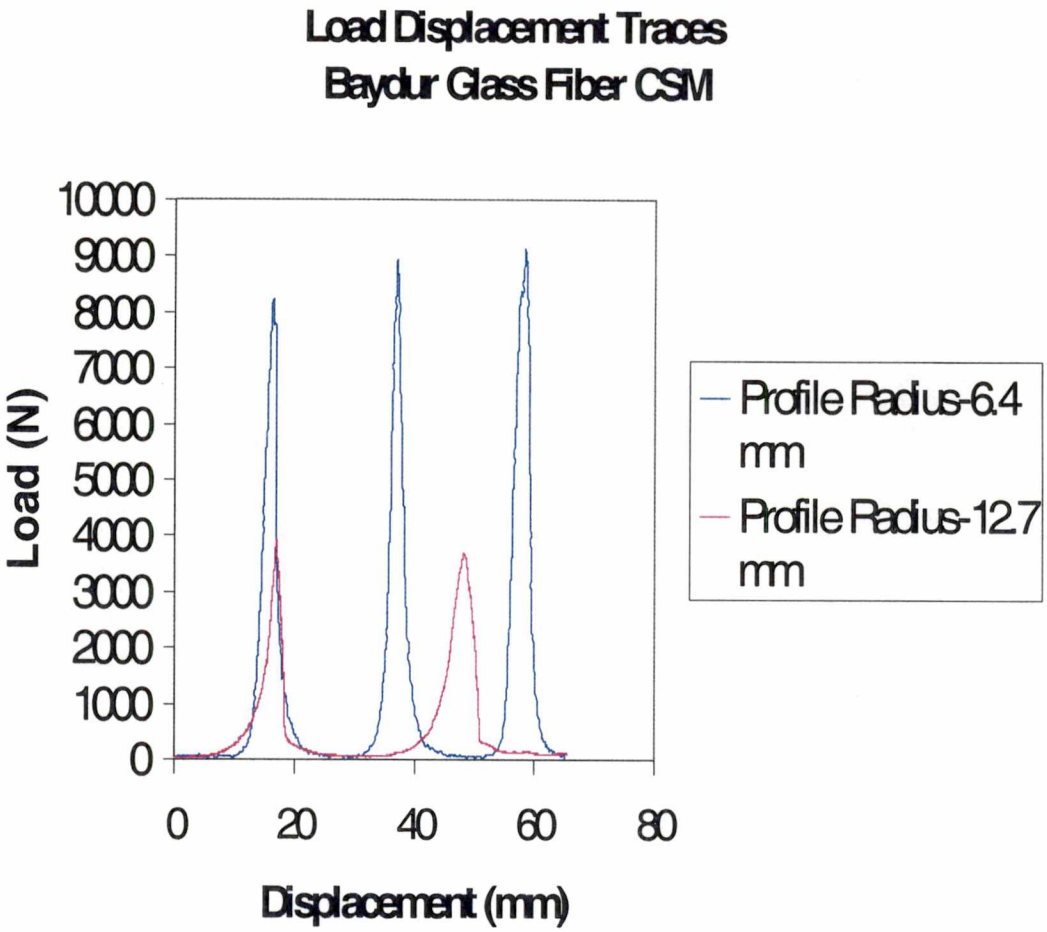

Figure 45. Load Displacement Traces for a Test Conducted on CSM in the Tight Constraint Condition at Loading Rates of 0.5 and 5 cm/min respectively.

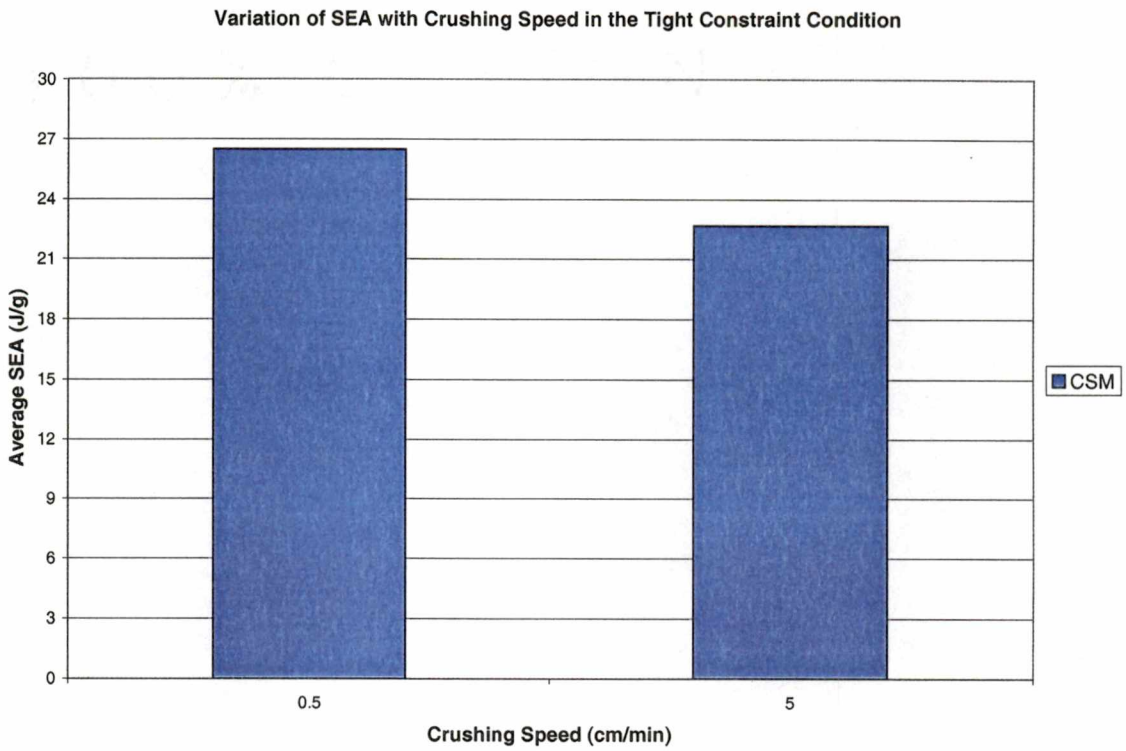

Figure 46. Variation of SEA with Crushing Speed for CSM in the Tight Constraint Condition.

3.4.3 Effect of Profile Radius

An increase in the profile radius caused a decrease in the specific energy absorption, SEA, of the CSM material. Please see Table 22. For a comparison of the load displacement traces recorded for a test conducted on a specimen using a profile block of radius 0.635 cm and on a specimen using a profile block of radius 1.27 cm please see Figure 47.

The decrease in SEA with an increase in the profile radius is due to the fact that a specimen loaded in compression is crushed through the contact profile as defined by the profile block and it follows a smoother curve when the profile block has a radius of 1.27 cm as when compared to a radius of 0.635 cm. Therefore less energy is absorbed in bending it. Please see Figure 48.

3.5 Chopped Carbon Fiber/Epoxy Material System: CCF

The material property variables that were tested for the chopped carbon fiber composites were

1. Fiber Volume Fraction: 40% and 50%
2. Fiber Tow Size: 150 gsm (12 K) and 300 gsm (48 K)
3. Fiber Length: 1 inch and 2 inch

8 panel groups of compression molded chopped carbon fiber/epoxy composites having different material properties were made. Descriptions of the various panel groups are given below.

1. Panel Group Name: CCF1

   Fiber Tow Size: 150 gsm (12 K)

   Fiber Volume Fraction: 40%

Table 22. Experimental Data from Tests Conducted with a Profile Block of Radius 0.635 cm and 1.27 cm at 0.5 cm/min Loading Rate in the No Constraint Condition on CSM.

Spec. Numb.	Spec. Width (cm)	Profile Radius (cm)	Const-raint	Load Rate (cm/ min)	Initial Peak Load (N)	Max. Peak Load (N)	Sustai-ned Crush Load (N)	SEA (J/g)	Avg. SEA (J/g)
CSM-1	5.070	0.635	None	0.5	7478.2	9556.5	4829.1	10.79	
CSM-3	5.073	0.635	None	0.5	8157.8	9064.7	4443.9	9.71	
CSM-6	5.070	0.635	None	0.5	8334.2	9460.9	4560.6	10.10	10.20
CSM-19	5.093	1.27	None	0.5	3228.0	4182.3	2199.0	7.00	
CSM-20	5.109	1.27	None	0.5	3913.8	3913.8	1908.6	6.62	6.81

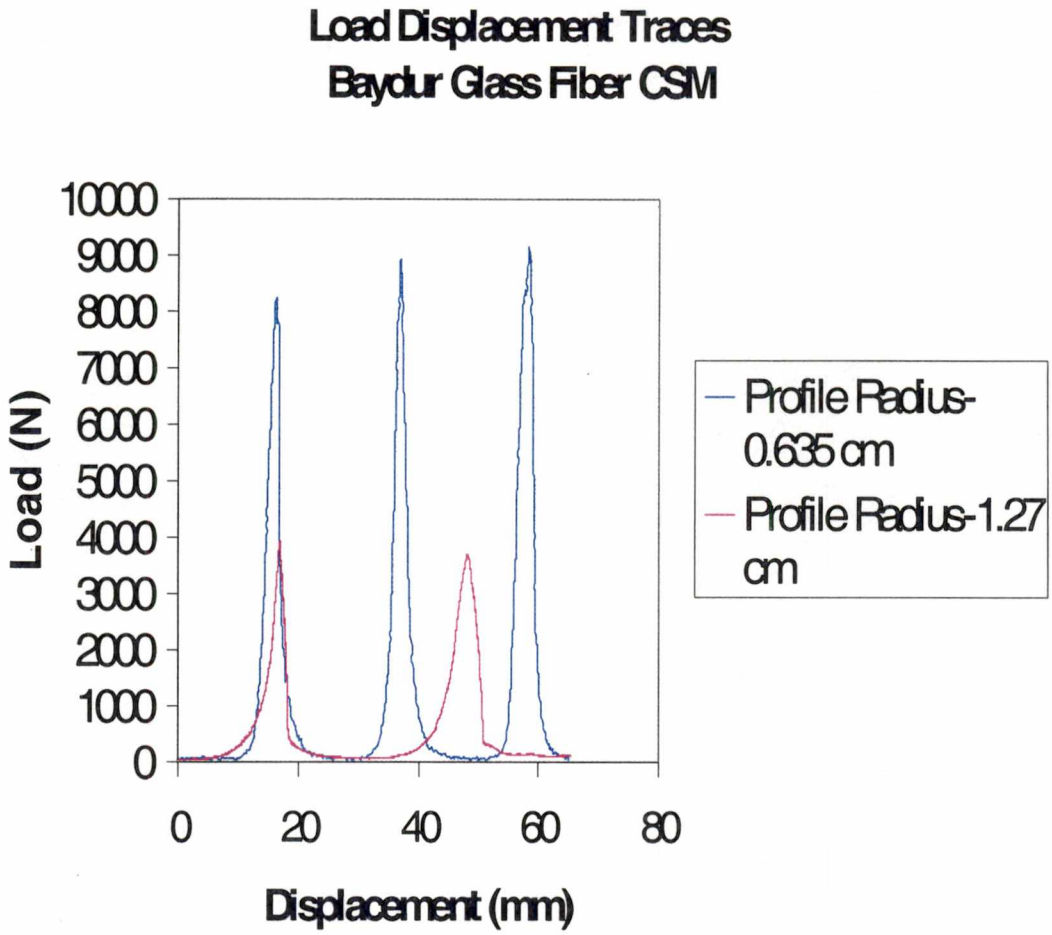

Figure 47. Load Displacement Traces for a Test Conducted with a Profile Block of Radius 0.635 cm and 1.27 cm respectively on CSM.

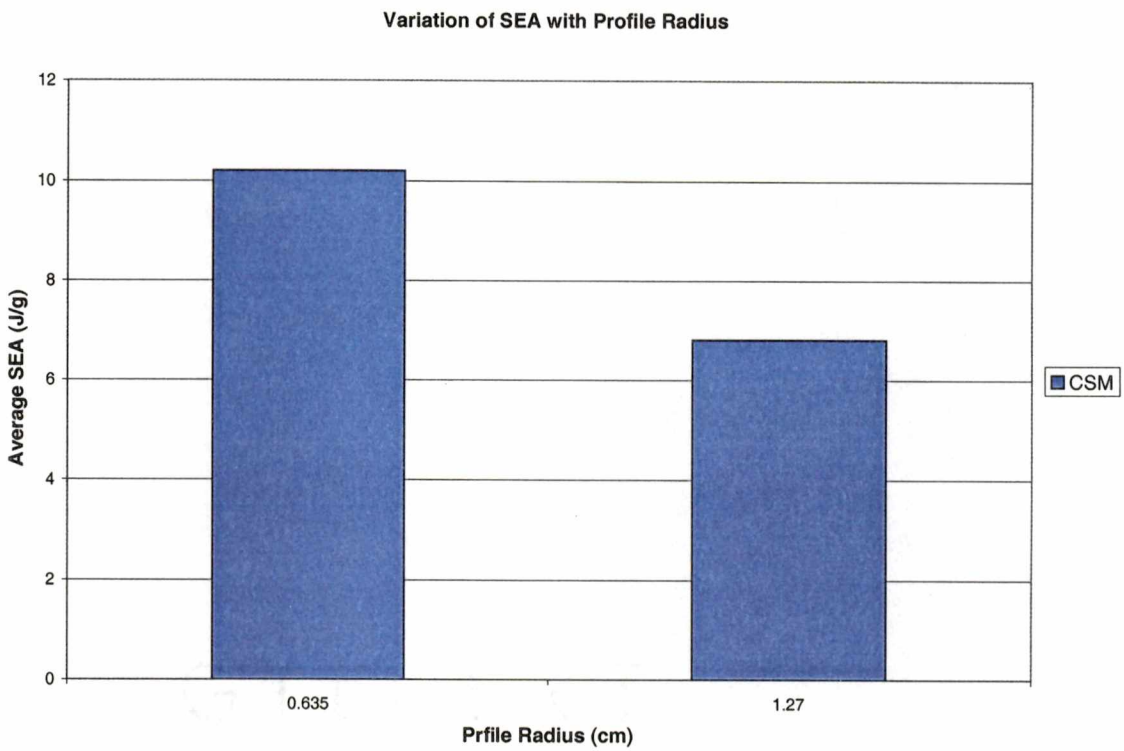

Figure 48. Variation of SEA with Profile Radius for CSM.

Fiber Length: 1 inch

2. Panel Group Name: CCF2

   Fiber Tow Size: 150 gsm (12 K)

   Fiber Volume Fraction: 40%

   Fiber Length: 2 inches

3. Panel Group Name: CCF3

   Fiber Tow Size: 300 gsm (48 K)

   Fiber Volume Fraction: 40%

   Fiber Length: 2 inches

4. Panel Group Name: CCF5

   Fiber Tow Size: 150 gsm (12 K)

   Fiber Volume Fraction: 50%

   Fiber Length: 1 inch

5. Panel Group Name: CCF6

   Fiber Tow Size: 150 gsm (12 K)

   Fiber Volume Fraction: 50%

   Fiber Length: 2 inches

6. Panel Group Name: CCF7

   Fiber Tow Size: 300 gsm (48 K)

   Fiber Volume Fraction: 50%

   Fiber Length: 2 inches

7. Panel Group Name: CCF8

   Fiber Tow Size: 300 gsm (48 K)

Fiber Volume Fraction: 40%

Fiber Length: 1 inch

8. Panel Group Name: CCF9

Fiber Tow Size: 300 gsm (48 K)

Fiber Volume Fraction: 50%

Fiber Length: 1 inch

For all specimens tested, local crushing took place at the chamfered end of the plates. Matrix cracking occurred at the ends of the fiber tows due to stress concentration at these ends. Fiber-matrix debonding also took place in a majority of the specimens that were tested. Flexural deformations controlled the damage process. Some of the test specimens when loaded in the no constraint condition experienced fiber pull out, fiber breakage in the tension side and fiber buckling in the compression side of the specimen. The fracture mechanism that took place in specimens crushed in the loose and tight constraint condition were the same in all of the specimens and the specimen failure was more or less predictable. On the contrary the specimens that were crushed in the no constraint condition fractured in rather erratic fashions and specimen failure was far less predictable. This was due to absence of the much needed roller constraint required to direct the crushing process. Some of the no constraint tests lead to catastrophic failure of the specimen where in the specimen broke in to 2 or 3 pieces. Please see Figure 49.

The specimens tested in the loose and tight constraint conditions generated load deflection curves that were similar to the ones generated during the progressive crushing of composite tubes. It had 4 stages, the first one being characterized by an initial rapid load increase. A rapid load drop occurred in the second stage of the load deflection

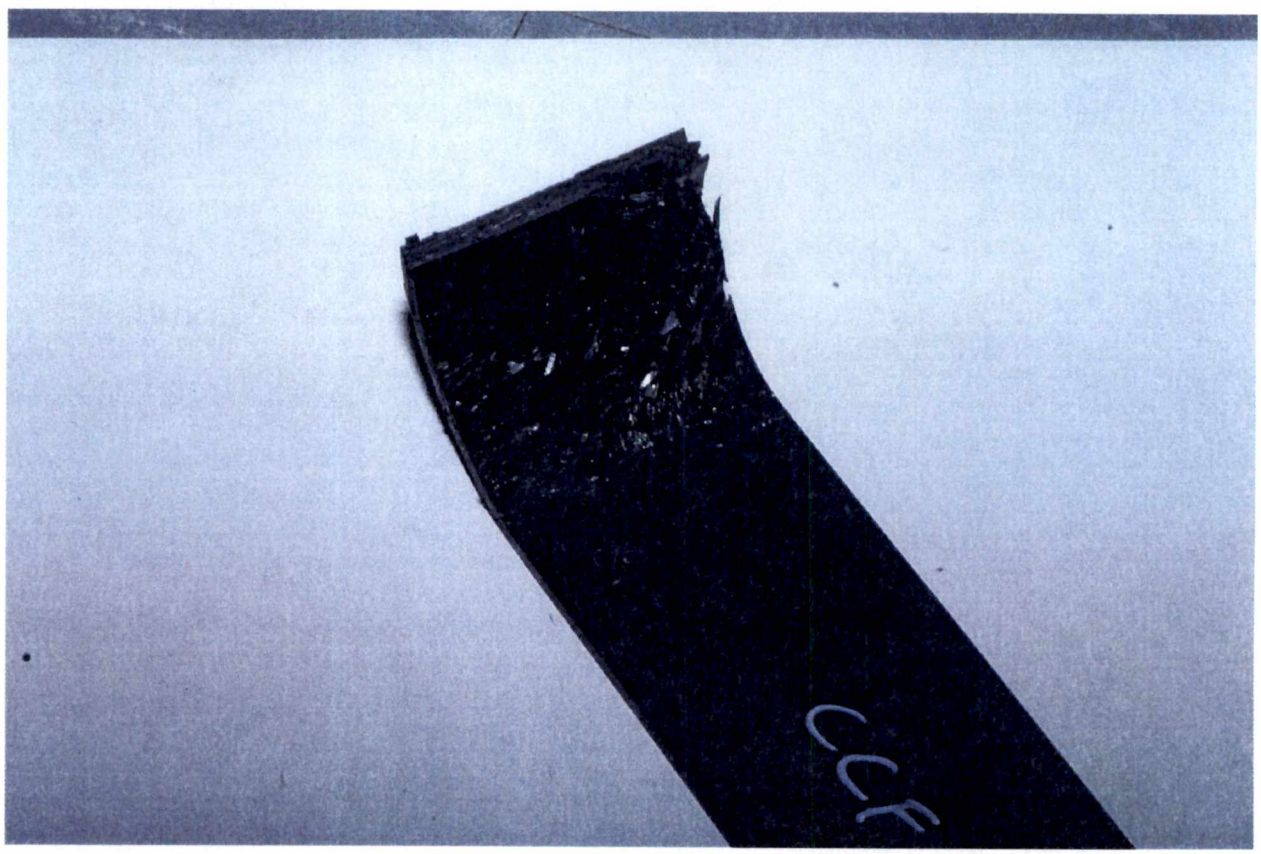

Figure 49. Crushed CCF Specimen.

curve followed by a gradual saturation of the load. The final stage was characterized by stable crushing at a constant mean load. Please see Figure 50. The small load fluctuations and serrations in the fourth stage of the curve are characteristic of stable crushing. The CCF material system recorded the highest initial peak load of all the material systems that were tested. Please see Appendix A to Appendix H in the Appendices, which lists the specific energy absorption, SEA, in all the tests conducted on the CCF material.

3.5.1 Effect of Tow Size

On comparing panel group CCF5 (150 gsm, 50% F.V., 1 inch F.L.) and panel group CCF9 (300 gsm, 50% F.V., 1 inch F.L.), the specific energy absorption of CCF5 was found to be greater than that of CCF9. Please see Appendix D and Appendix H. For a comparison of the load displacement traces recorded for a test conducted on a specimen belonging to panel group CCF5 and on a specimen belonging to panel group CCF9 please see Figure 51.

Panel group CCF1 (150 gsm, 40% F.V., 1 inch F.L.) and panel group CCF8 (300 gsm, 40% F.V., 1 inch F.L.) were also compared. It was found that the specific energy absorption of CCF1 was greater than that of CCF8. Please see Appendix A and Appendix G.

- Hence it was concluded that an increase in tow size caused a decrease in the specific energy absorption for chopped carbon fiber composite materials with 1 inch fiber length. Please see Figure 52 and Figure 53.

But on comparing panel group CCF6 (150 gsm, 50% F.V., 2 inch F.L.) and panel group CCF7 (300 gsm, 50% F.V., 2 inch F.L.), the specific energy absorption of

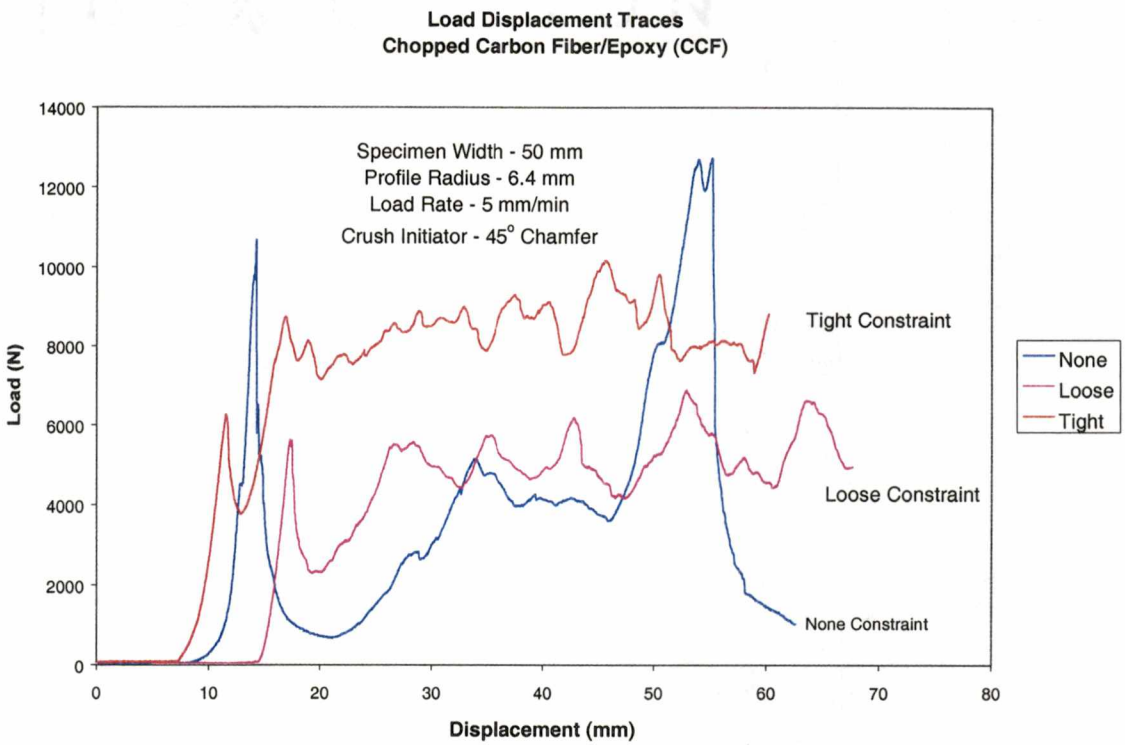

Figure 50. Load Displacement Traces for CCF.

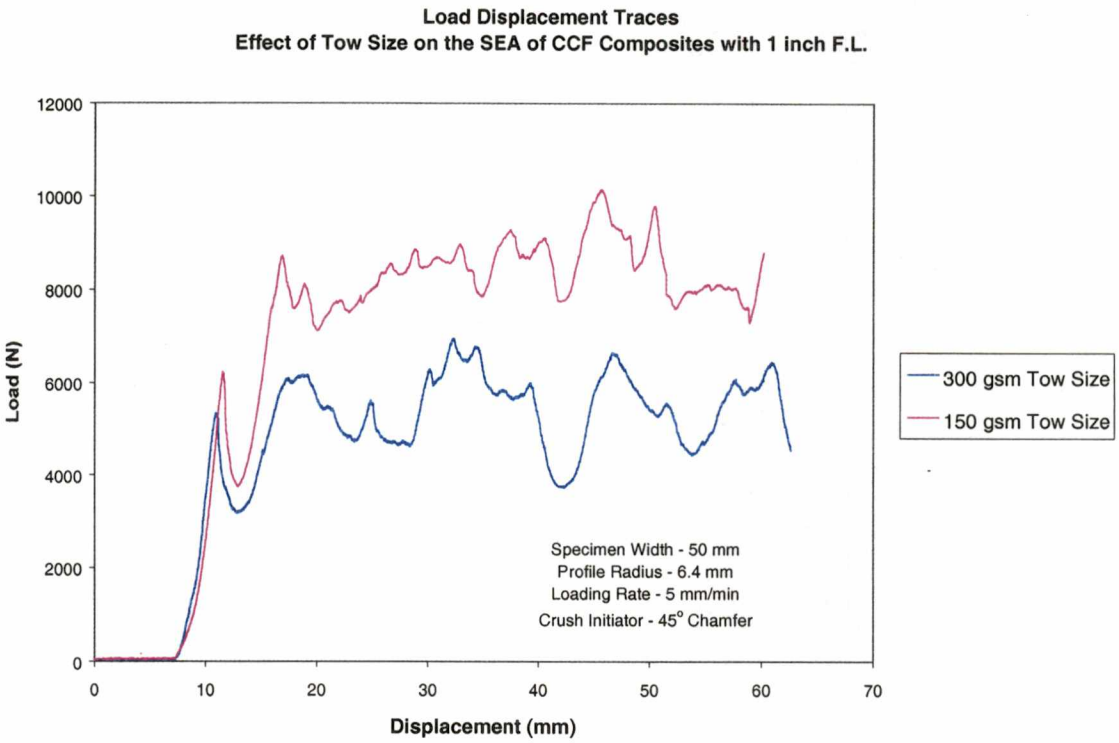

Figure 51. Load Displacement Traces Representing the Effect of Tow Size on the SEA of CCF with 1 inch Fiber Length.

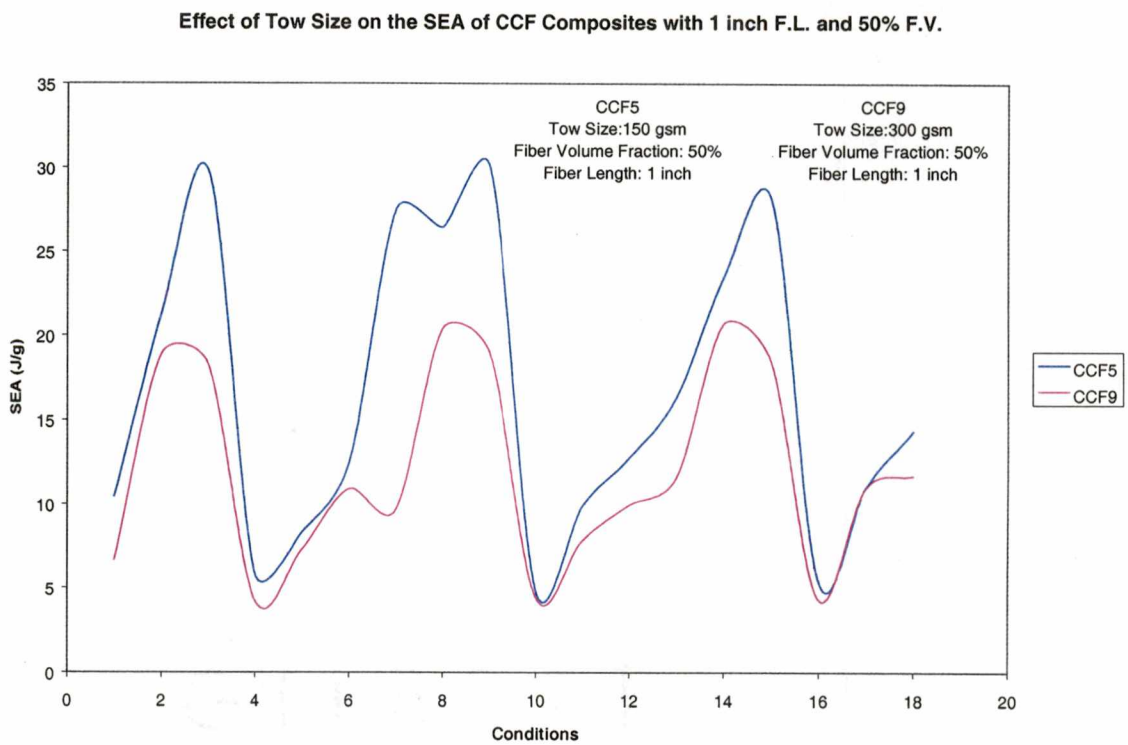

Figure 52. Effect of Tow Size on the SEA of CCF with 1 inch F.L. and 50% F.V..

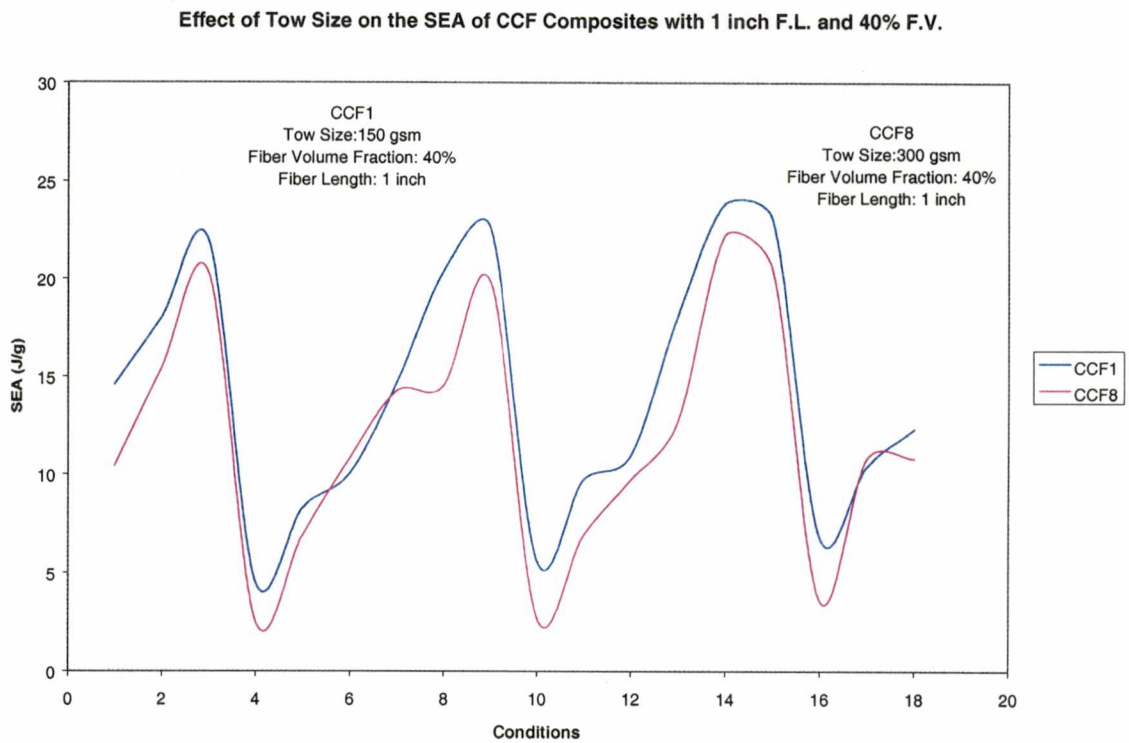

Figure 53. Effect of Tow Size on the SEA of CCF with 1 inch F.L. and 40% F.V..

CCF6 was found to be neither more nor less than the specific energy absorption of CCF7 for all conditions of specimen width, type of constraint and profile radius. Please see Appendix E and Appendix F. For a comparison of the load displacement traces recorded for a test conducted on a specimen belonging to panel group CCF6 and on a specimen belonging to panel group CCF7 please see Figure 54.

Similarly on comparing panel group CCF2 (150 gsm, 40% F.V., 2 inch F.L.) and panel group CCF3 (300 gsm, 40% F.V., 2 inch F.L.), the specific energy absorption of CCF2 was found to be neither more nor less than the specific energy absorption of CCF3 for all conditions of specimen width, type of constraint and profile radius. Please see Appendix B and Appendix C.

- Hence it was concluded that there was no serious effect of change in tow size on the specific energy absorption for chopped carbon fiber composite materials with fiber length of 2 inches. Please see Figure 55 and Figure 56.

For Figure 52, Figure 53, Figure 55 and Figure 56 the following are the details of the Y and X axis.

Y axis: Specific Energy Absorption (SEA)

X axis: Condition

1. Specimen Width: 1.27 cm (0.5 inches), Profile Radius: 0.635 cm (0.25 inches), No Constraint
2. Specimen Width: 1.27 cm (0.5 inches), Profile Radius: 0.635 cm (0.25 inches), Loose Constraint
3. Specimen Width: 1.27 cm (0.5 inches), Profile Radius: 0.635 cm (0.25 inches), Tight Constraint

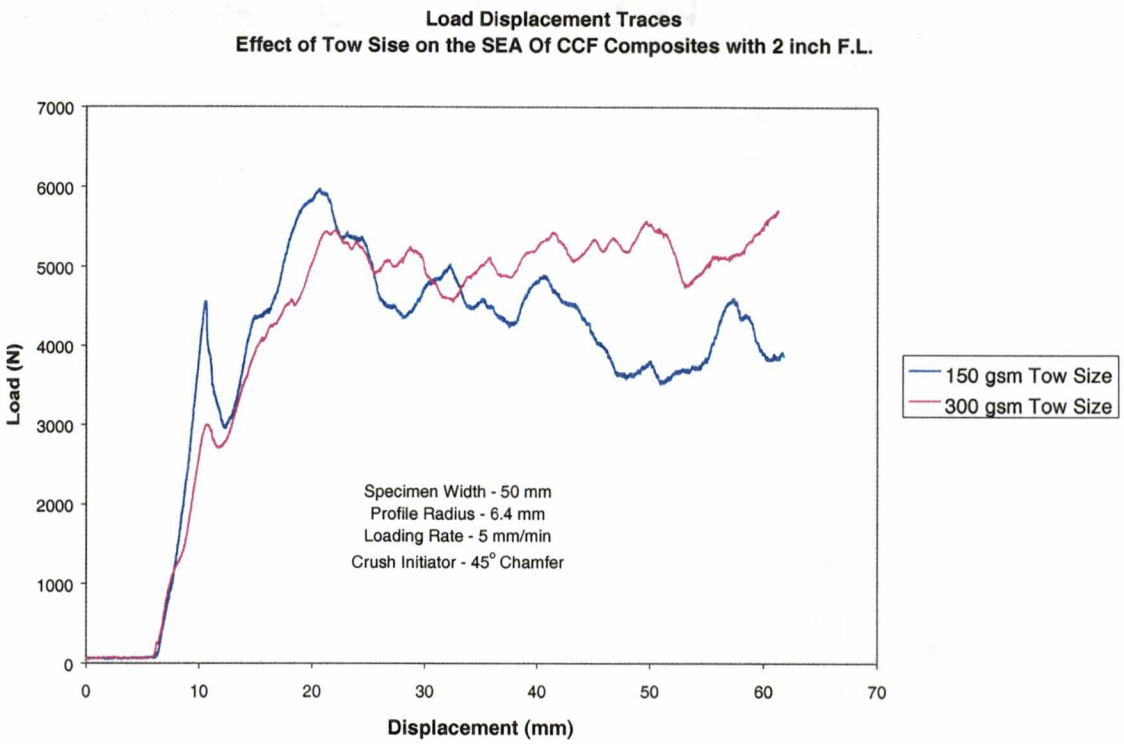

Figure 54. Load Displacement Traces Representing the Effect of Tow Size on the SEA of CCF with 2 inch Fiber Length.

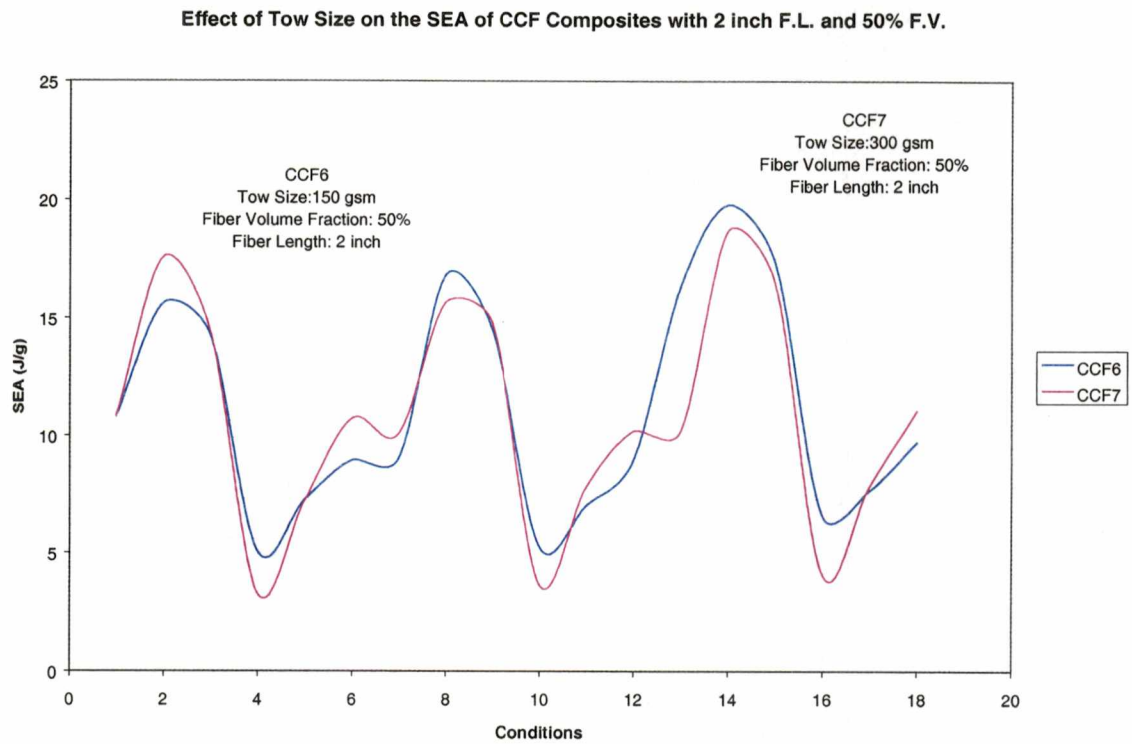

Figure 55. Effect of Tow Size on the SEA of CCF with 2 inch F.L. and 50% F.V..

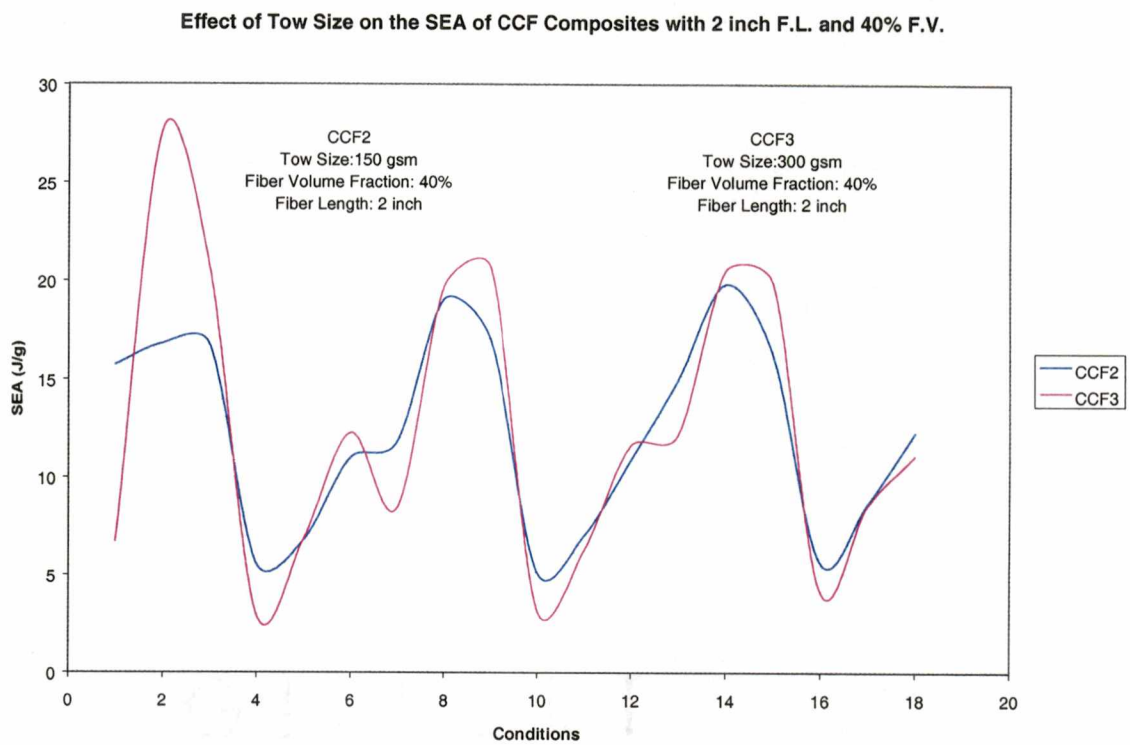

Figure 56. Effect of Tow Size on the SEA of CCF with 2 inch F.L. and 40% F.V..

4. Specimen Width: 1.27 cm (0.5 inches), Profile Radius: 1.27 cm (0.5 inches), No Constraint
5. Specimen Width: 1.27 cm (0.5 inches), Profile Radius: 1.27 cm (0.5 inches), Loose Constraint
6. Specimen Width: 1.27 cm (0.5 inches), Profile Radius: 1.27 cm (0.5 inches), Tight Constraint
7. Specimen Width: 2.54 cm (1.0 inch), Profile Radius: 0.635 cm (0.25 inches), No Constraint
8. Specimen Width: 2.54 cm (1.0 inch), Profile Radius: 0.635 cm (0.25 inches), Loose Constraint
9. Specimen Width: 2.54 cm (1.0 inch), Profile Radius: 0.635 cm (0.25 inches), Tight Constraint
10. Specimen Width: 2.54 cm (1.0 inch), Profile Radius: 1.27 cm (0.5 inches), No Constraint
11. Specimen Width: 2.54 cm (1.0 inch), Profile Radius: 1.27 cm (0.5 inches), Loose Constraint
12. Specimen Width: 2.54 cm (1.0 inch), Profile Radius: 1.27 cm (0.5 inches), Tight Constraint
13. Specimen Width: 5.08 cm (2.0 inches), Profile Radius: 0.635 cm (0.25 inches), No Constraint
14. Specimen Width: 5.08 cm (2.0 inches), Profile Radius: 0.635 cm (0.25 inches), Loose Constraint

15. Specimen Width: 5.08 cm (2.0 inches), Profile Radius: 0.635 cm (0.25 inches), Tight Constraint
16. Specimen Width: 5.08 cm (2.0 inches), Profile Radius: 1.27 cm (0.5 inches), No Constraint
17. Specimen Width: 5.08 cm (2.0 inches), Profile Radius: 1.27 cm (0.5 inches), Loose Constraint
18. Specimen Width: 5.08 cm (2.0 inches), Profile Radius: 1.27 cm (0.5 inches), Tight Constraint

3.5.2 Effect of Fiber Volume Fraction

On comparing panel group CCF2 (150 gsm, 40% F.V., 2 inch F.L.) and panel group CCF6 (150 gsm, 50% F.V., 2 inch F.L.), the specific energy absorption of CCF2 was found to be greater than that of CCF6. Please see Appendix B and Appendix E. Panel group CCF3 (300 gsm, 40% F.V., 2 inch F.L.) and panel group CCF7 (300 gsm, 50% F.V., 2 inch F.L.) were also compared. It was found that the specific energy absorption of CCF3 was greater than that of CCF7. Please see Appendix C and Appendix F. For a comparison of the load displacement traces recorded for a test conducted on a specimen belonging to panel group CCF3 and on a specimen belonging to panel group CCF7 please see Figure 57.

- Hence it was concluded that an increase in fiber volume fraction caused a decrease in the specific energy absorption for chopped carbon fiber composite materials with fiber length of 2 inches. Please see Figure 58 and Figure 59.

But on comparing panel group CCF5 (150 gsm, 50% F.V., 1 inch F.L.) and panel group CCF1 (150 gsm, 40% F.V., 1 inch F.L.) one found the specific energy

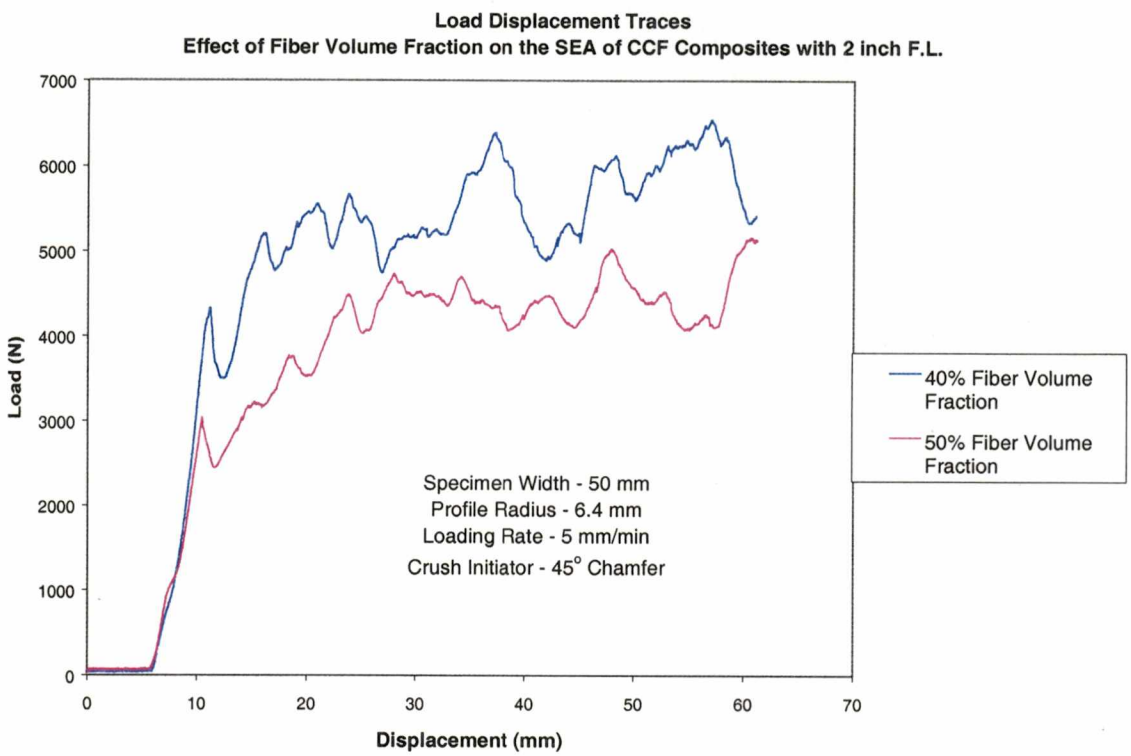

Figure 57. Load Displacement Traces Representing the Effect of Fiber Volume Fraction on the SEA of CCF with 2 inch Fiber Length.

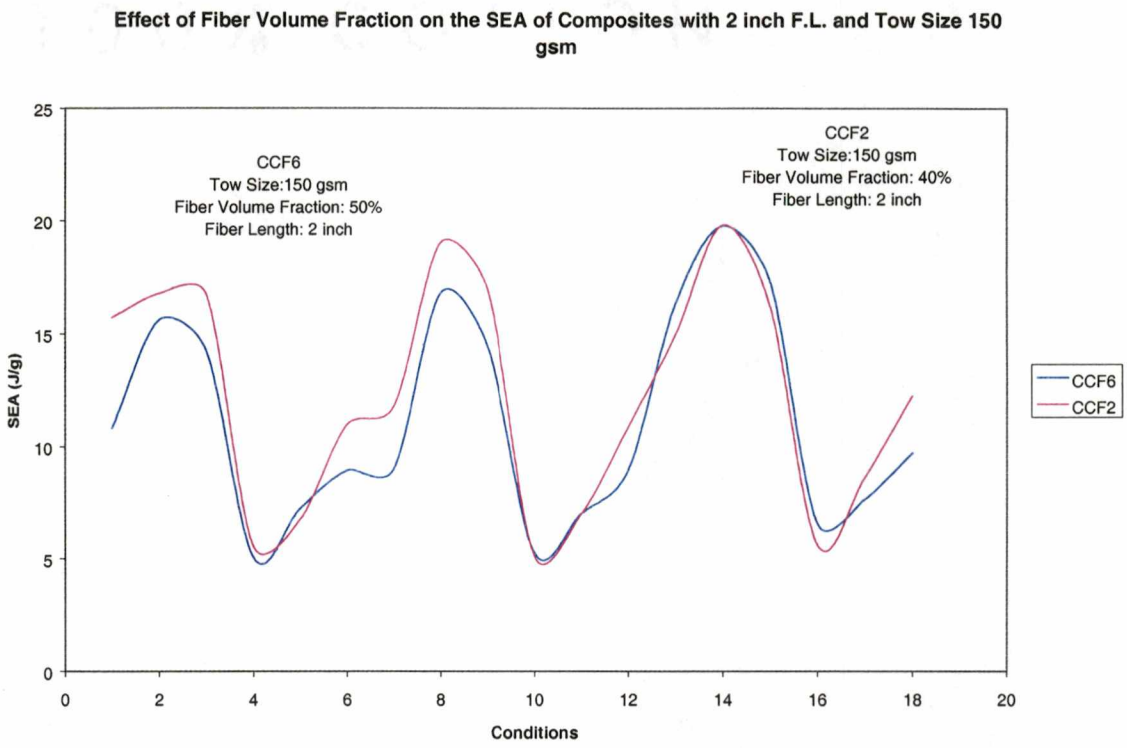

Figure 58. Effect of F.V. on SEA of CCF with 2 inch F.L. and Tow Size 150 gsm.

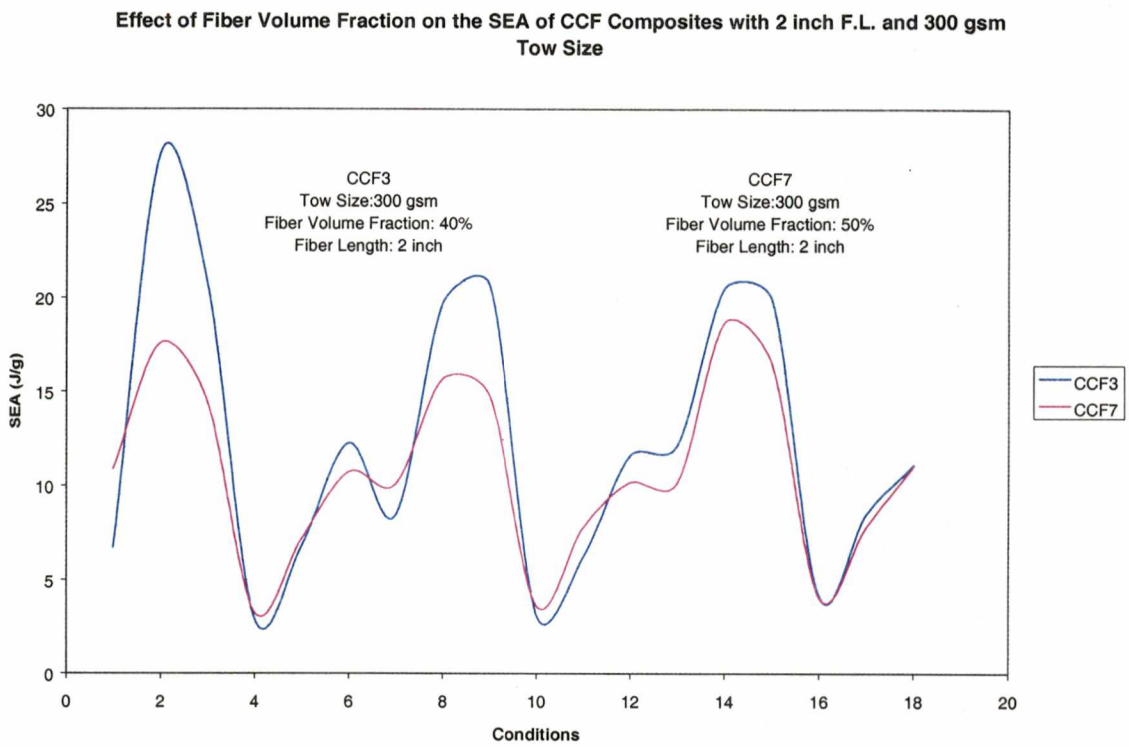

Figure 59. Effect of F.V. on SEA of CCF with 2 inch F.L. and Tow Size 300 gsm.

absorption of CCF5 to be greater than that of CCF1. Please see Appendix D and Appendix A. For a comparison of the load displacement traces recorded for a test conducted on a specimen belonging to panel group CCF5 and on a specimen belonging to panel group CCF1 please see Figure 60.

- Hence it was concluded that an increase in fiber volume fraction caused an increase in the specific energy absorption for chopped carbon fiber composite materials with 1 inch fiber length. Please see Figure 61.

One also compared panel group CCF9 (300 gsm, 50% F.V., 1 inch F.L.) and panel group CCF8 (300 gsm, 40% F.V., 1 inch F.L.). But the specific energy absorption of CCF9 was found to be neither more nor less than the specific energy absorption of CCF8 for all conditions of specimen width, type of Constraint and profile radius. Please see Appendix H, Appendix G and Figure 62.

For Figure 58, Figure 59, Figure 61 and Figure 62 the following are the details of the Y and X axis.

Y axis: Specific Energy Absorption (SEA)

X axis: Condition

1 Specimen Width: 1.27 cm (0.5 inches), Profile Radius: 0.635 cm (0.25 inches), No Constraint

2 Specimen Width: 1.27 cm (0.5 inches), Profile Radius: 0.635 cm (0.25 inches), Loose Constraint

3 Specimen Width: 1.27 cm (0.5 inches), Profile Radius: 0.635 cm (0.25 inches), Tight Constraint

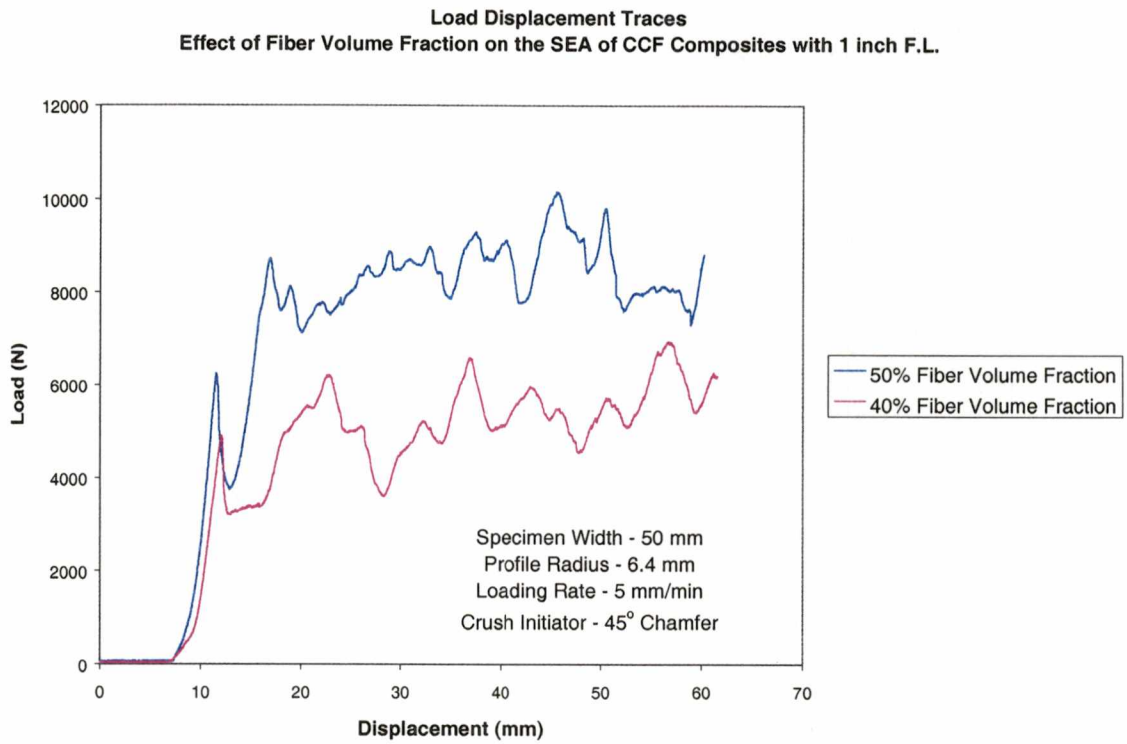

Figure 60. Load Displacement Traces Representing the Effect of Fiber Volume Fraction on the SEA of CCF with 1 inch Fiber Length.

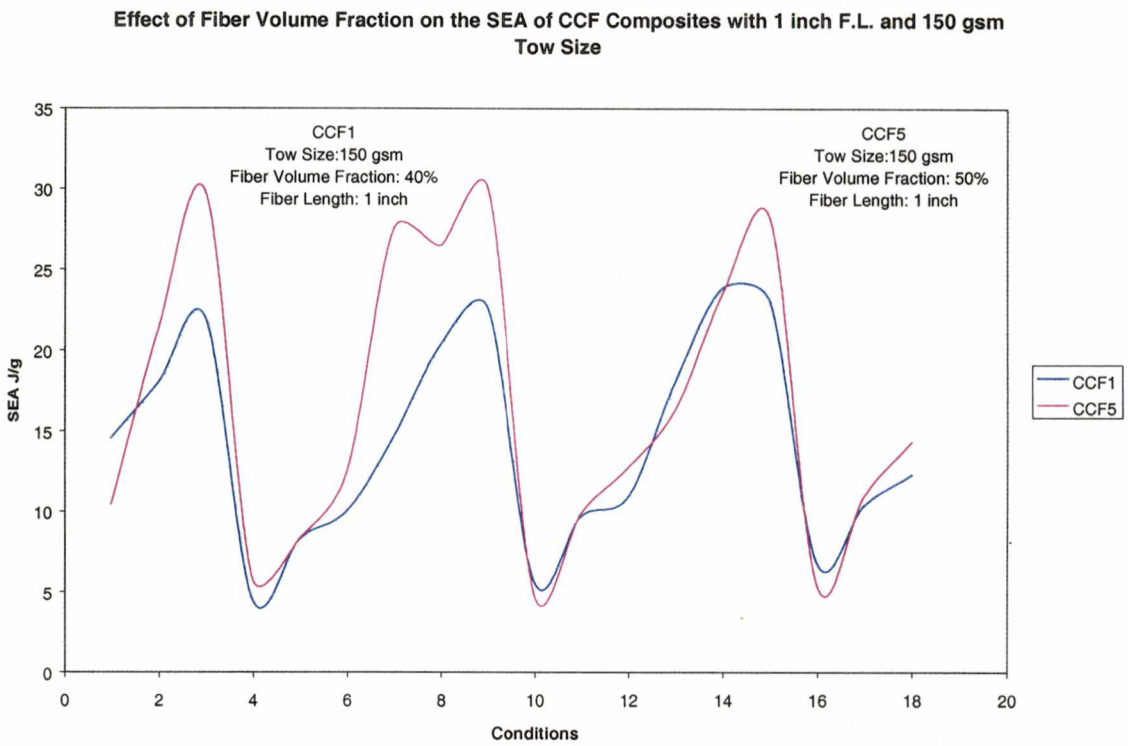

Figure 61. Effect of F.V. on SEA of CCF with 1 inch F.L. and Tow Size 150 gsm.

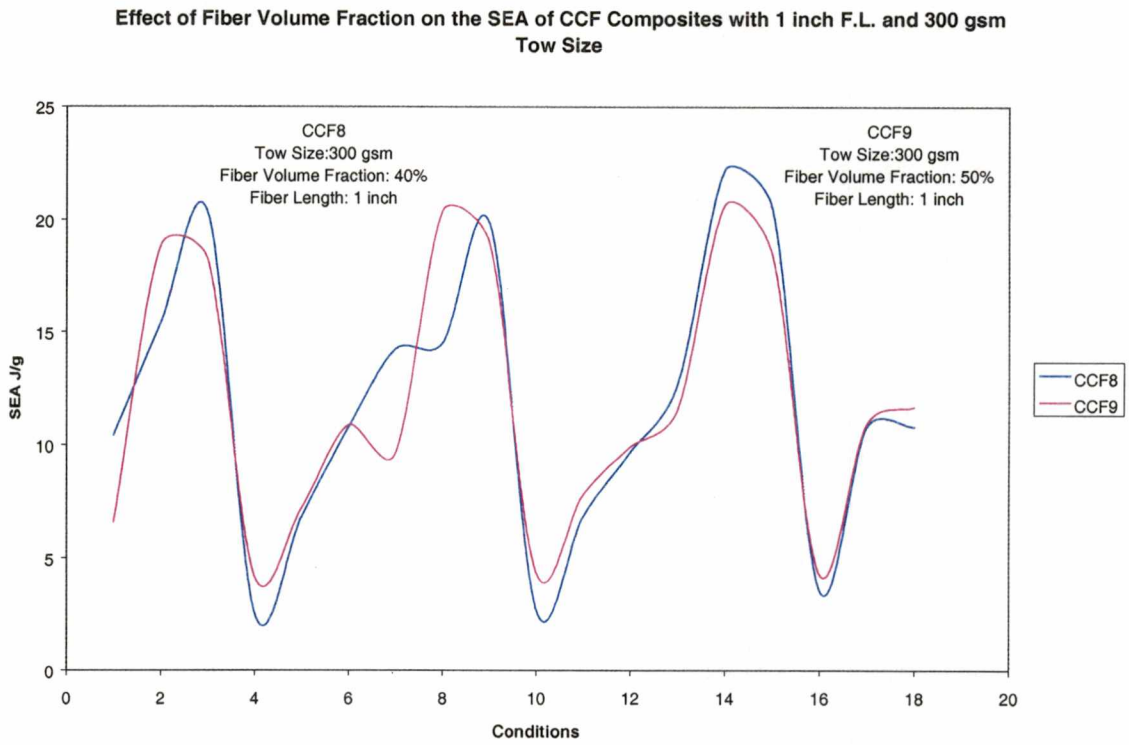

Figure 62. Effect of F.V. on SEA of CCF with 1 inch F.L. and Tow Size 300 gsm.

4 Specimen Width: 1.27 cm (0.5 inches), Profile Radius: 1.27 cm (0.5 inches), No Constraint

5 Specimen Width: 1.27 cm (0.5 inches), Profile Radius: 1.27 cm (0.5 inches), Loose Constraint

6 Specimen Width: 1.27 cm (0.5 inches), Profile Radius: 1.27 cm (0.5 inches), Tight Constraint

7 Specimen Width: 2.54 cm (1.0 inch), Profile Radius: 0.635 cm (0.25 inches), No Constraint

8 Specimen Width: 2.54 cm (1.0 inch), Profile Radius: 0.635 cm (0.25 inches), Loose Constraint

9 Specimen Width: 2.54 cm (1.0 inch), Profile Radius: 0.635 cm (0.25 inches), Tight Constraint

10 Specimen Width: 2.54 cm (1.0 inch), Profile Radius: 1.27 cm (0.5 inches), No Constraint

11 Specimen Width: 2.54 cm (1.0 inch), Profile Radius: 1.27 cm (0.5 inches), Loose Constraint

12 Specimen Width: 2.54 cm (1.0 inch), Profile Radius: 1.27 cm (0.5 inches), Tight Constraint

13 Specimen Width: 5.08 cm (2.0 inches), Profile Radius: 0.635 cm (0.25 inches), No Constraint

14 Specimen Width: 5.08 cm (2.0 inches), Profile Radius: 0.635 cm (0.25 inches), Loose Constraint

15 Specimen Width: 5.08 cm (2.0 inches), Profile Radius: 0.635 cm (0.25 inches), Tight Constraint

16 Specimen Width: 5.08 cm (2.0 inches), Profile Radius: 1.27 cm (0.5 inches), No Constraint

17 Specimen Width: 5.08 cm (2.0 inches), Profile Radius: 1.27 cm (0.5 inches), Loose Constraint

18 Specimen Width: 5.08 cm (2.0 inches), Profile Radius: 1.27 cm (0.5 inches), Tight Constraint

3.5.3 Effect of Fiber Length

On comparing panel group CCF5 (150 gsm, 50% F.V., 1 inch F.L.) and panel group CCF6 (150 gsm, 50% F.V., 2 inch F.L.), the specific energy absorption of CCF5 was found to be greater than that of CCF6. Please see Appendix D and Appendix E. For a comparison of the load displacement traces recorded for a test conducted on a specimen belonging to panel group CCF5 and on a specimen belonging to panel group CCF6 please see Figure 63.

Panel group CCF1 (150 gsm, 40% F.V., 1 inch F.L.) and panel group CCF2 (150 gsm, 40% F.V., 2 inch F.L.) were also compared. It was found that the specific energy absorption of CCF1 was greater than that of CCF2. Please see Appendix A and Appendix B.

- Hence it was concluded that an increase in fiber length caused a decrease in the specific energy absorption for chopped carbon fiber composite materials with 150 gsm tow Size. Please see Figure 64 and Figure 65.

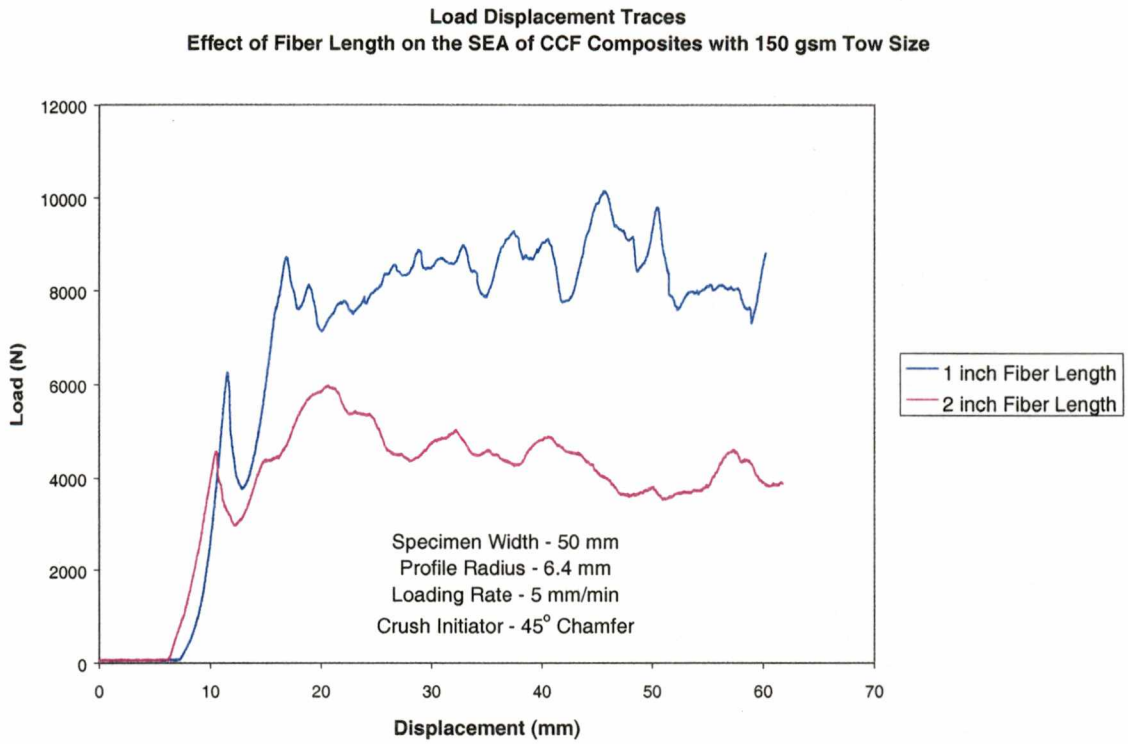

Figure 63. Load Displacement Traces Representing the Effect of Fiber Length on the SEA of CCF with 150 gsm Tow Size.

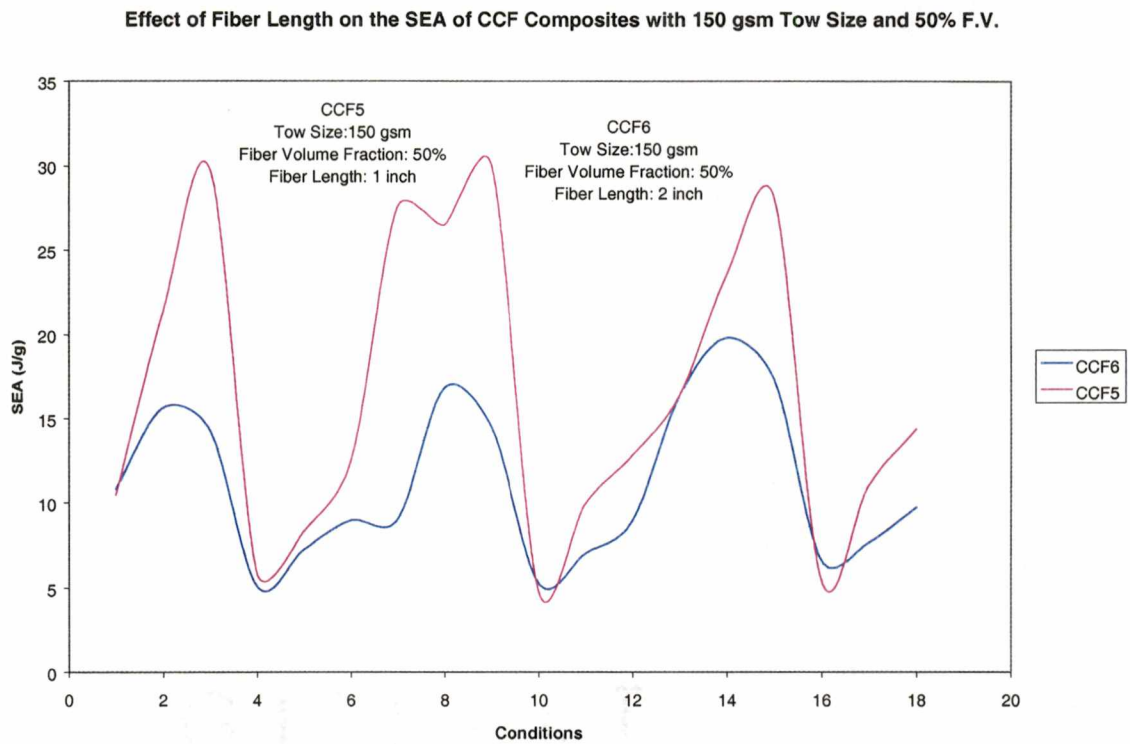

Figure 64. Effect of F.L. on the SEA of CCF with 150 gsm Tow Size and 50% F.V..

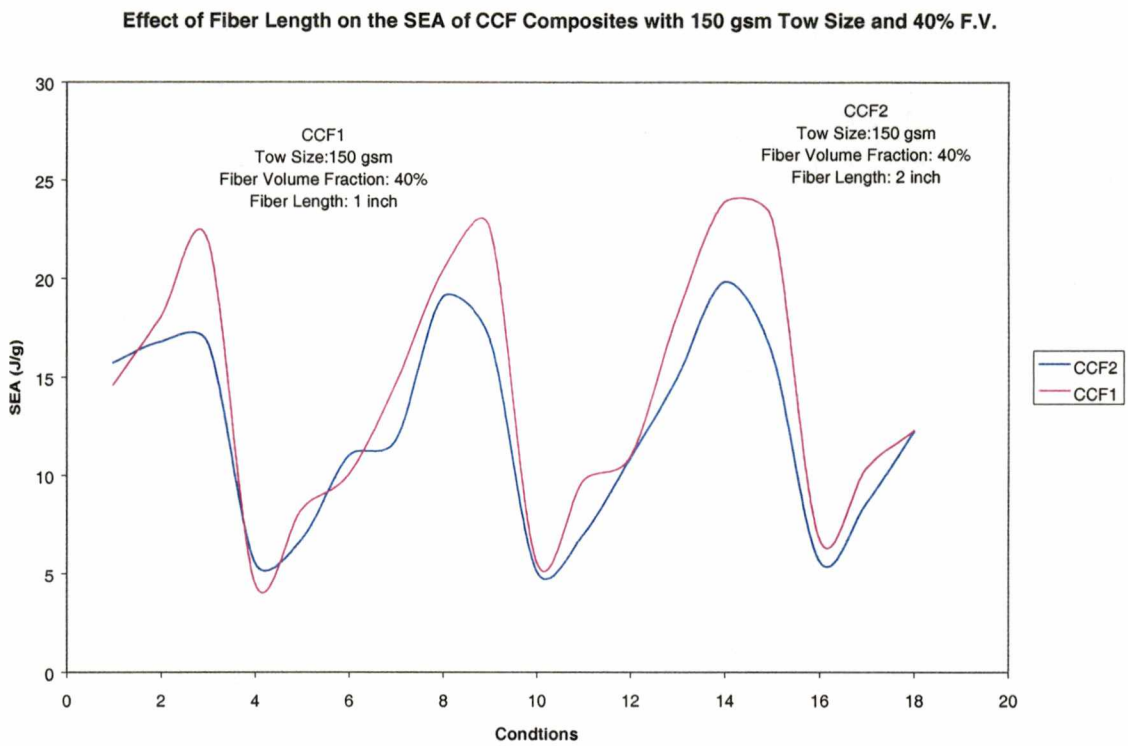

Figure 65. Effect of F.L. on the SEA of CCF with 150 gsm Tow Size and 40% F.V..

One also compared panel group CCF9 (300 gsm, 50% F.V., 1 inch F.L.) and panel group CCF7 (300 gsm, 50% F.V., 2 inch F.L.) to find the specific energy absorption of CCF9 to be greater than that of CCF7. Please see Appendix H and Appendix F. For a comparison of the load displacement traces recorded for a test conducted on a specimen belonging to panel group CCF9 and on a specimen belonging to panel group CCF7 please see Figure 66.

- Hence it was concluded that an increase in fiber length caused a decrease in the specific energy absorption for chopped carbon fiber composite materials with 300 gsm tow size. Please see Figure 67.

But on comparing panel group CCF8 (300 gsm, 40% F.V., 1 inch F.L.) and panel group CCF3 (300 gsm, 40% F.V., 2 inch F.L.), the specific energy absorption of CCF8 was found to be neither more nor less than the specific energy absorption of CCF3 for all conditions of specimen width, type of constraint and Profile Radius. Please see Appendix C, Appendix G and Figure 68.

For Figure 64, Figure 65, Figure 67 and Figure 68 the following are the details of the Y and X axis.

Y axis: Specific Energy Absorption (SEA)

X axis: Condition

1 Specimen Width: 1.27 cm (0.5 inches), Profile Radius: 0.635 cm (0.25 inches), No Constraint

2 Specimen Width: 1.27 cm (0.5 inches), Profile Radius: 0.635 cm (0.25 inches), Loose Constraint

3 Specimen Width: 1.27 cm (0.5 inches), Profile Radius: 0.635 cm (0.25 inches), Tight

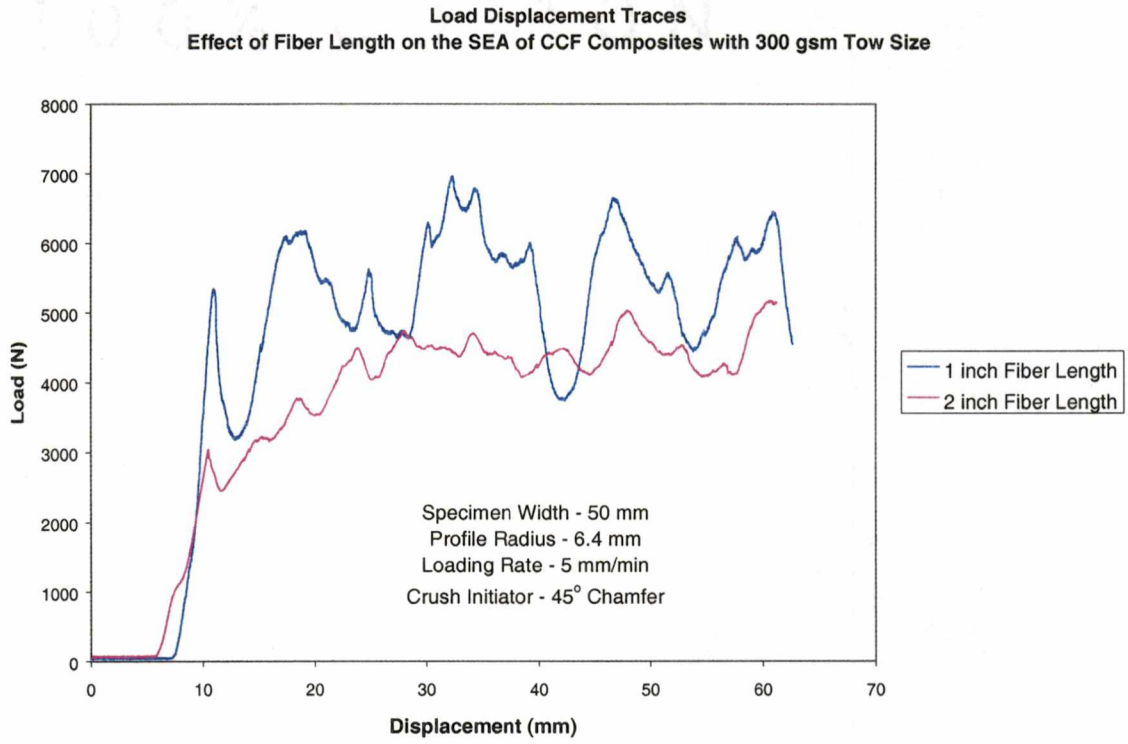

Figure 66. Load Displacement Traces Representing the Effect of Fiber Length on the SEA of CCF with 300 gsm Tow Size.

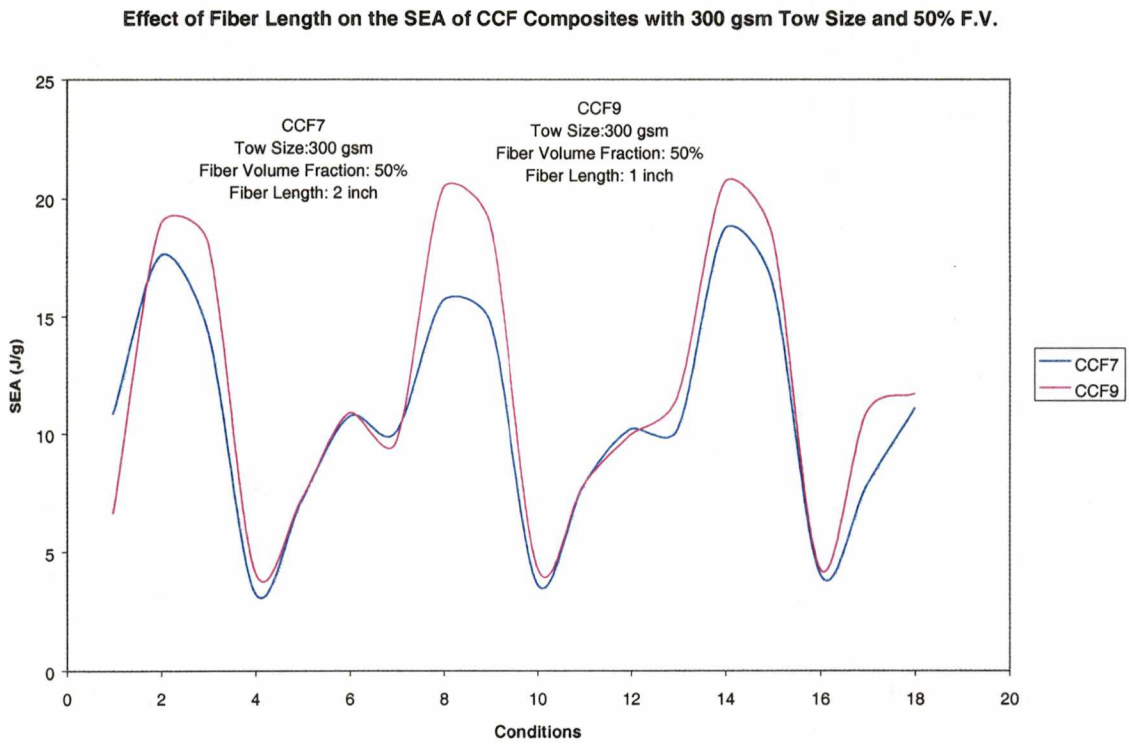

Figure 67. Effect of F.L. on the SEA of CCF with 300 gsm Tow Size and 50% F.V..

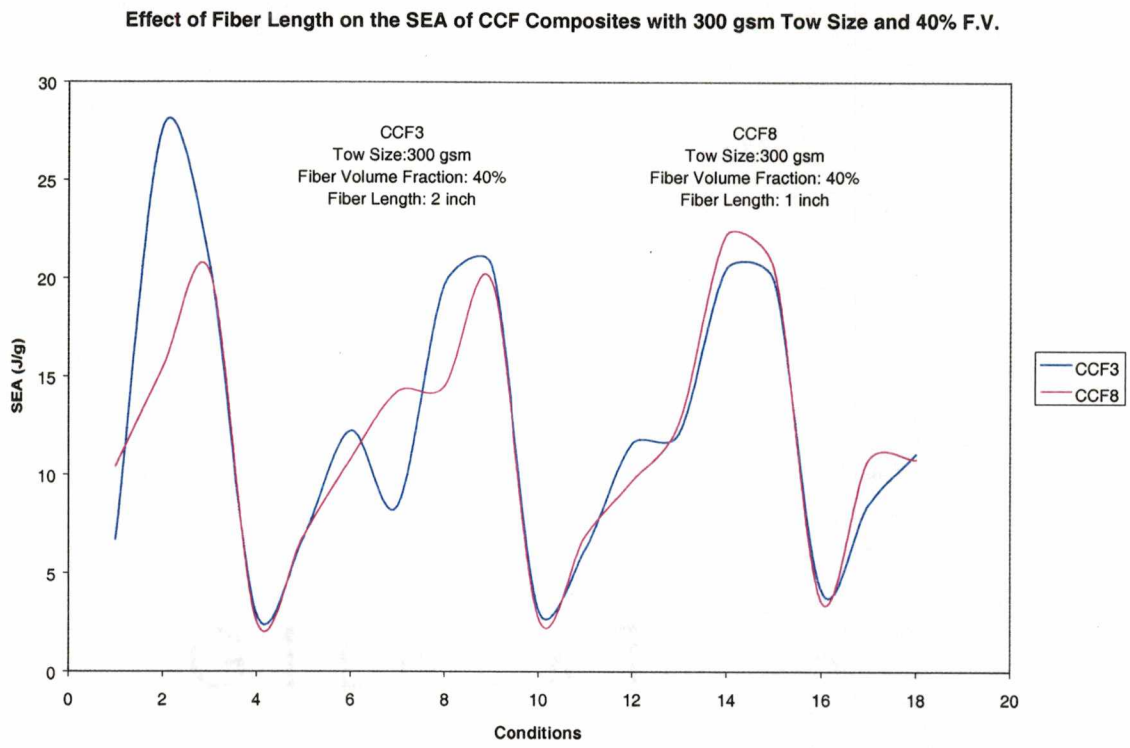

Figure 68. Effect of F.L. on the SEA of CCF with 300 gsm Tow Size and 40% F.V..

Constraint

4 Specimen Width: 1.27 cm (0.5 inches), Profile Radius: 1.27 cm (0.5 inches), No Constraint

5 Specimen Width: 1.27 cm (0.5 inches), Profile Radius: 1.27 cm (0.5 inches), Loose Constraint

6 Specimen Width: 1.27 cm (0.5 inches), Profile Radius: 1.27 cm (0.5 inches), Tight Constraint

7 Specimen Width: 2.54 cm (1.0 inch), Profile Radius: 0.635 cm (0.25 inches), No Constraint

8 Specimen Width: 2.54 cm (1.0 inch), Profile Radius: 0.635 cm (0.25 inches), Loose Constraint

9 Specimen Width: 2.54 cm (1.0 inch), Profile Radius: 0.635 cm (0.25 inches), Tight Constraint

10 Specimen Width: 2.54 cm (1.0 inch), Profile Radius: 1.27 cm (0.5 inches), No Constraint

11 Specimen Width: 2.54 cm (1.0 inch), Profile Radius: 1.27 cm (0.5 inches), Loose Constraint

12 Specimen Width: 2.54 cm (1.0 inch), Profile Radius: 1.27 cm (0.5 inches), Tight Constraint

13 Specimen Width: 5.08 cm (2.0 inches), Profile Radius: 0.635 cm (0.25 inches), No Constraint

14 Specimen Width: 5.08 cm (2.0 inches), Profile Radius: 0.635 cm (0.25 inches), Loose Constraint

15 Specimen Width: 5.08 cm (2.0 inches), Profile Radius: 0.635 cm (0.25 inches), Tight Constraint

16 Specimen Width: 5.08 cm (2.0 inches), Profile Radius: 1.27 cm (0.5 inches), No Constraint

17 Specimen Width: 5.08 cm (2.0 inches), Profile Radius: 1.27 cm (0.5 inches), Loose Constraint

18 Specimen Width: 5.08 cm (2.0 inches), Profile Radius: 1.27 cm (0.5 inches), Tight Constraint

Previous studies on the effect of fiber length on the energy absorption capabilities of composite plates have reported an increase in the specific energy absorption, SEA, with increased fiber lengths. As mentioned already, it was observed that an increase in fiber length from 1 inch to 2 inches caused a decrease in the specific energy absorption, SEA, for the compression molded chopped carbon fiber plates up to a factor of 2. This led to the conclusion that for compression molded chopped carbon fiber composites there was a decrease in the SEA with increased fiber lengths. The reason for this variation from the expected belief on how fiber length affects the SEA is speculated to be the result of the poor molding quality of the CCF plates causing poor fiber wetting by the resin, voids and holes, resin rich areas and poor continuity in the plate structure.

3.5.4 Effect of Profile Radius

In all the tests performed on chopped carbon fiber composite materials, irrespective of the specimen width or the constraint condition, an increase in the profile radius caused a decrease in the specific energy absorption, SEA. Please see Appendix D. For a comparison of the load displacement traces recorded for a test conducted on a

specimen using a profile bock of radius 0.635 cm and on a specimen using a profile block of radius 1.27 cm please see Figure 69.

The decrease in SEA with an increase in the profile radius is due to the fact that a specimen loaded in compression is crushed through the contact profile as defined by the profile block and it follows a smoother curve when the profile block has a radius of 1.27 cm as when compared to a radius of 0.635 cm. Therefore less energy is absorbed in bending it.

Please see Figure 70. The following are the details of Figure 70.

Series: Profile Radius = 0.635 cm

Y axis: Specific Energy Absorption (SEA)

X axis: Condition

1 Specimen Width: 1.27 cm (0.5 inches), Profile Radius: 0.635 cm (0.25 inches), No Constraint

2 Specimen Width: 1.27 cm (0.5 inches), Profile Radius: 0.635 cm (0.25 inches), Loose Constraint

3 Specimen Width: 1.27 cm (0.5 inches), Profile Radius: 0.635 cm (0.25 inches), Tight Constraint

4 Specimen Width: 2.54 cm (1.0 inch), Profile Radius: 0.635 cm (0.25 inches), No Constraint

5 Specimen Width: 2.54 cm (1.0 inch), Profile Radius: 0.635 cm (0.25 inches), Loose Constraint

6 Specimen Width: 2.54 cm (1.0 inch), Profile Radius: 0.635 cm (0.25 inches), Tight Constraint

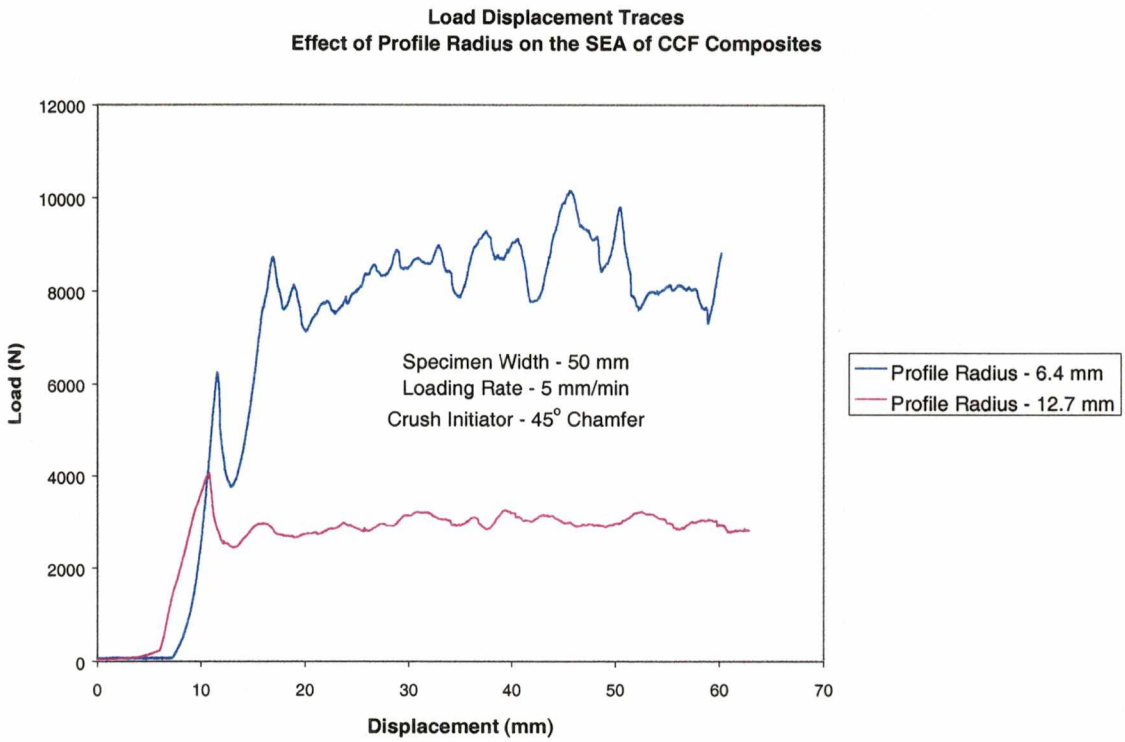

Figure 69. Load Displacement Traces Representing the Effect of Profile Radius on the SEA of CCF.

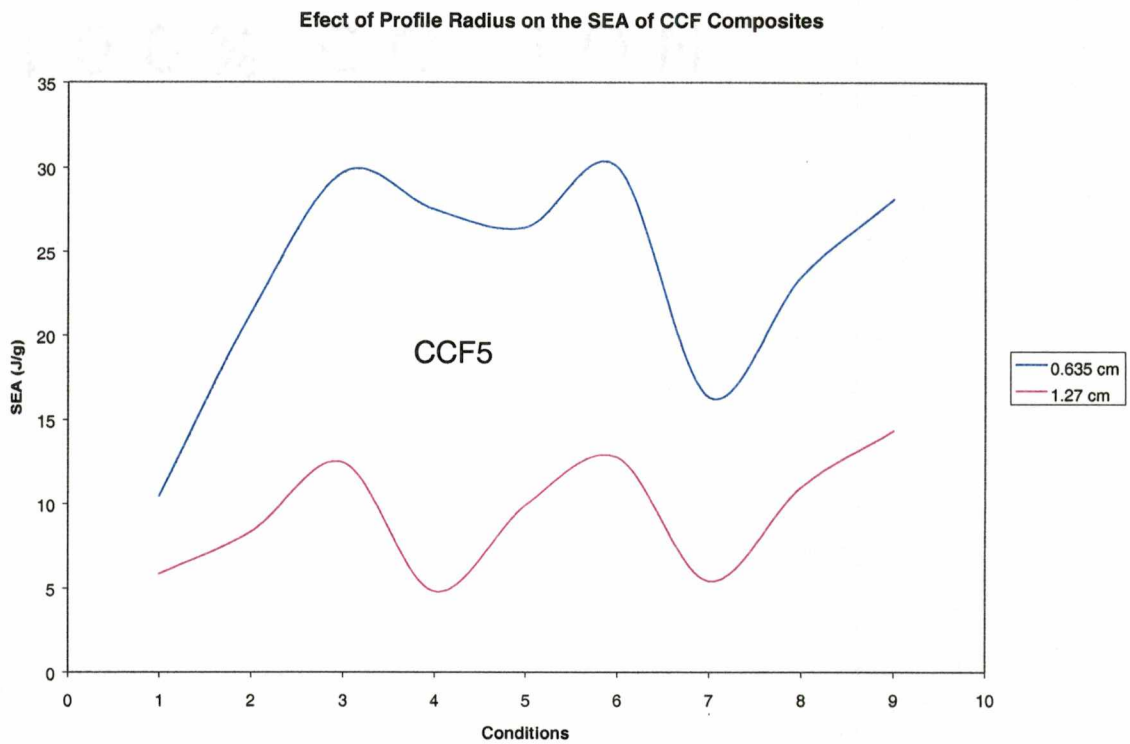

Figure 70. Variation of SEA with Profile Radius for CCF.

7 Specimen Width: 5.08 cm (2.0 inches), Profile Radius: 0.635 cm (0.25 inches), No Constraint

8 Specimen Width: 5.08 cm (2.0 inches), Profile Radius: 0.635 cm (0.25 inches), Loose Constraint

9 Specimen Width: 5.08 cm (2.0 inches), Profile Radius: 0.635 cm (0.25 inches), Tight Constraint

Series: Profile Radius = 1.27 cm

Y axis: Specific Energy Absorption (SEA)

X axis: Condition

1. Specimen Width: 1.27 cm (0.5 inches), Profile Radius: 1.27 cm (0.5 inches), No Constraint
2. Specimen Width: 1.27 cm (0.5 inches), Profile Radius: 1.27 cm (0.5 inches), Loose Constraint
3. Specimen Width: 1.27 cm (0.5 inches), Profile Radius: 1.27 cm (0.5 inches), Tight Constraint
4. Specimen Width: 2.54 cm (1.0 inch), Profile Radius: 1.27 cm (0.5 inches), No Constraint
5. Specimen Width: 2.54 cm (1.0 inch), Profile Radius: 1.27 cm (0.5 inches), Loose Constraint
6. Specimen Width: 2.54 cm (1.0 inch), Profile Radius: 1.27 cm (0.5 inches), Tight Constraint
7. Specimen Width: 5.08 cm (2.0 inches), Profile Radius: 1.27 cm (0.5 inches), No Constraint

8. Specimen Width: 5.08 cm (2.0 inches), Profile Radius: 1.27 cm (0.5 inches), Loose Constraint
9. Specimen Width: 5.08 cm (2.0 inches), Profile Radius: 1.27 cm (0.5 inches), Tight Constraint

3.5.5 Effect of Specimen Width

In all the tests conducted irrespective of the constraint condition or the radius of the profile block, the 2 inch wide specimens displayed the highest specific energy absorption. Either the 1 inch or the 0.5 inch wide specimens followed it. For a comparison of the load displacement traces recorded for a test conducted on a specimen of width 0.5 inch, 1 inch and 2 inch respectively please see Figure 71.

The reason for the superior energy absorption in the 2 inch wide specimens was due to the fact that the fibers in them had fiber lengths less than or equal to the width of the specimen unlike the case of the 0.5 and the 1 inch wide specimens that had fibers with fiber lengths greater than the width of the specimen. Please see Appendix E and Figure 72.

The following are the details of Figure 72.

Series: Specimen Width = 0.5 inches

Y axis: Specific Energy Absorption (SEA)

X axis: Condition

1 Specimen Width: 1.27 cm (0.5 inches), Profile Radius: 0.635 cm (0.25 inches), No Constraint

2 Specimen Width: 1.27 cm (0.5 inches), Profile Radius: 0.635 cm (0.25 inches), Loose Constraint

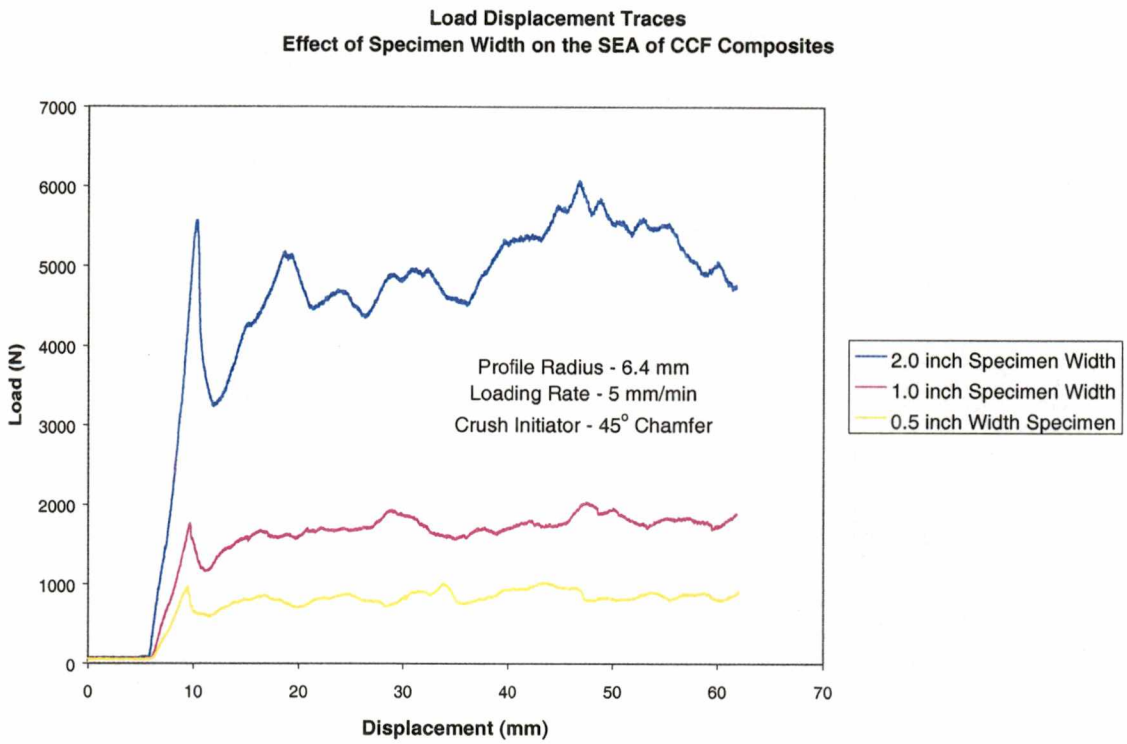

Figure 71. Load Displacement Traces Representing the Effect of Specimen Width on the SEA of CCF.

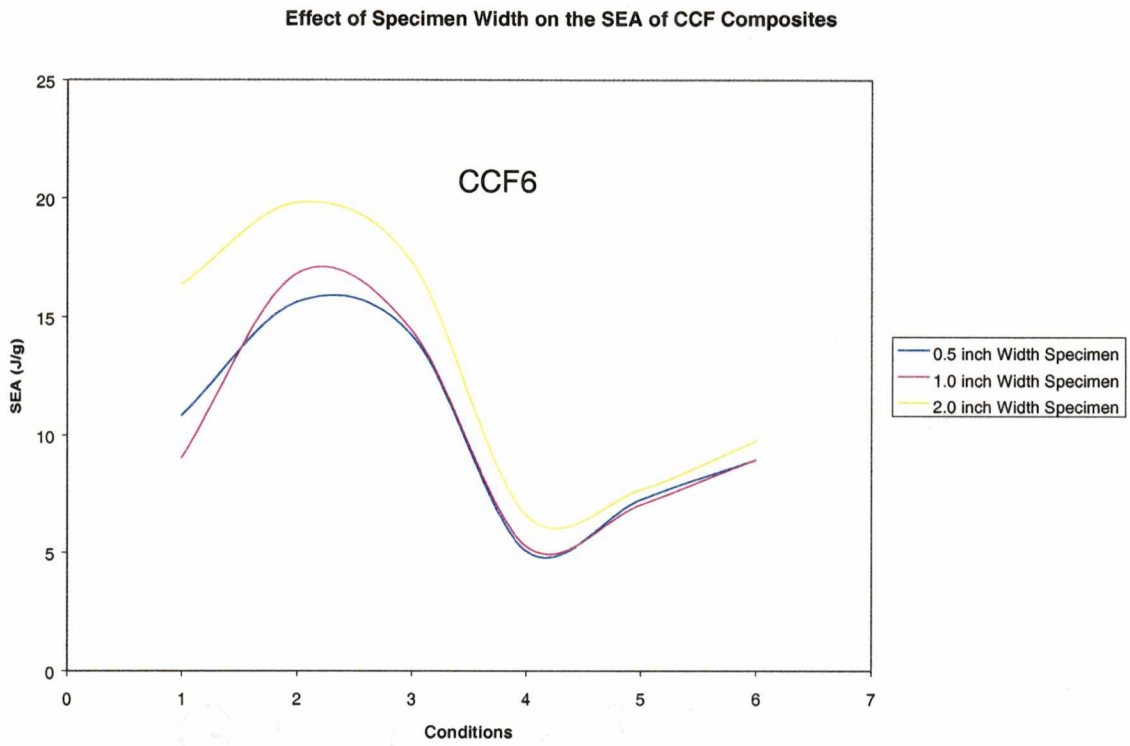

Figure 72. Variation of SEA with Specimen Width for CCF.

3 Specimen Width: 1.27 cm (0.5 inches), Profile Radius: 0.635 cm (0.25 inches), Tight Constraint

4 Specimen Width: 1.27 cm (0.5 inches), Profile Radius: 1.27 cm (0.5 inches), No Constraint

5 Specimen Width: 1.27 cm (0.5 inches), Profile Radius: 1.27 cm (0.5 inches), Loose Constraint

6 Specimen Width: 1.27 cm (0.5 inches), Profile Radius: 1.27 cm (0.5 inches), Tight Constraint

Series: Specimen Width = 1.0 inches

Y axis: Specific Energy Absorption (SEA)

X axis: Condition

Specimen Width: 2.54 cm (1.0 inch), Profile Radius: 0.635 cm (0.25 inches), No Constraint

1. Specimen Width: 2.54 cm (1.0 inch), Profile Radius: 0.635 cm (0.25 inches), Loose Constraint
2. Specimen Width: 2.54 cm (1.0 inch), Profile Radius: 0.635 cm (0.25 inches), Tight Constraint
3. Specimen Width: 2.54 cm (1.0 inch), Profile Radius: 1.27 cm (0.5 inches), No Constraint
4. Specimen Width: 2.54 cm (1.0 inch), Profile Radius: 1.27 cm (0.5 inches), Loose Constraint
5. Specimen Width: 2.54 cm (1.0 inch), Profile Radius: 1.27 cm (0.5 inches), Tight Constraint

Series: Specimen Width = 2.0 inches

Y axis: Specific Energy Absorption (SEA)

X axis: Condition

1. Specimen Width: 5.08 cm (2.0 inches), Profile Radius: 0.635 cm (0.25 inches), No Constraint
2. Specimen Width: 5.08 cm (2.0 inches), Profile Radius: 0.635 cm (0.25 inches), Loose Constraint
3. Specimen Width: 5.08 cm (2.0 inches), Profile Radius: 0.635 cm (0.25 inches), Tight Constraint
4. Specimen Width: 5.08 cm (2.0 inches), Profile Radius: 1.27 cm (0.5 inches), No Constraint
5. Specimen Width: 5.08 cm (2.0 inches), Profile Radius: 1.27 cm (0.5 inches), Loose Constraint
6. Specimen Width: 5.08 cm (2.0 inches), Profile Radius: 1.27 cm (0.5 inches), Tight Constraint

3.5.6 Effect of Constraint

- The tests conducted on the CCF material were only successful when the roller was positioned in the tight and loose constraint condition. When the no constraint condition was attempted the initial peak load increased and the CCF specimens buckled between the top plate and roller ways. The roller ways were unsuccessful in preventing out-of-plane buckling in the CCF material because of its low buckling strength. This resulted in having to use a metal push plate to reduce the unsupported specimen length. The metal plate was 76 mm in length and was bonded to the end of

the CCF specimens using 5-minute epoxy. This specimen configuration was successful when the roller was positioned in the no constraint condition.

- The no constraint condition resulted in the highest initial peak load relative to the other constraint conditions. Please see Appendix F.

For the profile block with a radius of 1.27 cm, the specific energy absorption, SEA, was highest in the tight constraint condition. No constraint to loose constraint to tight constraint condition resulted in larger specific energy absorption, SEA. For the profile block with a radius of 0.635 cm, in most cases, the specific energy absorption, SEA, followed the order: SEA for tests conducted in the loose constraint condition > SEA for tests conducted in the tight constraint condition > SEA for tests conducted in the no constraint condition, except in a few cases when it followed the order: SEA for tests conducted in the tight constraint condition > SEA for tests conducted in the loose constraint condition > SEA for tests conducted in the no constraint condition. Hence it was concluded that the specific energy absorption, SEA, was lowest in the tests that were conducted in the no constraint condition. The SEA was highest in tests conducted in either the tight or loose constraint condition. Please see Appendix F. For a comparison of the load displacement traces recorded for a test conducted on a specimen in the no constraint, the loose constraint and the tight constraint condition respectively please see Figure 73.

Please see Figure 74. The following are the details of Figure 74.

Series: Constraint Condition = No

Y axis: Specific Energy Absorption (SEA)

X axis: Condition

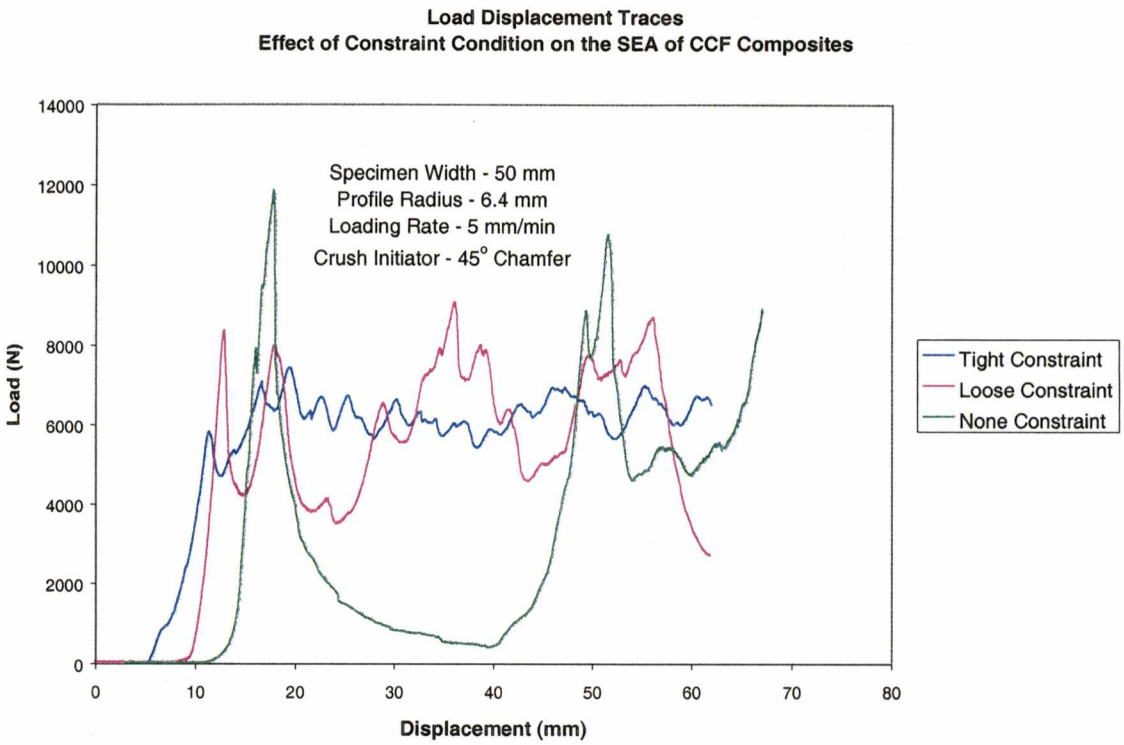

Figure 73. Load Displacement Traces Representing the Effect of Constraint Condition on the SEA of CCF.

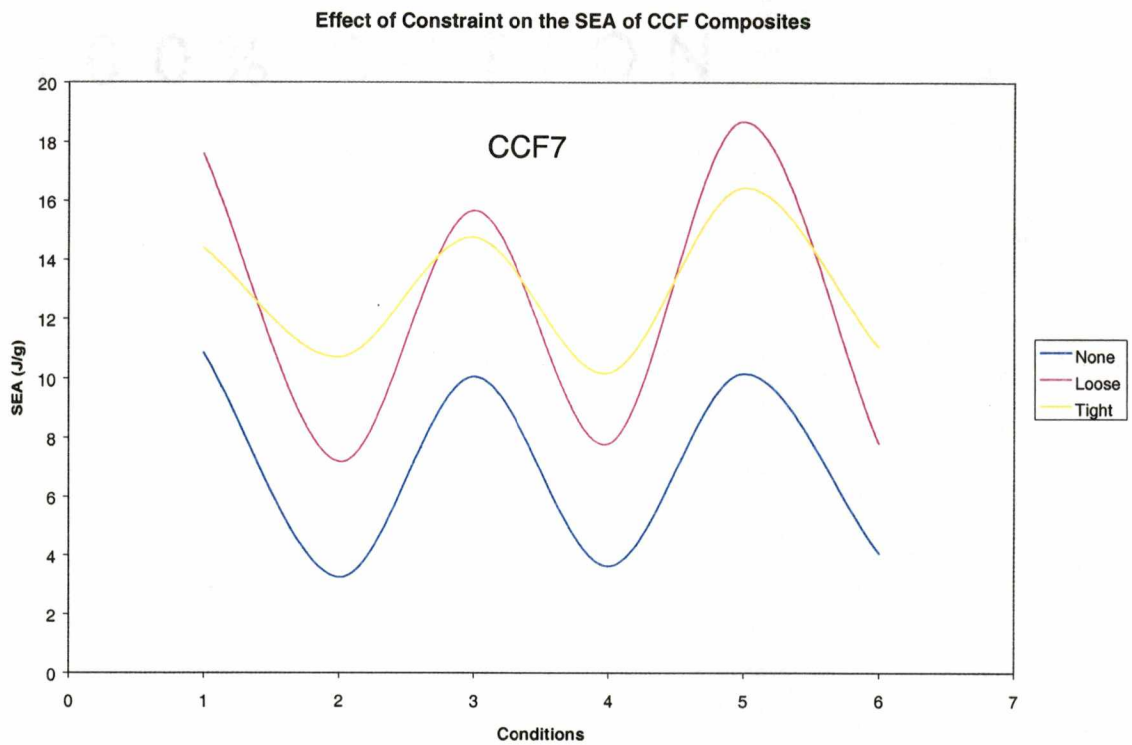

Figure 74. Variation of SEA with Constraint Condition for CCF.

1 Specimen Width: 1.27 cm (0.5 inches), Profile Radius: 0.635 cm (0.25 inches), No Constraint

2 Specimen Width: 1.27 cm (0.5 inches), Profile Radius: 1.27 cm (0.5 inches), No Constraint

3 Specimen Width: 2.54 cm (1.0 inch), Profile Radius: 0.635 cm (0.25 inches), No Constraint

4 Specimen Width: 2.54 cm (1.0 inch), Profile Radius: 1.27 cm (0.5 inches), No Constraint

5 Specimen Width: 5.08 cm (2.0 inches), Profile Radius: 0.635 cm (0.25 inches), No Constraint

6 Specimen Width: 5.08 cm (2.0 inches), Profile Radius: 1.27 cm (0.5 inches), No Constraint

Series: Constraint Condition = Loose

Y axis: Specific Energy Absorption (SEA)

X axis: Condition

1. Specimen Width: 1.27 cm (0.5 inches), Profile Radius: 0.635 cm (0.25 inches), Loose Constraint
2. Specimen Width: 1.27 cm (0.5 inches), Profile Radius: 1.27 cm (0.5 inches), Loose Constraint
3. Specimen Width: 2.54 cm (1.0 inch), Profile Radius: 0.635 cm (0.25 inches), Loose Constraint
4. Specimen Width: 2.54 cm (1.0 inch), Profile Radius: 1.27 cm (0.5 inches), Loose Constraint

5. Specimen Width: 5.08 cm (2.0 inches), Profile Radius: 0.635 cm (0.25 inches), Loose Constraint
6. Specimen Width: 5.08 cm (2.0 inches), Profile Radius: 1.27 cm (0.5 inches), Loose Constraint

Series: Constraint Condition = Tight

Y axis: Specific Energy Absorption (SEA)

X axis: Condition

1. Specimen Width: 1.27 cm (0.5 inches), Profile Radius: 0.635 cm (0.25 inches), Tight Constraint
2. Specimen Width: 1.27 cm (0.5 inches), Profile Radius: 1.27 cm (0.5 inches), Tight Constraint
3. Specimen Width: 2.54 cm (1.0 inch), Profile Radius: 0.635 cm (0.25 inches), Tight Constraint
4. Specimen Width: 2.54 cm (1.0 inch), Profile Radius: 1.27 cm (0.5 inches), Tight Constraint
5. Specimen Width: 5.08 cm (2.0 inches), Profile Radius: 0.635 cm (0.25 inches), Tight Constraint
6. Specimen Width: 5.08 cm (2.0 inches), Profile Radius: 1.27 cm (0.5 inches), Tight Constraint

3.5.7 Highest and Lowest Energy Absorbing Panel Groups

The panel group having the highest specific Energy absorption, SEA, was CCF5.

CCF5 Panel Description

Fiber Tow Size: 150 gsm (12 K)

Fiber Volume Fraction: 50%

Fiber Length: 1 inch

The 2 panel groups having the lowest specific energy absorption, SEA, was CCF6 and CCF7.

CCF6 Panel Description

Fiber Tow Size: 150 gsm (12 K)

Fiber Volume Fraction: 50%

Fiber Length: 2 inches

CCF7 Panel Description

Fiber Tow Size: 300 gsm (48 K)

Fiber Volume Fraction: 50%

Fiber Length: 2 inches

The above results indicate that it is the 2 inch long fibers that are causing the specific energy absorption, SEA, of the CCF6 and CCF7 panel groups to be the least among all the other CCF panel groups. The above observation was further proved when we looked at the effect the fiber length had on the specific energy absorption, SEA, where in it was observed that an increase in fiber length caused a decrease in the SEA of chopped carbon fiber composite materials. Therefore we conclude that the fiber length appears to be the most critical material parameter in determining the SEA of a composite material, with shorter fiber lengths leading to higher specific energy absorptions. This is contrary to the general belief that an increase in fiber length causes an increase in the specific energy absorption, SEA, of composite plates as it is widely reported in the

literature. The reason for this is speculated to be the result of the poor molding quality of the chopped carbon fiber, CCF, plates causing poor fiber wetting by the resin, voids and holes, resin rich areas and poor continuity in the plate structure.

3.6 Comparison of all Materials Tested

In order to identify the best material system among all the composites investigated in this document, a comparison of the specific energy absorption, SEA, recorded in all the tests conducted at a crushing speed of 5 mm/min on the 2 inch wide specimens under the tight constraint condition using a profile block having a radius of 0.635 cm was made. It was found that the specific energy absorption, SEA, of the chopped carbon fiber composite material, CCF, was the highest (28.11 Jg^{-1}), followed by that of the CSM material (26.50 Jg^{-1}), the CP#1 panel group (25.58 Jg^{-1}), and the CP#2 panel group (17.62 Jg^{-1}) in the order of decreasing SEA. Please see Figure 75. The lower SEA in panel CP#2 is attributed to the weaker interfacial bond strength, resulting from poor consolidation, requiring less energy to delaminate. The higher SEA in the CCF materials is attributed to the low density of the carbon fibers and the large amount of energy absorbed due to the matrix cracking at the ends of the chopped carbon fiber tows due to stress concentration at these ends.

3.7 Material Performance Requirements

Consider a midsize car of mass 1000 kg (2200 lbs) traveling at a velocity of 15.5 m/sec (35 mph). The kinetic energy of the car is equal to 0.5 m v^2 = $0.5*1000*(15.5)^2$ = 120125 J, where m is the mass of the car = 1000 kg (2200 lbs) and v is the velocity with which it is traveling = 15.5 m/sec (35 mph). In the event of an impact, the crash worthy materials have work done on it to absorb this kinetic energy

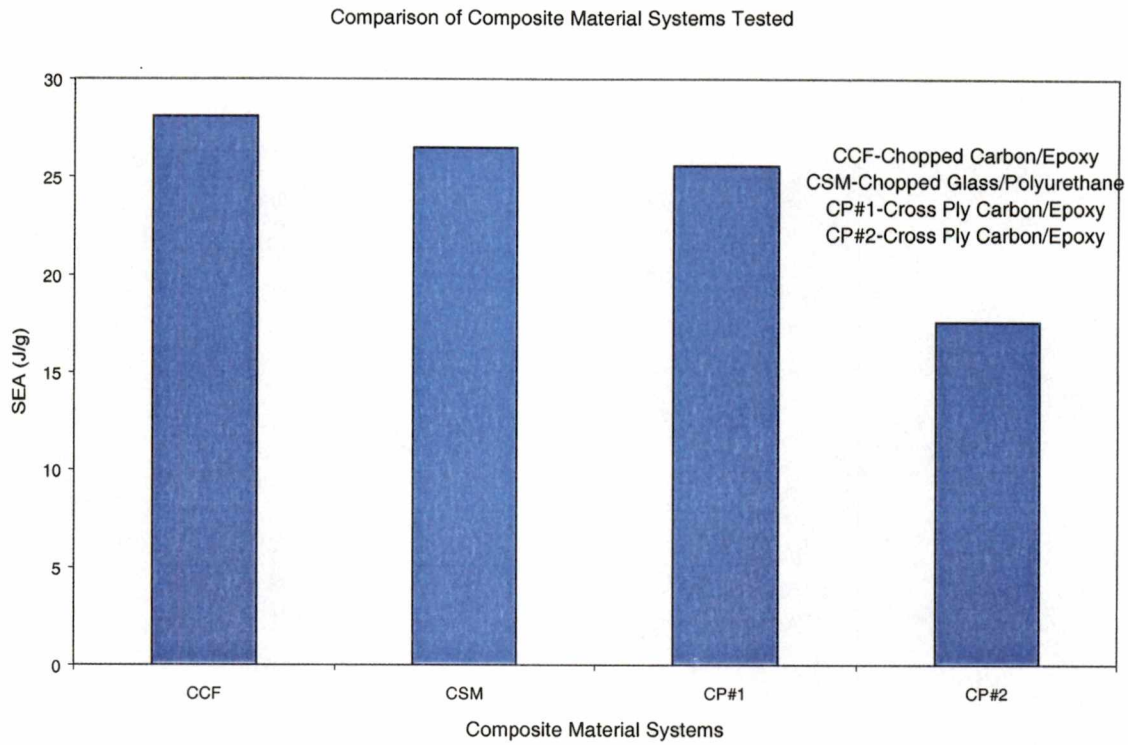

Figure 75. Comparison of Composite Material Systems Tested.

over a time frame that ensures the deceleration of the car to be less than 20g, above which the passengers will experience irreversible brain damage. Therefore 120 kJ of work needs to be done on the crash worthy material. One can calculate the minimum safe time frame over which this work needs to be done to ensure the safety of the passengers using the basic equation of motion

$$v = u - at \qquad \text{Eq. (10)}$$

where v is the final velocity of the car which is equal to zero since the car comes to rest, u is the initial impact speed and a is the maximum allowable deceleration which is equal to 20g. This minimum time was calculated to be equal to 0.079 seconds. Therefore the maximum allowable rate of work decay that will ensure the safety of the passengers is equal to 120125 / 0.079 = 1521 kJ/sec. The specific energy absorption, SEA, of the chopped carbon fiber/epoxy composite materials is recorded to be 28.11 kJ/kg. Therefore to absorb 120 kJ of kinetic energy one will only need 120125 / 28110 = 4.27 kg (9.39 lbs) of the CCF composite material located in specific places in the car. This clearly leads to an important practical conclusion that only a reasonable amount of this composite material is required to meet the necessary impact performance standard. Please see Figure 76 which shows the amount of the different composite materials that were tested in the lab that will be required in the event of a crash to ensure a safe rate of work decay in a car of mass 1000 kg (2200 lbs) traveling at a particular velocity.

3.8 Work Rate Decay

The maximum allowable rate of work decay that will ensure the safety of the passengers traveling in a car at 35 mph in the event of an impact is equal to kinetic energy with which the car is traveling divided by the minimum safe time frame over

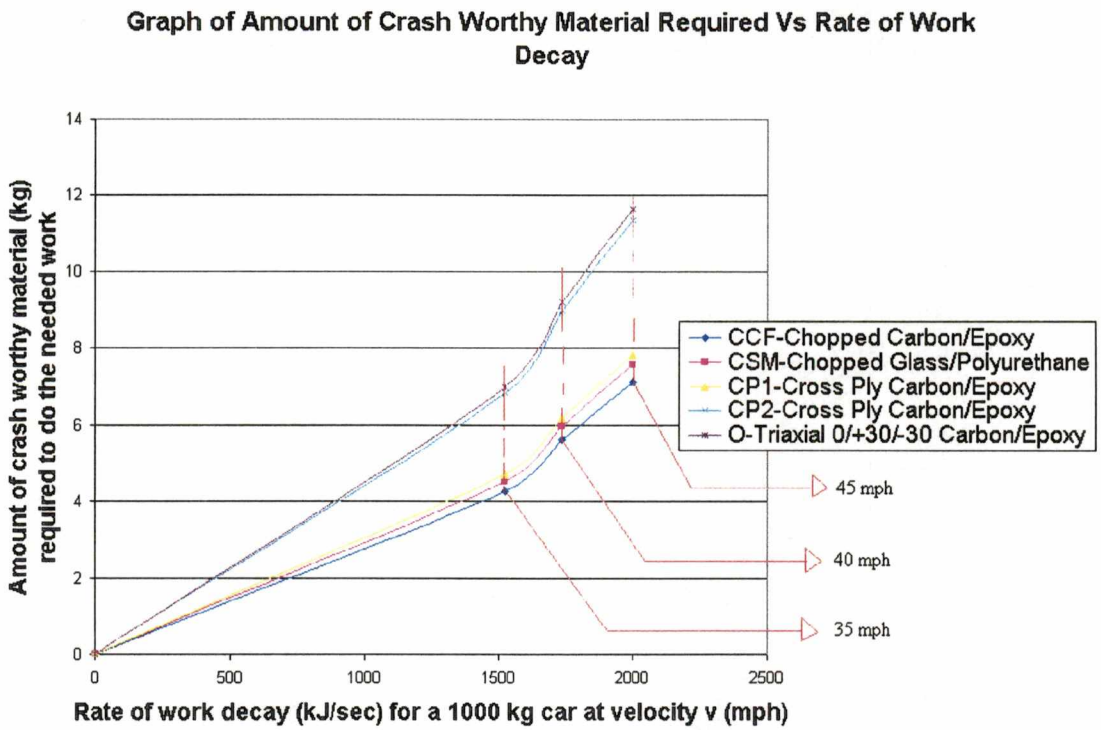

Figure 76. Graph of Amount of Crash Worthy Material Investigated in this Document Required to Rate of Work Decay.

which this work needs to be done. This has been calculated in the previous section (see page 160) to be 1521 kJ/sec. So while testing materials in the lab to determine their crash worthiness, it is equally important to determine the rate of energy absorption as it is to record the magnitude of energy that is being absorbed by the specimen. No discussion of energy absorption rates can be found in literature. The load increases very rapidly in the initial stages of the load displacement curve for materials undergoing crushing to some maximum value after which stable crushing takes place. Now it is in this initial stage of the crash that the work decay rate might exceed the safe allowable limits. So though these materials may record very high-energy absorption values they will not ensure the much needed passenger safety. The best material system among all the composites investigated was identified to be the chopped carbon fiber/epoxy composite, which recorded a specific energy absorption, SEA, of 28.11 J/g. One needs to further determine whether the rate of this energy absorption is within the safe allowable limits that would ensure passenger safety. The maximum allowable rate of work decay for the chopped carbon fiber, CCF, composite specimens when quasi-statically crushed in a 1000 kg car traveling at 5mm/min ($8.3 * 10^{-5}$ m/sec) is equal to the kinetic energy possessed by it divided by the minimum safe time frame over which this kinetic energy needs to be absorbed. The kinetic energy is equal to $0.5\ m\ v^2 = 0.5*1000*(8.3 * 10^{-5})^2 = 3.5 * 10^{-6}$ J, where m is the mass = 1000 kg (2200 lbs) and v is the crushing speed = ($8.3 * 10^{-5}$ m/sec). The minimum safe time frame over which this work needs to be done to can be calculated using the basic equation of motion

$$v = u - at \qquad \text{Eq. (11)}$$

where v is the final velocity which is equal to zero, u is the initial speed = $8.3 * 10^{-5}$ m/sec and a is the maximum allowable deceleration which is equal to 20g. This minimum time was calculated to be equal to $4.3 * 10^{-7}$ seconds. Therefore the maximum allowable rate of work decay is equal to $(3.5 * 10^{-6})/ (4.3 * 10^{-7}) = 8.175$ J/sec. Similar to other composites, when the CCF composites underwent crushing, the load increased very rapidly to some maximum value in the load displacement curve before stable crushing started taking place. It is in this initial stage of the crushing process that its work rate decay could exceed the safe allowable limits. Hence the rate of energy absorption in this initial stage of the crush process was determined and compared with the calculated maximum allowable rate of work decay, 8.175 J/sec. Calculating the area under the load displacement curve recorded during the initial stage of the crush process and dividing it by the time taken to absorb this energy accomplished this. The time quantity was determined by multiplying the X-coordinate of the initial peak in the load displacement curve by the crushing speed. The rate of energy absorption was found to be equal to 0.20 J/sec, which is far less than the maximum allowable rate of work decay. Hence it was concluded that the CCF material satisfied both criteria required for a material to be deemed highly crash worthy: A high magnitude of energy absorption and a safe allowable rate of this energy absorption.

It should be noted that the magnitude of energy absorption, the rate at which this energy is absorbed and the maximum allowable rate of work decay are all functions of the crushing speed. At a crushing speed of 5 mm/min, the rate of energy absorption (calculated to be 0.20 J/sec) is far less than the maximum allowable rate of work decay (calculated to be 8.175 J/sec) and also the energy absorbed by the CCF material is high.

But this might not be case at a different crushing speed. Cause one; the maximum allowable rate of work decay, a ratio of the kinetic energy of the car divided by the minimum safe time frame over which this kinetic energy can be absorbed by the CCF composite material, is a function of the crushing speed. Hence it is this ratio, which has velocity as a variable in both its numerator and denominator that will determine the safe allowable rate of work decay. And two; as reported in the literature and also in this document, the specific energy absorption, SEA, of a composite material is a function of crushing speed. Hence the load displacement curve, the initial peak load, the magnitude of energy absorbed calculated as the area under the load displacement curve and the time taken to absorb this energy are all functions of this crushing speed. Therefore though it was concluded that at a crushing speed of 5 mm/min, the CCF material satisfied both the criteria required for it to be deemed crash worthy: a high magnitude of energy absorption and a safe allowable rate of this energy absorption, one cannot be sure about its crash worthiness at an alternate crushing speed. The above discussion further emphases the need to investigate both the magnitude and the rate of energy absorption at various testing speeds while testing materials in the lab in order to determine their crash worthiness.

Chapter 4

Conclusion

- A test fixture had been developed for conducting progressive crush tests on composite plates.
- It was inferred that different damage mechanisms could be activated depending on the condition of the profile constraint. For example, in the braided material, the active damage mechanisms were localized crushing, fiber fracture on the tensile side of the specimen, and fiber buckling of the off-axis tows on the compressive side of the specimen. The fiber buckling was more extensive when the no constraint condition was used, whereas the fiber fracture was more predominant in the loose constraint tests.
- Modifications to the basic specimen geometry were required when testing material systems having a low axial stiffness. For example, the tests conducted on the CSM material were only successful when the roller was positioned in the no constraint condition. When the loose or tight constraint condition was attempted the initial peak load increased and the CSM specimens buckled between the top plate and roller ways. The roller ways were unsuccessful in preventing out-of-plane buckling in the CSM material because of its low buckling strength. This resulted in having to use a metal push plate to reduce the unsupported specimen length. The metal plate was 76 mm in length and was bonded to the end of the CSM specimens using 5-minute epoxy. This specimen configuration was successful when the roller was positioned in the loose and tight constraint condition.

- An increase in tow size causes a decrease in the specific energy absorption, SEA, for chopped carbon fiber composite materials with a fiber length of 1 inch. For chopped carbon fiber composite materials with 2 inch fiber lengths, there is no serious effect of a change in tow size on its specific energy absorption, SEA.
- An increase in fiber volume fraction causes a decrease in the specific energy absorption, SEA, for chopped carbon composite materials with a fiber length of 2 inches. On the contrary, an increase in the fiber volume fraction causes an increase in the specific energy absorption, SEA, for chopped carbon fiber composite materials with 1 inch fiber length.
- An increase in fiber length causes a decrease in the specific energy absorption, SEA, for chopped carbon fiber composite materials.
- An increase in the crushing speed causes a decrease in the specific energy absorption, SEA, for the Baydur glass polyurethane composite (CSM) when tested in the loose and tight constraint conditions. This confirmed the rate dependence of the specific energy absorption, SEA, of composite plates.
- An increase in the radius of the profile block causes a decrease in the specific energy absorption, SEA, for all material systems tested.
- In all the tests conducted, irrespective of the constraint condition or the radius of the profile block that was used, the 2 inch wide specimens displayed the highest specific energy absorption, SEA, when compared to that of the 0.5 inch and 1 inch wide specimens.
- The no constraint condition resulted in the highest initial peak load and the lowest specific energy absorption, SEA, relative to the other constraint conditions.

- The specific energy absorption, SEA, of the chopped carbon fiber composite material, CCF, was the highest compared to that of all the other composites investigated here in. The 2 inch wide specimens belonging to panel group CCF5 having fiber tow size 150 gsm, a fiber length of 1 inch and 50% fiber volume fraction recorded the highest SEA equal to 28.11 kJ/kg when tested at 5 mm/min crushing speed under the tight constraint condition using a profile block of radius 0.635 cm. Only a reasonable amount of it (4.27 kg) located in specific places in the car is required to meet the necessary impact performance standard. The CCF composite tested at 5 mm/min crushing speed met both the criteria that need to be satisfied before a material is deemed highly crash worthy: A high magnitude of energy absorption and a safe allowable rate of this energy absorption.
- The high specific energy absorption, SEA, recorded for the less costly CCF composite material, which by no means is an expensive aerospace grade, indicates how successful one might be in analyzing different grades and combinations of carbon fiber and resins for use in automotive applications. In design, researchers must try to better understand the design of composite parts through finite element analysis so carbon fiber composites can be concentrated in strategic locations for stiffness. The potential of using cheap glass-reinforced polymers for the basic component, then reinforcing it at critical points with the more costly carbon fiber also needs to be explored. Lastly, the use of carbon fiber composites for dual purposes other than just being used to improve the crash worthiness of vehicles must be explored. For example one could use the chopped carbon fiber composite material, CCF, for the reinforcements in the inside of a door in addition to its use as a crash

worthy material. Its use will improve the structural integrity of the door and also the acoustics in the car. However it must also be realized that it is going to be very difficult to replace the low cost metals that are currently being used for parts that satisfy the functional needs in a car with a more costly carbon composite material.

Based on the above, the profound conclusion one can arrive at is that the chopped carbon fiber composite material, CCF, is more crash worthy than any other composite material investigated in this document. When tested at a crushing speed of 5 mm/min, the CCF composite material met both the criteria that needed to be satisfied before it could be deemed as a highly crash worthy material: A high magnitude of energy absorption and a safe allowable rate of this energy absorption. The magnitude of the specific energy absorption, SEA, of the CCF composite material is highly dependent on changes in both its material (fiber volume fraction, fiber length and fiber tow size) parameters and its test (specimen width, loading rate, profile radius and constraint condition) parameters, the changes in its fiber length affecting the SEA most greatly. A 2 inch wide CCF composite plate having a high fiber volume fraction, a low value of fiber tow size and fiber length, tested at a crushing speed of 5 mm/min in the tight constraint condition using a small radius profile block yields the highest specific energy absorption, SEA. In fact it is calculated that only 4.27 kg of it is needed to be placed at specific places in the car to ensure passenger safety in the event of a crash at 35 mph. This clearly leads to an important practical conclusion that only a reasonable amount of this composite material is required to meet the necessary impact performance standard.

Chapter 5

Future Work

- Splaying mode and frond formation is only part of the total energy absorbing process while crushing of composite plates. Alternative tests are needed to isolate and quantify the other damage mechanisms that absorb energy. An attempt will be made in the above regard to evaluate the functionality of constraint roller brackets as a load cell for measuring frictional forces.
- Results from tube testing show that the dynamic SEA in tubes is less than the static SEA. The tests conducted on the CSM plates also showed that the SEA in them is rate dependent. A detailed understanding of the rate dependency of damage mechanisms and specific energy absorption, SEA, calls for experimental data at intermediate and high strain rates. In the above regard modifications and/or adaptations of the existing fixture for intermediate strain rate testing will be attempted in the near future.
- From the tests conducted on the chopped carbon fiber composites plates it was concluded that fiber length appears to be the most critical material parameter controlling the specific energy absorption, SEA, with shorter fiber lengths resulting in higher specific energy absorptions. Keeping that in mind an attempt will be made to determine the effect of fiber length in tube tests.
- Static strength and modulus comparison between the 8 different panel groups of the CCF material system will be attempted by conducting tension, compression and flexure tests. An attempt will also be made to determine the fracture toughness of the CCF material system.

List of References

1. D. C. Worley, ***"Damage Assessment and Progression in a Polyisocyanurate Based Continuos Swirl Mat Composite"***, Ph.D., Thesis, University of Tennessee, Knoxville, USA, (1999).
2. G. L. Farley, "Energy Absorption of Composite Material and Structures", ***Proc. 43rd American Helicopter Society Annual Forum***, St. Louis, USA, (1987), p. 613-627.
3. G. L. Farley, "Effect of specimen geometry on the energy absorption capability of composite materials", ***J. Comp. Mater.***, Vol. 20 (July 1986) p. 390-400.
4. G. L. Farley, "Energy Absorption of Composite Materials", ***J. Comp. Mater.***, Vol. 17 (May 1983) p. 267-279.
5. G. L. Farley, "Effect of Fiber And Matrix Maximum Strain on the Energy Absorption of Composite Materials", ***J. Comp. Mater.***, Vol. 20 (July 1986) p. 322-334.
6. G. L. Farley, "Energy Absorption in Composite Materials for Crashworthy Structures", ***Proc. Of ICCM 6***, Edited by F. L. Matthews, N. C. R. Buskell, J. M. Hodgkinson and J. Mortan, Elsevier Science Publishers Limited, London, (1987) p. 3.57-3.66.
7. P. H. Thornton, P. J. Edwards, "Energy absorption in composite tubes", ***J. Comp. Mater.***, Vol. 16 (November 1982) p. 521-545.
8. D. Hull, "A Unified Approach to Progressive Crushing of Fiber-Reinforced Composite Tubes", ***Comp. Sci. & Tech.***, Vol. 40 (1991) p. 377-421.
9. D. Hull, ***In Structural Crash Worthiness***, Editors N. Jones and T. Weirzbicki, Butterworths, London, (1983), p. 118-135.
10. H. Hamada, S. Ramakrishna, Z. Maekawa, M. Nakamura, "Energy Absorption Behavior of Hybrid Composite Tubes", ***Proc. 10th Annual ASM/ESD Advanced***

Composite Conference, Dearborn, Michigan, USA, (7th–10th November 1994) p. 511-522.

11. D. W. Schmuesser, L. E. Wickliffe, "Impact Energy Absorption of Continuous Fiber Composite Tubes", ***J. Engg. Mat. & Tech.***, Vol. 109 (January 1987) p. 72-77.
12. H. Hamada, S. Ramakrishna, H. Sato, Z. Maekawa, "Effect of fiber material on the energy absorption behavior of Thermoplastic composite tubes", ***J. Thermoplastic Composite Materials***, (in press).
13. G. L. Farley, R. M. Jones, "Analogy for the Effect of Material and Geometrical Variables on Energy Absorption Capability of Composite Tubes", ***J. Comp. Mater.***, Vol. 26, No. 1 (1992) p. 78-89.
14. G. L. Farley, "Prediction of the Energy Absorption Capability of Composite Tubes", ***J. Comp. Mater.***, Vol. 26, No. 3 (1992) p. 388-404.
15. P. H. Thornton, "Energy Absorption in Composite Structures", ***J. Comp. Mater.***, Vol. 13 (July 1979) p. 247-262.
16. C. H. Chiu, C. K. Lu, "Crushing Characteristics of 3-D Braided Composite SQUARE Tubes", ***J. Comp. Mater.***, Vol. 31, No. 22 (1997) p. 2309-2327.
17. C. H. Chiu, C. K. Lu, C. M. Wu, "Energy Absorption of Three-Dimensional Braided Composite Tubes", ***Proc. Of ICCM 10***, Edited by B. C. Whistler, Canada, (August 1995) p. 4.187-4.194.
18. S. Ramakrishna, H. Hamada, Z. Maekawa, H. Sato, "Energy Absorption Behavior of Carbon Fiber Reinforced Thermoplastic Composite Tubes", ***J. Thermo. Comp. Mater.***, Vol. 8 (July 1995) p. 323-344.
19. I. Y. Chang, J. K. Lees, ***J. Thermo. Comp. Mater.***, Vol. 1 (1998) p. 277-295.

20. I. Y. Chang, "Thermoplastic Matrix Continuous Filament Composites of Kevlar, Aramid or Graphite Fiber", ***Comp. Sci. & Techn.***, Vol. 24 (1985) p. 61-79.

21. H. Satoh, H. Hirakawa, Z. Maekawa, H. Hamada, M. Nakamura, D. Hull, "Comparison of Energy Absorption Among Carbon/Thermoplastic Tubes", ***38th International SAMPE Symposium, Science of Advanced Materials and Process Engineering Series***, Vol. 38 (10th–13th May, 1993) p. 952–966.

22. H. Hamada, J. C. Coppola, D. Hull, Z. Maekawa, H. Sato, "Comparison of Energy Absorption of Carbon/Epoxy and Carbon/PEEK Composite Tubes", ***Composites***, Vol. 23, No. 4 (1992) p. 245-252.

23. G. L. Farley, R. M. Jones, "Energy Absorption Capability of Composite Tubes and Beams", ***NASA TM-101634, AVSCOM TR-89-B-003***, (1989).

24. D. Hull, "Energy Absorption of Composite Materials Under Crash Conditions", ***Proc. Of ICCM-4***, Edited by T. Hayashi, K. Kawata and S. Umekawa, Tokyo, Japan, (1982) p. 861-870.

25. J.P. Berry, ***"Energy Absorption and Failure Mechanisms of Axially Crushed GRP Tubes"***, Ph.D., Thesis, University of Liverpool, UK, (1984).

26. G. L. Farley, "Crash Energy Absorbing Composite Sub-floor Structure", ***27th SDM conference***, (May 1986). Also submitted for publication to ***The American Helicopter Society***.

27. G. L. Farley, R. M. Jones, "Crushing Characteristics of Composite Tubes with 'Near-Elliptical' Cross Sections", ***J. Comp. Mater.***, Vol. 26, No. 12 (1992) p. 1741-1751.

28. P. H. Thornton, J. J. Harwood, P. Beardmore, "Fiber Reinforced Plastic Composites for Energy Absorption Purposes", ***Comp. Sci. & Tech.***, Vol. 24 (1985) p. 275-298.

29. D. D. Dubey, J. A. Vizzini, "Energy Absorption of Composite Plates and Tubes", ***J. Comp. Mater.***, Vol. 32 (February 1998) p. 158-176.

30. H. Hamada, S. Ramakrishna, Z. Maekawa, M. Nakamura, "Energy Absorption Characteristics of Composite Tubes with Different Cross Sectional Shapes", ***Proc. 10th Annual ASM/ESD Advanced Composite Conference***, Dearborn, Michigan, USA, (7th–10th November 1994), p. 523-534.

31. A. G. Mamalis, Y. B. Yuan, G. L. Viegelahn, "Collapse of Thin Wall Composite Sections Subjected to High Speed Axial Loading", ***Int. J. of Vehicle Design***, Vol. 13:5/6 (1992) p. 564–579.

32. A. H. Fairfull, ***"Scaling Effects in the Energy Absorption of Axially Crushed Composite Tubes"***, Ph.D., Thesis, University of Liverpool, UK, (1986).

33. A. H. Fairfull and D. Hull, ***Proc. Of ICCM 6***, Edited by F. L. Matthews, N. C. R. Buskell, J. M.Hodgkinson, J. Morton, Elsevier Science and Publishers, (1987) p. 3.36-3.45.

34. G. L. Farley, "Energy Absorption Capability and Scalability Of Square Cross Section Composite Tube Specimens", ***U.S. Army Research and Technology Activity–AVSCOM***, p. 1–17.

35. S. Ramakrishna, H. Hamada, "Energy Absorption Characteristic of Crash Worthy Structural Composite Materials", ***Key Engineering Materials***, Vol. 141–143 (1998) p. 585–620.

36. S. Hanagud, J. I. Craig, P. Sriram, W. Zhou, "Energy Absorption Behavior of Graphite Epoxy Composite Sine Webs", ***J. Comp. Mater.***, Vol. 23 (May 1989) p. 448-459.

37. H. Hamada, S. Ramakrishna, Z. Maekawa, H. Sato, "Effect of Cooling Rate on the Energy Absorption Capability of Carbon Fibre/PEEK Composite Tubes", ***J. Poly. & Poly. Comp.***, Vol. 3,No. 2 (1995) p. 99-104.

38. S. Ramakrishna, D. Hull, "Energy Absorption Capability of Epoxy Composite Tubes With Knitted Carbon Fibre Fabric Reinforcement", ***Comp. Sci. & Tech.***, Elsevier Science Publishers Limited, Vol. 49 (1993) p. 349-356.

39. S. Ramakrishna, "Energy Absorption Characteristics of Knitted Fabric Reinforced Composite Tubes", ***J. Reinf. Plast. & Comp.***, Vol. 14 (October 1995) p. 1121-1141.

40. P. Snowdon, D. Hull, "Energy Absorption of SMC Under Crash Conditions", ***Proc. Fiber Reinforced Composites Conference'84***, Plastics and Rubber Institute, (3rd–5th April 1984) p. 5.1-5.10.

41. P. H. Thornton, W. H. Tao, R. E. Robertson, "Crash Energy Management: Axial Crush of Unidirectional Fiber Composite Rods", ***Advanced Composite Materials: New Development and Applications Conference Proceedings***, Detroit, Michigan, USA, (30th September-3rd October 1991) p. 489-496.

42. D. C. Bannerman, C. M. Kindervater, ***Proc. 4th International SAMPE European Chapter***, Bordeaux, France, (1984) p. 155-167.

43. P. H. Thornton, "The Crush Behavior of Pultruded Tubes at High Strain Rate", ***J. Comp. Mater.***, Vol. 24 (June 1990) p. 594-615.

44. G. L. Farley, "The Effects of Crushing Speed on the Energy Absorption Capability of Composite Tubes", ***J. Comp. Mater.***, Vol. 25 (October 1991) p. 1314-1329.

45. C. M. Kindervater, ***National Specialists Meeting, Composite Structures of the American Helicopter Society***, Philadelphia, Pennsylvania, (23rd–25th March 1983).

46. M. Botkin, E. Zywicz, S. Simunovic, R. Averill, E. Plaskacz, D. Lo, J. Benner, G. Kay, "Computational Analysis of Composite Structures for Crash Worthiness", ***Annual Automotive Technology Development Customers' Coordination Meeting, Advanced Automotive Technologies***, Vol. 1 (27th–30th October, 1997).

47. S. Ramakrishna, ***"Knitted Fabric Reinforced Polymer Composites"***, Ph.D., Thesis, University of Cambridge, UK, (1992).

48. S. Ramakrishna, H. Hamada, D. Hull, "Impact and dynamic fracture of polymers and composites", ***(ESIS19)***, Edited by J. G. Williams, A. Pavan, Mechanical Engineering Publications, London (1995) p. 453-464.

49. S. Ramakrishna, D. Hull, ***Proc. International Conference on Advances in Structural Testing, Analysis and Design***, Bangalore, India, Edited by B. Dattaguru, Tata McGraw-Hill, New Delhi, (1990), p. 69-74.

50. H. Hamada, A. Nakai, T. Nakatani, ***Proc. First Canada-Japan Seminar on Composite Materials***, Kyoto, (August 1996) p. 44.1-44.4.

51. G. L. Farley, "Relationship Between Mechanical Property and Energy Absorption Trends for Composite Tubes", ***NASA TP-3284, ARL-TR-29***, (December 1992).

52. Lavoie, Morton, ***Nasa Contractor Report*** 4526, (July 1993).

Appendices

Appendix A

Table of Experimental Data for CCF1

Panel group name: CCF1

Fiber tow size: 150 gsm (12 K)

Fiber volume fraction: 40%

Fiber length: 1 inch

Spec. Number	**Spec. Width (cm)**	**Profile Radius (cm)**	**Const-raint**	**Initial Peak Load (N)**	**Max. Peak Load (N)**	**Sustain-ed Crush Load (N)**	**SEA (J/g)**
CCF11	1.286	0.635	None	3890.7	3890.7	967.9	14.54
CCF12	1.270	0.635	None	3299.2	3299.2	920.7	14.03
CCF13	1.285	0.635	None	3216.5	3216.5	920.7	15.15
CCF14	1.276	0.635	Loose	1503.9	1834.3	1149.1	18.70
CCF15	1.263	0.635	Loose	1422.9	1824.4	1168.9	18.41
CCF16	1.313	0.635	Loose	1501.2	2102.9	1120.7	16.91
CCF17	1.267	0.635	Tight	1116.4	1897.7	1259.7	19.75
CCF18	1.285	0.635	Tight	1036.6	1974.7	1259.7	19.51
CCF19	1.268	0.635	Tight	1250.2	3033.5	1607.3	26.49
CCF110	1.283	1.27	None	1115.1	1115.1	262.8	4.18
CCF111	1.276	1.27	None	1729.7	1729.7	309.5	4.86

CCF112	1.267	1.27	None	1818.5	1818.5	284.0	4.48
CCF113	1.263	1.27	Loose	1098.8	1098.8	553.1	8.88
CCF114	1.285	1.27	Loose	1152.4	1152.4	494.9	7.68
CCF115	1.268	1.27	Loose	1217.5	1222.3	523.8	8.26
CCF116	1.281	1.27	Tight	977.4	977.4	619.2	9.57
CCF117	1.269	1.27	Tight	982.9	982.9	633.2	10.46
CCF118	1.283	1.27	Tight	900.8	900.8	624.6	10.02
CCF119	2.545	0.635	None	6993.2	6993.2	1746.6	13.83
CCF120	2.555	0.635	None	6397.7	6397.7	2059.0	16.00
CCF121	2.559	0.635	None	5526.1	5526.1	1802.4	13.99
CCF122	2.566	0.635	Loose	3025.2	4137.6	2541.3	19.29
CCF123	2.547	0.635	Loose	3213.4	4055.2	2647.0	20.88
CCF124	2.560	0.635	Loose	3212.3	4313.8	2702.7	20.92
CCF125	2.540	0.635	Tight	1933.0	4338.2	2907.3	22.93
CCF126	2.561	0.635	Tight	2322.6	4254.4	2943.6	23.03
CCF127	2.5553	0.635	Tight	2783.5	3912.8	2781.6	21.81
CCF128	2.562	1.27	None	2283.8	2643.3	768.1	5.97
CCF129	2.588	1.27	None	2178.7	2353.0	780.4	6.03
CCF130	2.598	1.27	None	2364.5	2364.5	619.3	4.79
CCF131	2.542	1.27	Loose	2616.2	2616.2	1259.2	9.80
CCF132	2.537	1.27	Loose	2511.7	2511.7	1244.4	9.80
CCF133	2.547	1.27	Loose	2351.0	2351.0	1218.8	9.56

CCF134	2.542	1.27	Tight	1836.2	1836.2	1367.9	10.63
CCF135	2.539	1.27	Tight	1767.6	1767.6	1390.3	11.00
CCF136	2.536	1.27	Tight	1999.0	1999.0	1411.1	11.15
CCF137	5.083	0.635	None	13470.2	13470.2	4534.8	17.80
CCF138	5.080	0.635	None	13976.9	13976.9	4306.0	18.16
CCF139	5.067	0.635	None	10672.8	12345.5	4750.7	18.25
CCF140	5.082	0.635	Loose	3860.6	10763.7	6219.6	23.70
CCF141	5.068	0.635	Loose	6443.1	8686.2	6167.9	26.48
CCF142	5.114	0.635	Loose	6512.2	7668.7	5217.0	21.38
CCF143	5.080	0.635	Tight	6452.0	7925.9	5680.5	23.01
CCF144	5.091	0.635	Tight	4889.1	6928.1	4829.5	19.64
CCF145	5.132	0.635	Tight	6420.3	10571.5	6543.1	26.41
CCF146	5.079	1.27	None	3580.0	5507.1	1791.3	7.13
CCF147	5.100	1.27	None	4282.1	5526.8	1838.5	7.64
CCF148	5.096	1.27	None	5895.7	5895.7	1329.9	5.57
CCF149	5.124	1.27	Loose	4415.0	4415.0	2394.7	9.42
CCF150	5.103	1.27	Loose	4895.9	4895.9	2622.6	10.87
CCF151	5.086	1.27	Loose	5723.5	5723.5	2631.2	10.84
CCF152	5.147	1.27	Tight	3698.1	3871.7	2789.1	11.18
CCF153	5.134	1.27	Tight	4879.0	4879.0	3413.2	13.63
CCF154	5.113	1.27	Tight	3921.9	3921.9	3011.2	12.04

Appendix B

Table of Experimental Data for CCF2

Panel group name: CCF2

Fiber tow size: 150 gsm (12 K)

Fiber volume fraction: 40%

Fiber length: 2 inches

Spec. Number	**Spec. Width (cm)**	**Profile Radius (cm)**	**Const-raint**	**Initial Peak Load (N)**	**Max. Peak Load (N)**	**Sustain-ed Crush Load (N)**	**SEA (J/g)**
CCF21	1.281	0.635	None	3276.8	3276.8	1084.8	16.94
CCF22	1.271	0.635	None	3848.6	3848.6	1209.3	18.65
CCF23	1.276	0.635	None	3312.8	3312.8	780.0	12.78
CCF24	1.277	0.635	Loose	1466.5	1466.5	752.9	12.52
CCF25	1.275	0.635	Loose	1147.7	1724.9	1160.3	18.47
CCF26	1.300	0.635	Loose	1371.5	2676.6	1250.9	19.36
CCF27	1.281	0.635	Tight	807.8	1533.6	1171.9	17.74
CCF28	1.278	0.635	Tight	947.6	1547.9	1196.7	18.27
CCF29	1.275	0.635	Tight	957.8	1460.4	862.7	14.16
CCF210	1.285	1.27	None	1231.7	1897.2	428.1	7.07
CCF211	1.271	1.27	None	1320.7	1320.7	312.3	4.82

CCF212	1.280	1.27	None	1762.2	1762.2	309.7	4.76
CCF213	1.283	1.27	Loose	858.0	858.0	417.8	6.96
CCF214	1.271	1.27	Loose	1221.6	1221.6	449.5	7.49
CCF215	1.281	1.27	Loose	978.1	978.1	348.9	5.83
CCF216	1.273	1.27	Tight	1057.4	1057.4	683.3	11.26
CCF217	1.275	1.27	Tight	884.5	913.0	665.4	10.92
CCF218	1.281	1.27	Tight	865.5	886.5	657.3	10.80
CCF219	2.588	0.635	None	9475.8	9475.8	2457.7	19.05
CCF220	2.576	0.635	None	7523.0	7523.0	1792.2	13.92
CCF221	2.564	0.635	None	7539.2	7539.2	1805.2	14.38
CCF222	2.564	0.635	Loose	2842.1	3040.8	2113.1	16.69
CCF223	2.561	0.635	Loose	2758.6	4489.6	2597.7	20.46
CCF224	2.548	0.635	Loose	2939.7	3318.2	2443.6	19.99
CCF225	2.563	0.635	Tight	1796.8	3169.7	2071.4	16.46
CCF226	2.570	0.635	Tight	2164.4	3247.0	2580.0	19.68
CCF227	2.566	0.635	Tight	2180.7	2564.6	1853.6	14.74
CCF228	2.560	1.27	None	2348.3	2348.3	608.5	4.80
CCF229	2.547	1.27	None	1771.7	1909.4	538.2	4.31
CCF230	2.564	1.27	None	2085.1	2566.7	822.9	6.26
CCF231	2.559	1.27	Loose	2148.2	2148.2	917.2	7.19
CCF232	2.573	1.27	Loose	2356.4	2356.4	929.1	7.40
CCF233	2.596	1.27	Loose	2238.4	2238.4	831.2	6.40

CCF234	2.589	1.27	Tight	1551.2	1704.5	1316.6	10.45
CCF235	2.578	1.27	Tight	1724.9	1876.2	1431.9	11.30
CCF236	2.579	1.27	Tight	1578.4	1928.4	1407.9	10.83
CCF237	5.113	0.635	None	9488.7	12969.7	6215.1	25.37
CCF238	5.120	0.635	None	17443.7	17443.7	3686.1	15.53
CCF239	5.088	0.635	None	12842.9	12842.9	3612.4	14.37
CCF240	5.121	0.635	Loose	6773.5	6869.8	5510.3	20.93
CCF241	5.127	0.635	Loose	5895.7	6174.5	4655.3	19.11
CCF242	5.098	0.635	Loose	6734.8	6734.8	4534.7	19.43
CCF243	5.109	0.635	Tight	3319.6	5665.8	4058.5	15.76
CCF244	5.106	0.635	Tight	4141.0	4520.9	3654.7	15.52
CCF245	5.102	0.635	Tight	4364.2	5718.7	4409.5	17.45
CCF246	5.115	1.27	None	4865.4	4865.4	1581.9	5.97
CCF247	5.079	1.27	None	4859.3	4859.3	1417.5	5.76
CCF248	5.123	1.27	None	5745.2	5745.2	1135.8	4.87
CCF249	5.105	1.27	Loose	4829.5	4829.5	2223.0	8.46
CCF250	5.125	1.27	Loose	5018.1	5018.1	2201.8	8.44
CCF251	5.105	1.27	Loose	4649.7	4649.7	2355.7	8.94
CCF252	5.099	1.27	Tight	4140.3	4140.3	3053.2	11.68
CCF253	5.151	1.27	Tight	3997.9	3997.9	2950.9	11.14
CCF254	5.091	1.27	Tight	3957.9	4815.9	3719.6	13.97

In the previous table, the data for CCF21 and CCF237 corresponds to an erroneous test where in the specimen buckled between the top plate and the roller ways.

Appendix C

Table of Experimental Data for CCF3

Panel group name: CCF3

Fiber tow size: 300 gsm (48 K)

Fiber volume fraction: 40%

Fiber Length: 2 inches

Spec. Number	**Spec. Width (cm)**	**Profile Radius (cm)**	**Const-raint**	**Initial Peak Load (N)**	**Max. Peak Load (N)**	**Sustain-ed Crush Load (N)**	**SEA (J/g)**
CCF31	1.282	0.635	None	2180.7	2422.9	323.2	5.24
CCF32	1.275	0.635	None	2439.8	2439.8	387.4	6.22
CCF33	1.281	0.635	None	2037.6	2037.6	526.4	8.65
CCF34	1.271	0.635	Loose	1424.4	1997.6	1017.6	16.50
CCF35	1.272	0.635	Loose	1357.3	1852.4	2866.9	46.59
CCF36	1.281	0.635	Loose	1347.1	1934.5	1223.7	20.05
CCF37	1.272	0.635	Tight	378.5	1950.8	1354.0	20.68
CCF38	1.280	0.635	Tight	880.4	1561.5	1246.8	18.92
CCF39	1.274	0.635	Tight	1581.8	1865.3	1458.7	22.33
CCF310	1.281	1.27	None	456.5	853.3	276.2	4.13
CCF311	1.284	1.27	None	996.4	996.4	159.0	2.58

CCF312	1.268	1.27	None	599.0	599.0	124.8	2.03
CCF313	1.275	1.27	Loose	403.6	668.8	352.6	5.75
CCF314	1.280	1.27	Loose	702.0	702.0	386.5	6.35
CCF315	1.288	1.27	Loose	869.6	1032.4	551.8	8.27
CCF316	1.268	1.27	Tight	936.0	1191.1	769.8	11.70
CCF317	1.272	1.27	Tight	953.7	1092.1	771.1	12.53
CCF318	1.283	1.27	Tight	913.7	1100.2	772.5	12.48
CCF319	2.560	0.635	None	4435.4	4435.4	950.5	7.19
CCF320	2.568	0.635	None	4883.1	4883.1	1341.2	10.53
CCF321	2.633	0.635	None	5092.0	5092.0	974.1	7.44
CCF322	2.562	0.635	Loose	2998.7	3468.1	2256.8	17.42
CCF323	2.541	0.635	Loose	2481.2	4090.1	2761.8	21.92
CCF324	2.572	0.635	Loose	2711.1	3406.4	2520.1	19.75
CCF325	2.558	0.635	Tight	1560.8	3498.0	2599.0	20.14
CCF326	2.579	0.635	Tight	1842.9	3853.4	2714.0	20.38
CCF327	2.565	0.635	Tight	1894.5	4005.3	2761.9	21.35
CCF328	2.560	1.27	None	1782.6	1782.6	377.4	2.83
CCF329	2.562	1.27	None	1853.1	1853.1	444.5	3.51
CCF330	2.548	1.27	None	1811.7	1811.7	388.3	3.05
CCF331	2.559	1.27	Loose	1221.6	1221.6	665.6	5.05
CCF332	2.580	1.27	Loose	1154.5	1441.4	746.5	5.84
CCF333	2.545	1.27	Loose	1562.1	1608.9	1002.2	7.76

CCF334	2.592	1.27	Tight	1992.2	2334.7	1442.1	10.80
CCF335	2.563	1.27	Tight	1744.6	2105.4	1571.7	12.30
CCF336	2.541	1.27	Tight	1816.5	2281.1	1520.9	11.67
CCF337	5.104	0.635	None	11356.1	11356.1	3769.9	14.32
CCF338	5.132	0.635	None	9555.2	9555.2	2456.6	9.41
CCF339	5.124	0.635	None	10136.4	10136.4	3384.3	12.67
CCF340	5.133	0.635	Loose	6326.5	7441.6	5329.4	19.62
CCF341	5.088	0.635	Loose	6844.7	8140.2	5382.3	20.34
CCF342	5.112	0.635	Loose	5646.1	10270.8	5853.3	21.58
CCF343	5.102	0.635	Tight	4320.1	6534.4	5115.0	21.30
CCF344	5.093	0.635	Tight	3822.9	6193.5	4735.7	18.98
CCF345	5.106	0.635	Tight	4221.0	6048.4	4679.8	19.29
CCF346	5.128	1.27	None	3856.1	3856.1	847.7	3.38
CCF347	5.085	1.27	None	3329.7	3329.7	1097.1	4.24
CCF348	5.101	1.27	None	3921.2	3921.2	1261.5	4.77
CCF349	5.120	1.27	Loose	2491.4	3611.9	1874.9	7.18
CCF350	5.135	1.27	Loose	3755.7	4115.9	2502.5	9.42
CCF351	5.104	1.27	Loose	3922.6	3922.6	2206.4	8.85
CCF352	5.112	1.27	Tight	3360.3	3768.0	2790.0	11.56
CCF353	5.130	1.27	Tight	4126.1	4927.8	3079.8	11.66
CCF354	5.170	1.27	Tight	3699.4	4149.1	2691.4	10.03

Appendix D

Table of Experimental Data for CCF5

Panel group name: CCF5

Fiber tow size: 150 gsm (12 K)

Fiber volume fraction: 50%

Fiber length: 1 inch

Spec. Number	**Spec. Width (cm)**	**Profile Radius (cm)**	**Const-raint**	**Initial Peak Load (N)**	**Max. Peak Load (N)**	**Sustain-ed Crush Load (N)**	**SEA (J/g)**
CCF51	1.271	0.635	None	2104.3	3044.0	537.2	10.44
CCF52	1.277	0.635	None	3399.1	3399.1	817.3	15.81
CCF53	1.268	0.635	None	3308.8	3308.8	979.7	18.65
CCF54	1.278	0.635	Loose	1673.7	1976.6	1416.3	26.82
CCF55	1.283	0.635	Loose	1398.8	1472.1	807.4	15.71
CCF56	1.276	0.635	Loose	1436.1	1766.8	1097.0	21.43
CCF57	1.280	0.635	Tight	625.4	2009.9	1541.5	29.75
CCF58	1.271	0.635	Tight	1266.3	2478.4	1644.6	31.87
CCF59	1.270	0.635	Tight	1659.5	2428.9	1408.2	27.47
CCF510	1.272	1.27	None	1494.3	1494.3	251.6	4.95
CCF511	1.270	1.27	None	1178.9	1178.9	365.3	7.19

CCF512	1.281	1.27	None	1279.9	1279.9	271.8	5.29
CCF513	1.280	1.27	Loose	1402.0	1402.0	448.5	8.75
CCF514	1.278	1.27	Loose	1118.5	1118.5	412.4	8.02
CCF515	1.270	1.27	Loose	1031.0	1031.0	416.2	8.16
CCF516	1.275	1.27	Tight	1005.9	1005.9	740.0	14.43
CCF517	1.277	1.27	Tight	1050.0	1050.0	565.6	11.07
CCF518	1.277	1.27	Tight	995.7	995.7	609.2	11.82
CCF519	2.531	0.635	None	1328.8	5529.9	1814.3	17.50
CCF520	2.549	0.635	None	4829.5	5561.1	2691.2	25.49
CCF521	2.552	0.635	None	5923.6	6252.6	3156.4	29.50
CCF522	2.549	0.635	Loose	3344.8	5614.8	3242.8	30.34
CCF523	2.540	0.635	Loose	3407.3	4059.8	2521.5	24.67
CCF524	2.542	0.635	Loose	3081.4	3773.3	2582.1	24.37
CCF525	2.541	0.635	Tight	3795.0	4226.2	2656.4	25.44
CCF526	2.540	0.635	Tight	3284.4	6107.1	3759.9	35.92
CCF527	2.547	0.635	Tight	3556.0	4617.3	2931.8	28.69
CCF528	2.544	1.27	None	1410.8	2015.9	565.2	5.54
CCF529	2.546	1.27	None	1497.7	2514.4	495.0	4.77
CCF530	2.540	1.27	None	1138.2	1603.5	413.3	4.08
CCF531	2.546	1.27	Loose	2395.1	2395.1	1052.3	9.80
CCF532	2.540	1.27	Loose	2352.3	2352.3	1071.0	10.15
CCF533	2.549	1.27	Loose	1962.3	1962.3	1015.2	9.78

CCF534	2.560	1.27	Tight	2062.7	2062.7	1293.3	12.22
CCF535	2.554	1.27	Tight	1954.2	1954.2	1225.2	11.67
CCF536	2.540	1.27	Tight	1883.6	1883.6	1490.7	14.37
CCF537	5.067	0.635	None	10657.8	12686.0	3736.0	17.54
CCF538	5.071	0.635	None	10477.2	11752.4	3472.1	15.93
CCF539	5.069	0.635	None	8024.6	10487.4	3343.5	15.54
CCF540	5.063	0.635	Loose	5593.7	6826.8	4756.6	22.02
CCF541	5.058	0.635	Loose	6742.0	7554.7	5587.0	26.00
CCF542	5.061	0.635	Loose	7858.2	8002.9	4854.0	22.48
CCF543	5.063	0.635	Tight	6169.5	8804.8	5460.5	25.13
CCF544	5.061	0.635	Tight	6050.2	7081.4	5155.8	23.89
CCF545	5.096	0.635	Tight	6203.1	10095.1	7739.4	35.31
CCF546	5.081	1.27	None	3197.5	3774.0	1214.9	5.61
CCF547	5.080	1.27	None	3432.9	3916.5	1315.8	6.02
CCF548	5.081	1.27	None	4887.1	4887.1	992.8	4.57
CCF549	5.080	1.27	Loose	4183.1	4183.1	2222.3	11.04
CCF550	5.088	1.27	Loose	4675.5	4675.5	2233.9	11.01
CCF551	5.083	1.27	Loose	4065.0	4065.0	2243.3	10.87
CCF552	5.088	1.27	Tight	4031.1	4031.1	2882.4	13.47
CCF553	5.082	1.27	Tight	2288.4	4026.4	3149.8	14.41
CCF554	5.080	1.27	Tight	3051.0	4103.0	3283.5	15.15

In the previous table, the data for CCF52, CCF53 and CCF520 corresponds to an erroneous test where in the specimen buckled between the top plate and the roller ways.

Appendix E

Table of Experimental Data for CCF6

Panel group name: CCF6

Fiber tow size: 150 gsm (12 K)

Fiber volume fraction: 50%

Fiber length: 2 inches

Spec. Number	Spec. Width (cm)	Profile Radius (cm)	Const-raint	Initial Peak Load (N)	Max. Peak Load (N)	Sustain-ed Crush Load (N)	SEA (J/g)
CCF61	1.278	0.635	None	3722.5	4225.8	968.0	14.98
CCF62	1.275	0.635	None	3728.6	3728.6	835.8	12.70
CCF63	1.218	0.635	None	2971.6	2971.6	277.9	4.80
CCF64	1.277	0.635	Loose	1876.2	1876.2	1035.8	16.75
CCF65	1.281	0.635	Loose	1517.4	1517.4	891.8	14.54
CCF66	1.276	0.635	Loose	1569.6	1569.6	956.2	15.56
CCF67	1.283	0.635	Tight	962.5	1018.8	814.1	12.97
CCF68	1.281	0.635	Tight	835.7	885.2	725.6	11.73
CCF69	1.282	0.635	Tight	1002.5	1535.7	1173.9	18.00
CCF610	1.275	1.27	None	1397.3	1397.3	297.3	4.59
CCF611	1.280	1.27	None	1096.8	1096.8	349.6	5.40

CCF612	1.278	1.27	None	1052.0	1052.0	335.2	5.19
CCF613	1.283	1.27	Loose	1054.9	1054.9	467.2	7.19
CCF614	1.278	1.27	Loose	971.3	971.3	483.4	7.46
CCF615	1.293	1.27	Loose	972.0	972.0	432.2	7.09
CCF616	1.273	1.27	Tight	833.6	833.6	537.6	8.72
CCF617	1.277	1.27	Tight	788.9	814.6	584.0	9.07
CCF618	1.281	1.27	Tight	993.0	993.0	583.9	9.04
CCF619	2.546	0.635	None	5950.7	5950.7	2023.1	15.95
CCF620	2.563	0.635	None	6541.5	6541.5	2037.1	15.73
CCF621	2.559	0.635	None	5252.7	5252.7	1432.7	11.31
CCF622	2.558	0.635	Loose	3290.4	3340.6	2278.4	17.66
CCF623	2.571	0.635	Loose	3830.3	3830.3	2079.5	16.04
CCF624	2.573	0.635	Loose	3552.9	3552.9	2119.1	16.74
CCF625	2.560	0.635	Tight	2145.4	2215.3	1804.2	13.81
CCF626	2.545	0.635	Tight	1758.8	2035.6	1652.4	12.92
CCF627	2.553	0.635	Tight	2201.0	3153.0	2161.7	16.60
CCF628	2.544	1.27	None	2373.4	2373.4	632.6	4.86
CCF629	2.552	1.27	None	2671.8	2671.8	678.3	5.21
CCF630	2.569	1.27	None	1952.1	2110.8	741.2	5.74
CCF631	2.563	1.27	Loose	2234.3	2234.3	983.8	7.55
CCF632	2.565	1.27	Loose	2069.5	2069.5	837.9	6.52
CCF633	2.553	1.27	Loose	2186.1	2186.1	890.6	7.00

CCF634	2.553	1.27	Tight	1590.6	1590.6	1202.5	9.36
CCF635	2.557	1.27	Tight	1809.1	1809.1	1112.0	8.76
CCF636	2.548	1.27	Tight	1999.0	1999.0	1087.2	8.69
CCF637	5.137	0.635	None	10117.5	10516.3	3543.3	12.81
CCF638	5.113	0.635	None	11275.3	11275.3	4008.5	15.89
CCF639	5.095	0.635	None	10264.0	10264.0	4274.1	16.34
CCF640	5.090	0.635	Loose	8029.0	8029.0	5483.4	20.87
CCF641	5.097	0.635	Loose	8471.2	8471.2	5416.4	20.90
CCF642	5.132	0.635	Loose	8163.3	8163.3	4638.6	17.58
CCF643	5.100	0.635	Tight	4575.1	5043.8	4043.2	15.82
CCF644	5.135	0.635	Tight	5560.7	6066.7	4738.9	18.14
CCF645	5.132	0.635	Tight	4546.6	5961.5	4236.3	17.93
CCF646	5.105	1.27	None	4963.1	4963.1	1563.4	6.24
CCF647	5.105	1.27	None	5722.1	5722.1	1668.8	6.62
CCF648	5.131	1.27	None	4462.5	4462.5	1705.4	6.90
CCF649	5.088	1.27	Loose	3966.0	3966.0	1908.4	7.49
CCF650	5.131	1.27	Loose	3931.4	3931.4	2097.3	8.82
CCF651	5.096	1.27	Loose	4101.0	4101.0	1727.2	6.64
CCF652	5.152	1.27	Tight	4195.3	4195.3	2756.8	10.49
CCF653	5.089	1.27	Tight	3910.4	3910.4	2212.0	8.97
CCF654	5.090	1.27	Tight	4186.4	4186.4	2294.9	9.70

In the previous table, the data for CCF619, CCF637 and CCF638 corresponds to an erroneous test where in the specimen buckled between the top plate and the roller ways.

Appendix F

Table of Experimental Data for CCF7

Panel group name: CCF7

Fiber tow size: 300 gsm (48 K)

Fiber volume fraction: 50%

Fiber length: 2 inches

Spec. Number	**Spec. Width (cm)**	**Profile Radius (cm)**	**Const-raint**	**Initial Peak Load (N)**	**Max. Peak Load (N)**	**Sustain-ed Crush Load (N)**	**SEA (J/g)**
CCF71	1.268	0.635	None	2363.2	2363.2	464.7	7.43
CCF72	1.286	0.635	None	2542.3	2542.3	927.7	14.86
CCF73	1.281	0.635	None	2019.3	2019.3	637.2	10.25
CCF74	1.292	0.635	Loose	1238.9	1703.5	1071.2	16.87
CCF75	1.284	0.635	Loose	1141.7	1756.2	1016.5	16.33
CCF76	1.271	0.635	Loose	968.8	1777.3	1210.1	19.50
CCF77	1.270	0.635	Tight	774.2	1228.0	916.2	14.77
CCF78	1.281	0.635	Tight	733.8	1072.3	914.2	14.75
CCF79	1.280	0.635	Tight	513.7	1048.1	842.4	13.65
CCF710	1.272	1.27	None	788.8	826.8	214.1	3.44
CCF711	1.273	1.27	None	514.1	780.7	213.3	3.27

CCF712	1.278	1.27	None	1083.2	1083.2	198.1	3.07
CCF713	1.279	1.27	Loose	771.9	771.9	466.9	7.14
CCF714	1.274	1.27	Loose	795.0	795.0	491.1	7.61
CCF715	1.275	1.27	Loose	828.0	828.0	426.5	6.83
CCF716	1.281	1.27	Tight	899.4	899.4	562.5	8.39
CCF717	1.278	1.27	Tight	833.6	1135.5	801.8	11.99
CCF718	1.275	1.27	Tight	889.2	1136.1	769.4	11.76
CCF719	2.568	0.635	None	3080.8	3974.1	1296.0	9.93
CCF720	2.553	0.635	None	3972.1	4305.2	1346.1	10.22
CCF721	2.557	0.635	None	4807.1	4807.1	1308.9	10.04
CCF722	2.566	0.635	Loose	2412.0	3189.4	1675.5	13.05
CCF723	2.586	0.635	Loose	2370.6	4451.0	2256.7	17.06
CCF724	2.588	0.635	Loose	2909.9	3273.5	2159.2	16.88
CCF725	2.551	0.635	Tight	1691.1	2670.6	2126.3	16.40
CCF726	2.562	0.635	Tight	1421.0	2223.4	1790.0	14.00
CCF727	2.559	0.635	Tight	1343.5	2218.5	1825.8	13.87
CCF728	2.576	1.27	None	1829.4	1829.4	353.0	2.76
CCF729	2.568	1.27	None	1334.2	1794.1	582.1	4.66
CCF730	2.558	1.27	None	991.0	1379.0	447.6	3.51
CCF731	2.555	1.27	Loose	1608.2	1676.1	1133.1	8.68
CCF732	2.570	1.27	Loose	1784.6	1916.9	971.4	7.41
CCF733	2.548	1.27	Loose	1690.3	1728.3	947.5	7.31

CCF734	2.549	1.27	Tight	1626.6	1767.6	1248.0	9.78
CCF735	2.580	1.27	Tight	1789.3	1818.5	1374.7	10.39
CCF736	2.546	1.27	Tight	1576.3	1805.0	1354.6	10.38
CCF737	5.105	0.635	None	8768.3	8768.3	2877.2	10.81
CCF738	5.111	0.635	None	8280.6	9426.3	2569.0	9.69
CCF739	5.092	0.635	None	7864.9	7864.9	2641.8	9.99
CCF740	5.079	0.635	Loose	5428.4	7436.2	4687.6	17.77
CCF741	5.094	0.635	Loose	4586.2	7909.9	5166.1	19.45
CCF742	5.133	0.635	Loose	4437.7	7932.9	5039.6	18.81
CCF743	5.090	0.635	Tight	3098.7	5910.2	4409.3	16.85
CCF744	5.076	0.635	Tight	2980.7	5699.3	4628.3	17.48
CCF745	5.099	0.635	Tight	3029.7	5139.8	3927.3	14.98
CCF746	5.120	1.27	None	3171.0	3171.0	1035.1	3.92
CCF747	5.109	1.27	None	2487.3	3698.1	1066.6	4.06
CCF748	5.131	1.27	None	3286.3	3299.9	1103.1	4.22
CCF749	5.126	1.27	Loose	3111.3	3111.3	2099.6	8.19
CCF750	5.080	1.27	Loose	3770.7	3770.7	2182.1	8.88
CCF751	5.149	1.27	Loose	3956.5	3956.5	1674.0	6.36
CCF752	5.050	1.27	Tight	3184.6	3761.2	3067.8	11.81
CCF753	5.097	1.27	Tight	3376.6	3870.4	2739.2	10.80
CCF754	5.072	1.27	Tight	3156.8	3352.1	2536.2	10.54

Appendix G

Table of Experimental Data for CCF8

Panel group name: CCF8

Fiber tow size: 300 gsm (48 K)

Fiber volume fraction: 40%

Fiber length: 1 inch

Spec. Number	**Spec. Width (cm)**	**Profile Radius (cm)**	**Const-raint**	**Initial Peak Load (N)**	**Max. Peak Load (N)**	**Sustain-ed Crush Load (N)**	**SEA**
CCF81	1.276	0.635	None	2242.4	3185.3	644.2	10.25
CCF82	1.272	0.635	None	2917.4	2917.4	743.3	12.19
CCF83	1.269	0.635	None	2340.8	2340.8	538.7	8.78
CCF84	1.283	0.635	Loose	1262.1	1454.8	775.2	12.37
CCF85	1.279	0.635	Loose	1284.3	1708.0	1058.4	16.86
CCF86	1.270	0.635	Loose	1506.9	1530.9	1050.6	17.04
CCF87	1.280	0.635	Tight	1159.3	1849.9	1543.0	23.49
CCF88	1.268	0.635	Tight	1002.5	1838.2	1326.9	20.38
CCF89	1.271	0.635	Tight	516.0	1279.3	1034.3	16.92
CCF810	1.280	1.27	None	288.2	688.5	134.5	2.13
CCF811	1.276	1.27	None	378.5	743.4	157.7	2.53

CCF812	1.276	1.27	None	668.1	668.1	178.2	2.92
CCF813	1.267	1.27	Loose	813.3	837.7	482.7	7.39
CCF814	1.281	1.27	Loose	722.4	790.9	380.9	5.81
CCF815	1.266	1.27	Loose	657.9	967.6	475.7	7.39
CCF816	1.280	1.27	Tight	788.2	1109.0	611.1	9.41
CCF817	1.281	1.27	Tight	930.0	1197.9	777.3	11.84
CCF818	1.267	1.27	Tight	993.0	1204.7	738.6	11.08
CCF819	2.559	0.635	None	5349.7	5349.7	1888.8	14.44
CCF820	2.542	0.635	None	4725.0	5269.7	1972.4	15.49
CCF821	2.548	0.635	None	4969.9	4969.9	1649.0	12.73
CCF822	2.552	0.635	Loose	2790.0	4238.0	2182.3	17.01
CCF823	2.543	0.635	Loose	2756.4	3942.9	2700.5	5.26
CCF824	2.549	0.635	Loose	2640.2	3869.0	2766.5	21.22
CCF825	2.559	0.635	Tight	2119.2	3650.0	3149.2	23.65
CCF826	2.558	0.635	Tight	1686.9	3598.4	2603.6	19.62
CCF827	2.545	0.635	Tight	1888.4	3468.1	2092.0	16.18
CCF828	2.544	1.27	None	1113.8	1321.3	299.5	2.36
CCF829	2.548	1.27	None	1446.1	1446.1	364.7	2.82
CCF830	2.538	1.27	None	1683.5	1683.5	370.5	2.93
CCF831	2.549	1.27	Loose	1541.7	2164.5	1035.8	7.99
CCF832	2.550	1.27	Loose	1651.0	1715.4	891.9	6.98
CCF833	2.552	1.27	Loose	1463.1	1634.7	733.9	5.66

CCF834	2.566	1.27	Tight	1606.9	2129.9	1314.5	10.04
CCF835	2.566	1.27	Tight	1708.6	2207.8	1248.2	9.52
CCF836	2.541	1.27	Tight	1663.2	1910.1	1223.7	9.47
CCF837	5.091	0.635	None	9934.4	9934.4	3109.5	11.87
CCF838	5.067	0.635	None	11829.7	11829.7	3582.9	13.60
CCF839	5.097	0.635	None	10425.4	10425.4	3287.8	12.55
CCF840	5.072	0.635	Loose	6530.1	9984.0	6447.2	24.62
CCF841	5.069	0.635	Loose	8361.2	9064.2	5662.9	21.86
CCF842	5.109	0.635	Loose	6343.6	9303.6	5272.1	20.17
CCF843	5.086	0.635	Tight	5805.5	7415.8	5755.5	23.78
CCF844	5.100	0.635	Tight	3889.0	7210.6	5016.6	19.34
CCF845	5.133	0.635	Tight	3654.4	6740.6	4845.0	18.35
CCF846	5.096	1.27	None	3626.8	3662.8	952.6	3.68
CCF847	5.095	1.27	None	3437.6	3437.6	867.8	3.37
CCF848	5.046	1.27	None	3081.5	3245.0	943.1	3.64
CCF849	5.060	1.27	Loose	4394.7	4394.7	2767.6	11.85
CCF850	5.088	1.27	Loose	3891.4	3891.4	2386.6	9.82
CCF851	5.071	1.27	Loose	4149.1	4149.1	2488.6	10.63
CCF852	5.092	1.27	Tight	2989.9	3998.6	2581.1	10.65
CCF853	5.132	1.27	Tight	2930.9	3867.0	2447.4	9.62
CCF854	5.059	1.27	Tight	4018.2	4018.2	3004.2	12.10

Appendix H

Table of Experimental Data for CCF9

Panel group name: CCF9

Fiber tow size: 300 gsm (48 K)

Fiber volume fraction: 50%

Fiber length: 1 inch

Spec. Number	Spec. Width (cm)	Profile Radius (cm)	Const-raint	Initial Peak Load (N)	Max. Peak Load (N)	Sustain-ed Crush Load (N)	SEA (J/g)
CCF91	1.281	0.635	None	2399.8	2399.8	433.3	6.79
CCF92	1.269	0.635	None	2277.1	2277.1	294.1	4.54
CCF93	1.280	0.635	None	2638.6	2638.6	536.0	8.53
CCF94	1.266	0.635	Loose	1661.1	2128.5	1269.0	20.41
CCF95	1.268	0.635	Loose	1128.7	1627.2	1096.5	17.57
CCF96	1.275	0.635	Loose	1132.1	2055.9	1179.0	18.61
CCF97	1.275	0.635	Tight	849.2	1495.0	1176.1	18.05
CCF98	1.269	0.635	Tight	930.6	1579.1	1200.4	18.69
CCF99	1.277	0.635	Tight	889.2	1381.0	1125.9	17.80
CCF910	1.268	1.27	None	1373.6	1373.6	276.1	4.41
CCF911	1.278	1.27	None	737.3	919.1	271.0	4.14

CCF912	1.268	1.27	None	610.5	771.2	244.0	3.73
CCF913	1.274	1.27	Loose	811.9	811.9	446.6	
CCF914	1.270	1.27	Loose	746.1	779.4	487.5	7.81
CCF915	1.278	1.27	Loose	778.0	846.5	430.8	6.86
CCF916	1.267	1.27	Tight	683.0	792.2	540.7	8.69
CCF917	1.268	1.27	Tight	790.2	954.0	804.2	12.41
CCF918	1.277	1.27	Tight	925.9	945.6	750.1	11.54
CCF919	2.536	0.635	None	4571.7	4571.7	1022.8	7.90
CCF920	2.546	0.635	None	5764.8	5764.8	1340.4	10.36
CCF921	2.536	0.635	None	5766.2	5766.2	1365.2	10.63
CCF922	2.544	0.635	Loose	2725.4	3858.8	2702.7	20.80
CCF923	2.540	0.635	Loose	2559.9	4013.5	2615.5	20.53
CCF924	2.539	0.635	Loose	2826.4	3618.0	2571.4	19.84
CCF925	2.540	0.635	Tight	1942.0	3041.5	2212.2	17.00
CCF926	2.540	0.635	Tight	2018.6	3921.9	2804.8	21.63
CCF927	2.538	0.635	Tight	2074.2	3536.0	2361.5	18.20
CCF928	2.540	1.27	None	1412.2	1448.2	461.2	3.59
CCF929	2.540	1.27	None	1517.3	1690.0	494.4	3.77
CCF930	2.542	1.27	None	2148.9	2148.9	593.5	5.74
CCF931	2.542	1.27	Loose	1954.9	1954.9	1157.8	9.02
CCF932	2.541	1.27	Loose	1639.4	1639.4	892.2	6.79
CCF933	2.543	1.27	Loose	1371.5	1589.2	1003.4	7.67

CCF934	2.535	1.27	Tight	1586.5	1627.2	1282.9	10.06
CCF935	2.542	1.27	Tight	1419.7	1643.5	1213.0	9.39
CCF936	2.547	1.27	Tight	1854.5	1854.5	1351.1	10.35
CCF937	5.088	0.635	None	8306.4	8306.4	2777.8	10.69
CCF938	5.086	0.635	None	9535.3	9535.3	3005.7	12.26
CCF939	5.110	0.635	None	10914.2	10914.2	3069.0	11.69
CCF940	5.082	0.635	Loose	5359.2	7959.8	5368.5	20.50
CCF941	5.125	0.635	Loose	5964.9	6981.0	5151.5	19.50
CCF942	5.031	0.635	Loose	6854.8	8789.3	5572.5	21.99
CCF943	5.104	0.635	Tight	3603.1	5566.8	4282.0	17.30
CCF944	5.075	0.635	Tight	4375.7	5863.9	4260.4	17.63
CCF945	5.071	0.635	Tight	5311.0	6944.4	5201.7	20.44
CCF946	5.105	1.27	None	3449.1	3449.1	812.4	3.14
CCF947	5.067	1.27	None	3639.0	3941.6	1400.8	5.75
CCF948	5.118	1.27	None	2736.9	3370.5	981.3	3.99
CCF949	5.111	1.27	Loose	3990.4	3990.4	2009.8	7.83
CCF950	5.076	1.27	Loose	4074.5	4074.5	2568.5	10.22
CCF951	5.109	1.27	Loose	3254.4	3680.4	2458.0	9.50
CCF952	5.081	1.27	Tight	3873.8	4208.8	3380.7	13.06
CCF953	5.107	1.27	Tight	2843.4	3913.1	2606.0	10.48
CCF954	5.078	1.27	Tight	3214.5	3346.7	2697.2	11.49

VITA

The author of this text was born in Chennai, India on February 4, 1976 to Mrs. Mary C. Jacob and Raju C. Jacob. He attended The D.A.V. Higher Secondary School in Chennai, India. After high school, he attended The Manipal Institute of Technology at Karnataka, India, in pursuit of a B.S. in Chemical Engineering which was completed February 1998. His B.S. was followed by graduate studies at The University of Tennessee in Polymer Engineering at the masters level which was completed January 9, 2001. He plans to pursue his Ph.D. in Polymer Engineering at The University of Tennessee.